692
1/10/79

NO STOCK

TID-28271
Distribution Category UC-66a

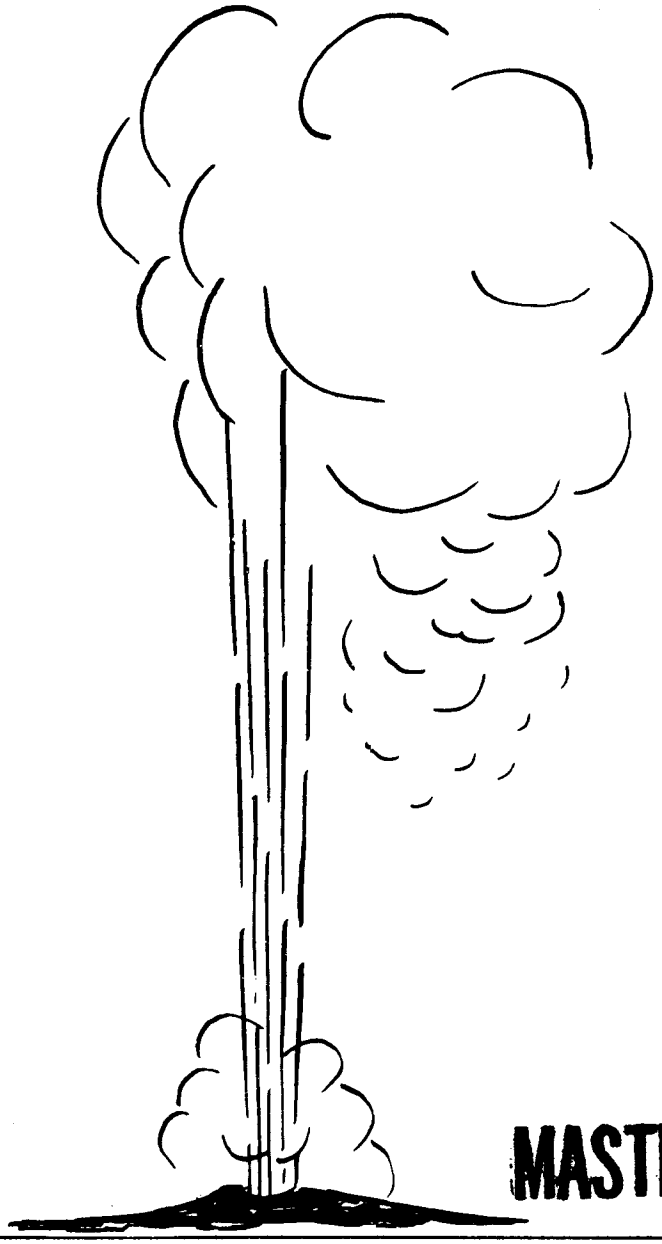

GEOLOGICAL AND GEOPHYSICAL STUDY OF THE ORIGIN OF THE WARM SPRINGS IN BATH COUNTY, VIRGINIA

Final Report, June 1, 1975—April 30, 1976

By
John K. Costain
G. V. Keller
R. A. Crewdson

Work Performed Under Contract No. EY-76-S-05-4920

Department of Geological Sciences
Virginia Polytechnic Institute and State University
Blacksburg, Virginia

U. S. DEPARTMENT OF ENERGY
Geothermal Energy

DISCLAIMER

NOTICE

Available from the National Technical Information Service, U. S. Department of Commerce, Springfield, Virginia 22161.

Price: Paper Copy $9.00
Microfiche $3.00

Table of Contents

	Page
Introduction	1
Purpose of the Investigation	4
Previous Investigations	6
Procedure	12
Topography of the Region	13
Electrical Resistivity Dipole Survey	17
Geothermal Gradient and Heat Flow from Existing Holes in Bath County	27
Drilling Site in the Warm Springs Anticline	30
Temperature Increase from Radiogenic Sources	35
Relationship of 38th Parallel Fracture Zone to Resistivity Anomalies	38
Conclusions	39
Acknowledgements	41
References	42
Personnel of Project	44
Appendix	45

Introduction

In the northwestern part of Virginia and adjacent parts of West Virginia there are approximately 100 springs that have temperatures ranging from slightly above the mean annual air temperature (9-12°C) to about 41°C (105.8°F). In Virginia, nearly all of the warm springs appear to issue from limestone formations of Middle Ordovician age where these formations are brought to the surface by anticlinal folding. The geographic distribution of the springs has been described by Reeves (1932).

Table I from Reeves (1932, p. 8) shows the number of springs in Virginia grouped according to their temperature. The hottest springs are located in the Warm Springs anticline in Bath and Alleghany Counties in Virginia where there are four groups of springs known as the Warm Springs, Hot Springs, Healing Springs, and Falling Springs. Since these are the hottest springs in the region, the present study has focused principally on the region centered around the Warm Springs anticline (Figure 1). Each group of springs in the Warm Springs anticline consists of at least three separate springs in close proximity. The group at Warm Springs is made up of three springs within about 30 meters of each other and a fourth about 250 meters to the southwest. At Hot Springs, eight warm springs occur over an area of about 4000 m^2. Healing Springs consists of three separate springs less than three meters apart. Falling Springs are

Table 1. Thermal springs in Virginia grouped according to their temperature.

Temperature, °C	Number of Springs
38 - 41	2
32 - 37	8
25 - 30	3
16 - 24	27
13 - 15	45

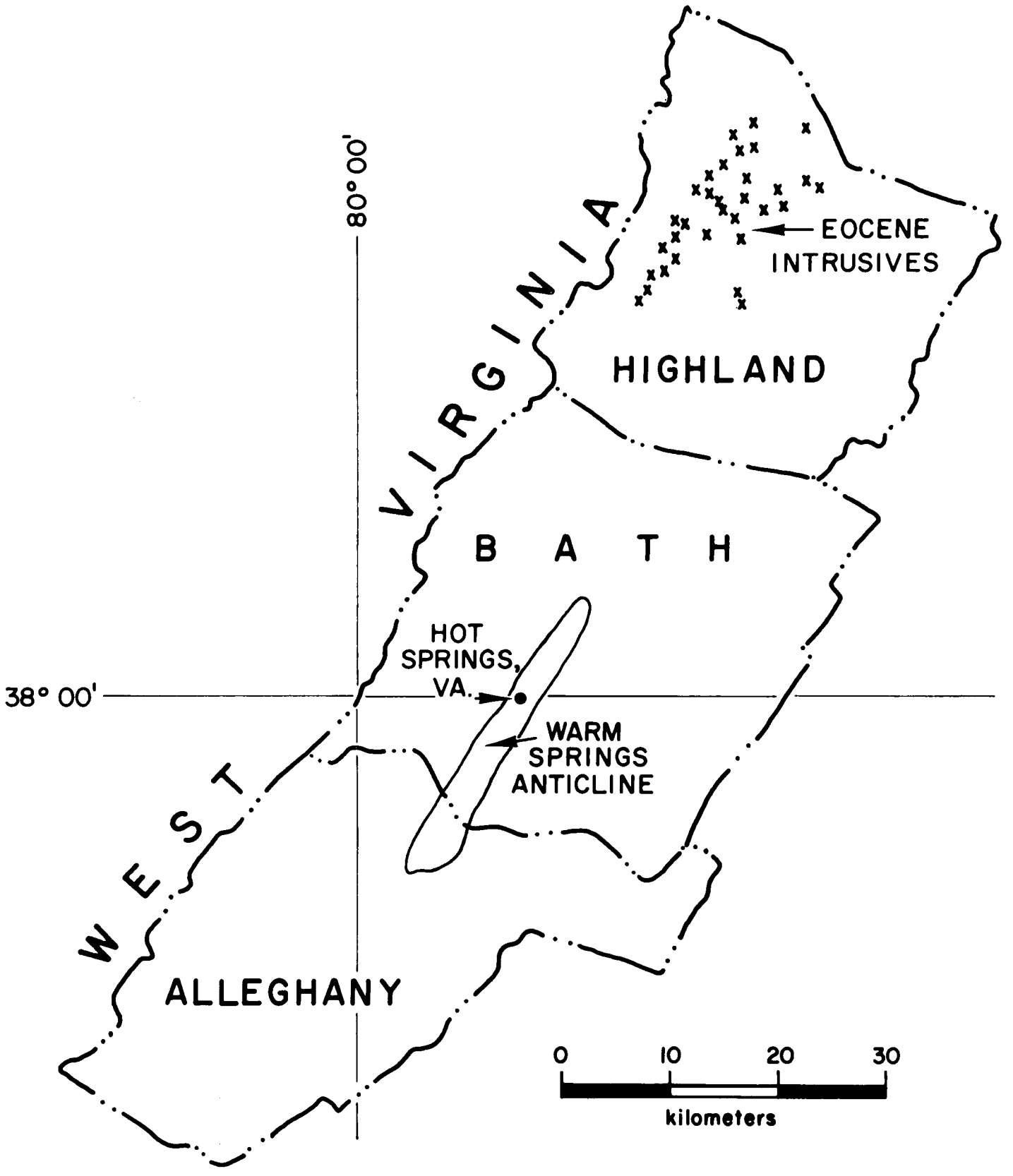

Figure 1. Location of Warm Springs Anticline in Bath and Alleghany Counties, Virginia.

made up of a number of flows and seepages at a much lower temperature than the other warm springs in the Warm Springs anticline, and with a much greater discharge than any other warm springs in the region.

Purpose of the Investigation

The purpose of this study was to determine the origin of the warm springs and to evaluate the geothermal resource potential of the area in the vicinity of the Warm Springs anticline in Bath and Alleghany Counties, Virginia. The Warm Springs anticline is shown on the geologic map of Figure 2.

Source of Data for Figure 2

1. Warm Springs Anticline: Reconnaissance mapping by Dr. C.E. Sears assisted by Mr. L.N. Ford.
2. Clifton Forge Iron District: Virginia Engineering Experiment Station Bulletin 118, F.G. Lesure, 1957.
3. Geologic map of the Appalchian Valley in Virginia, by Charles Butts, Virginia Geological Survey, 1933.
4. Geologic Map of Virginia, Commonwealth of Virginia, Department of Conservation and Economic Development, Division of Mineral Resources, 1963.
5. Bick, K.F., 1960, Geology of the Lexington quadrangle, Virginia: Virginia Division of Mineral Resources Rept. Invest. 2, 40 p.
6. Bick, K.F., 1962, Geology of the Williamsville quadrangle, Virginia: Virginia Division of Mineral Resources Rept. Invest. 2, 40 p.
7. Geologic Atlas of the United States, Monterey Folio, Virginia-West Virginia, 1899.

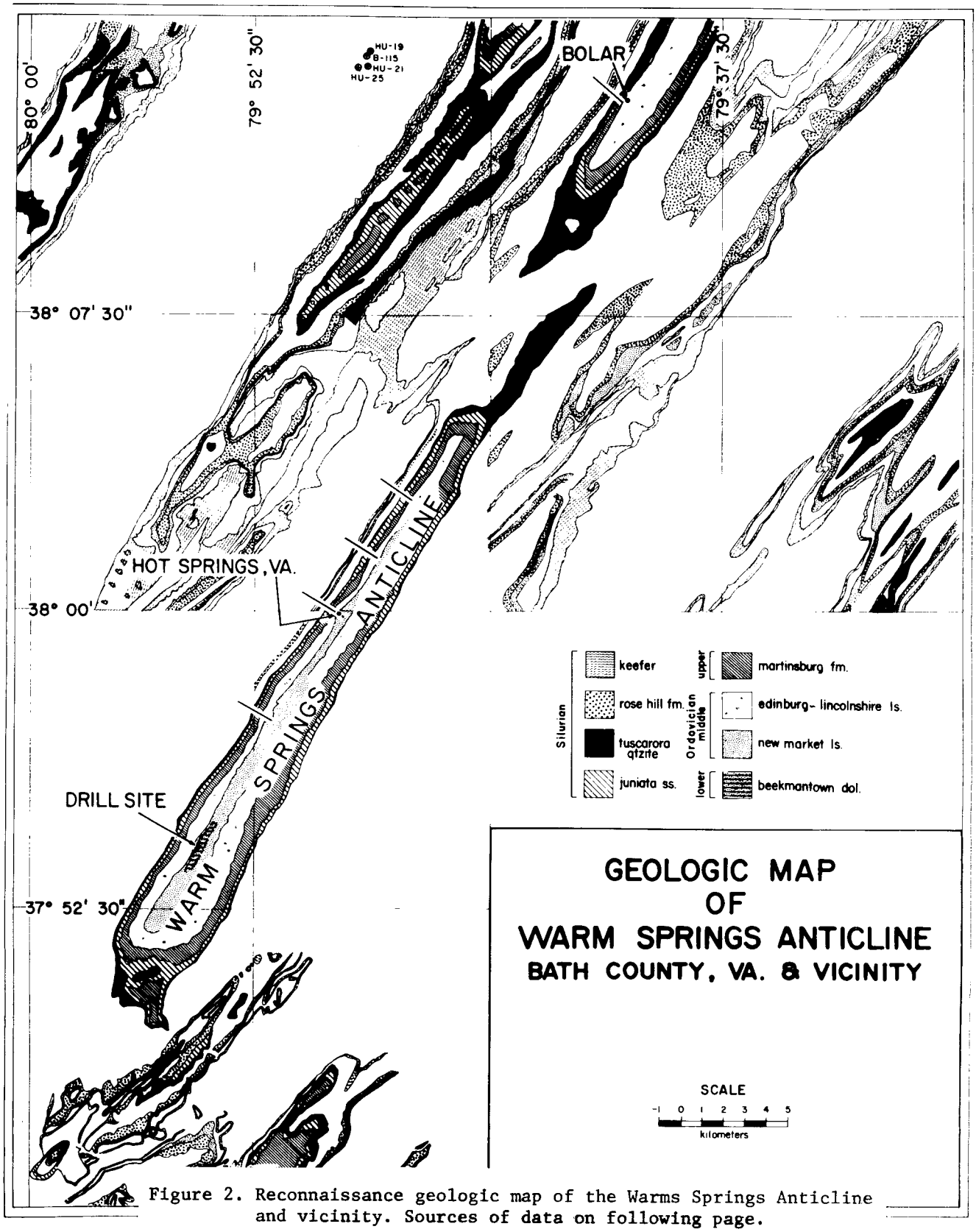

Figure 2. Reconnaissance geologic map of the Warms Springs Anticline and vicinity. Sources of data on following page.

Previous Investigations

Nearly a century ago, Rogers (1884) noted that the principal warm springs then known in Virginia were located along anticlinal fold axes. This observation has been corroborated by subsequent investigators. The most comprehensive study of the geology of the area was that of Reeves (1939) who reported on the geographic distribution of the springs, the temperature, discharge, chemistry, and gas content of the spring water, and the general geology of the area including topography, structural geology, and stratigraphy. Reeves' study was hampered by lack of complete topographic map coverage, and much of the stratigraphic nomenclature used by him, particularly that relating to the formations from which the springs issue, is now considered inappropriate for the area.

Rogers (1884) and Reeves (1932) both concluded that the warm and moderately warm springs issue from rocks of Cambrian and Ordovician age where these formations rise from considerable depths as the result of anticlinal folding. Rogers proposed that surface water entering the rocks at their outcrop in high anticlinal ridges sinks to considerable depths along joints and fissures until it reaches a permeable bed, and then rises along the dip of this bed to its outcrop in an adjacent valley. According to Reeves (1932, p. 26), however, some of the anticlines are broken by thrust faults, but he states that there is no positive

evidence that any of the warm springs are along faults. Reeves further concluded that most of the springs of the region undoubtedly are not so located, and that few of the springs are probably fed by water rising along fault planes or through fissures bordering fault planes. Reeves (1932, p. 28) concluded that the springs are produced by meteoric waters entering a permeable bed along its outcrop at a relatively high altitude on the crest or limb of one anticline and rising to the surface where the same bed crops out at a lower altitude in another anticline, the temperature of the waters being an expression of the normal earth temperature in the deep synclinal basins through which the water circulates. Reeves' hypothesis is similar to Rogers' in that it attributes the temperature of the springs to normal earth temperatures. It differs from Rogers' hypothesis in that it predicts movement through permeable beds from one anticline to another rather than movement through joints and fissures from an anticlinal ridge to adjacent valleys.

Rogers (1884), Watson (1924), and Reeves (1932) have thus all postulated that the spring waters are of meteoric origin. The chief basis for this conclusion is the similarity in the chemical character of the water from the cold and warm springs, the fact that the dissolved gases appeared to be principally of atmospheric origin (Reeves, 1932, p. 28; 1974), and the observation that the geologic setting in which the springs occur is indeed compatible

with a model of artesian circulation of meteoric water through permeable beds. Additional geochemical studies of the spring waters are now in progress by the U.S. Geological Survey (W. Hobba, personal communication, 1975).

Recognition of albite-felsite sills and dikes of Eocene age in Highland County by Fullagar and Bottino (1969) suggested to Dennison and Johnson (1971) an alternative heat source other than deep circulation of meteoric water. The igneous intrusions are exposed just 30 km north of Hot Springs, Virginia. Dennison and Johnson suggested a causal relationship between the Schooley erosion surface and the known site of igneous activity. The generally accordant and flat profiles of the highest ridges in the Appalachian Plateau and adjacent Ridge and Valley region have been interpreted as an ancient erosion surface known as the Schooley peneplane. The age of this Schooley surface is variously interpreted as Cretaceous or early Tertiary (Wright, 1934, p. 10). The position of maximum uplift of a dome on the Schooley surface with 1000 feet of arching is close to the presumably younger Eocene intrusions in Highland County. Dennison and Johnson (1971, p. 503) proposed that thermal and mechanical energy associated with igneous intrusions at depth could upwarp the erosion surface.

Dennison and Johnson also noted a negative simple Bouguer gravity anomaly with its maximum negative value in western Bath County. Large granitic plutons usually have associated with them

negative density contrasts (Bott and Smithson, 1967). Dennison and Johnson suggested, therefore, that the large negative gravity anomaly is related to a deep felsic pluton that provides heat to the thermal springs centered in Bath County. They suggest that the pluton is either the source of the andesite dikes in Highland County, or possible represents a later thermal (volcanic) pulse related to the same deep crustal fracture zone. The intrusives of igneous age represent the youngest known igneous activity in the eastern United States. The range of rock types represented is from basalt through andesite to trachytes, all of which can be related to the basalt by a crystal separation, differentiation process (Hall, 1974; Bollinger and Gilbert, 1974); there is no clear correlation, therefore, between these intrusives of shallow origin (Hall, 1974) and a proposed deeper-seated granitic body.

All of these phenomena are located near the apparent termination eastward of the "38th parallel fracture zone" (Snyder and Gerdemann, 1965; Heyl and others, 1965; Zartman and others, 1967). The extent of this fracture zone and its geographic relationship to Bath and Highland Counties are shown in Figure 3. The 38th parallel fracture zone has apparently been a site of sporadic igneous activity from late Precambrian to Eocene time. There is some suggestion that the intrusive activity is older toward the west. Dennison and Johnson (1971, p. 506) conclude that the 38th parallel fracture zone is still a geologically

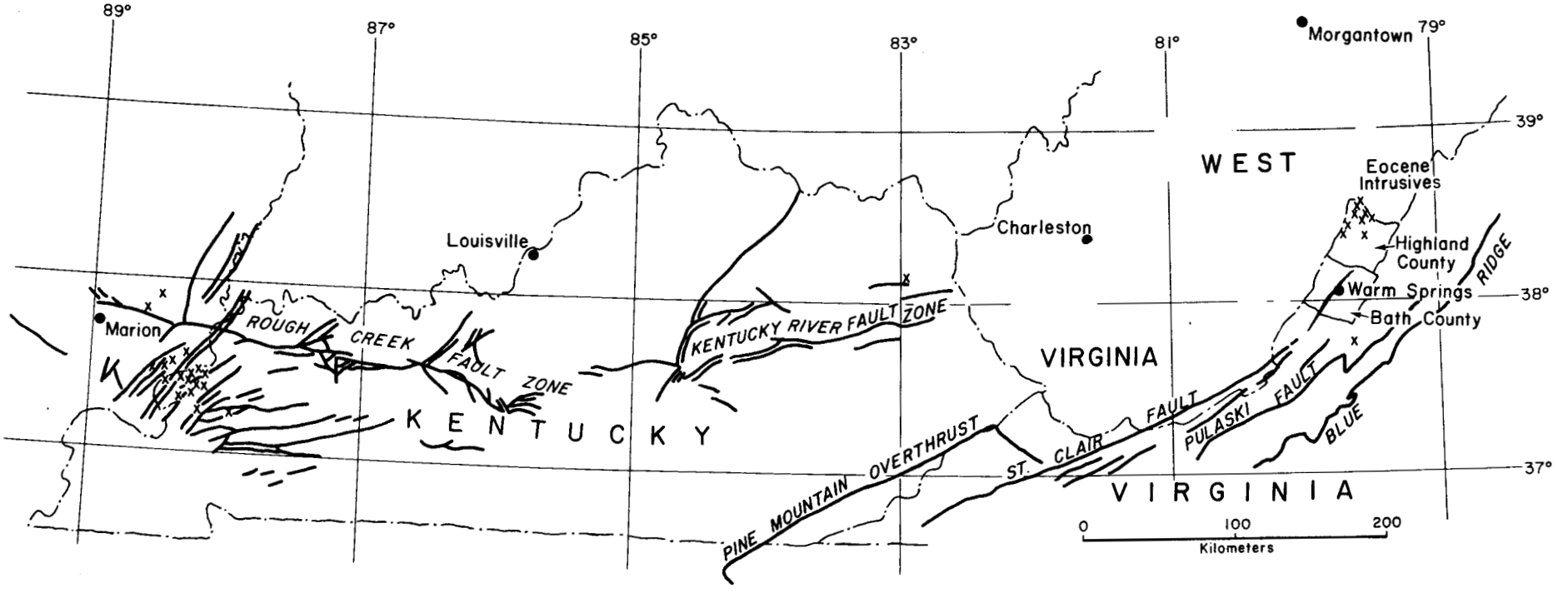

Figure 3. Relationship of the Warm Springs Anticline and Eocene intrusives in Highland County to the 38th parallel fracture zone. Map adapted from the Tectonic Map of the United States, 1962.

active zone of weakness along which additional activity will probably occur in the geologic future.

Bollinger and Gilbert (1974) reported on a reconnaissance microearthquake survey at six sites in Bath County and one in Highland County. A swarm of 43 microshocks was recorded at Duncan Knob, about 20 km north of Hot Springs; however, the swarm stopped before the other two instruments could be moved into the area. The remaining six stations recorded no definite microearthquake activity during the recording program. Since no seismic events were recorded on more than one instrument, it must be concluded that the area is one of low microearthquake activity.

Prior to the present investigation, no detailed geophysical studies have been published in Bath and Highland Counties. This report describes the results of heat flow determinations and a reconnaissance dipole electrical resistivity survey in Bath County. Both of these geophysical approaches must be used to defend the credibility of any model of the origin of the hot springs in western Virginia.

Procedure

Pase I of the study was the compilation of a geologic map based on published maps and supported by reconnaissance geologic mapping in areas where published maps were not available. Phase II consisted of a regional bipole-dipole electrical resistivity survey made in order to detect the presence of resistivity lows that might be associated with a geothermal system at depth. Phase III involved the drilling of a single hole to a depth of approximately 300 m (∿1000 feet) to obtain a heat flow value that is representative of the area.

The above data were used to attempt to arrive at a model that unambiguously explains the origin of the thermal springs. Additional data other than that discussed above will have to be considered at a later date. Topographic maps combined with geologic maps will help to define the source of the water that feeds the springs. The geochemistry of the spring water will provide important data on the origin of the thermal springs. The geochemical study is being done by the U. S. Geological Survey.

Topography of the Region

Conditions for the generation of springs by deep artesian circulation of meteoric ground water include 1) folded beds, 2) permeability along bedding planes and/or joints extending to depths great enough to heat the water in the presence of the normal geothermal gradient, and 3) a source area of large enough areal extent such that precipitation can enter permeable beds at a relatively high outcrop and be discharged by springs at a lower elevation. The elevations of the hottest springs at Hot Springs vary from 686 to 693 meters above sea level. Figure 4 shows the extent of surface area in the region above an elevation of 731 meters (about 2400 feet). It appears that an adequate source area is present to satisfy condition (3) above, and to provide a hydrostatic head sufficient for deep artesian circulation. The present model for the origin of the warm springs favors the area beneath Warm Springs Mountain as the source area for downward-percolating ground water.

Figures 5 and 6 show structural cross sections across the Warm Springs Anticline. It is apparent that condition (1) also appears to be satisfied. The extent of vertical permeability in the area will be evaluated during the summer of 1976 under ERDA Contract No. E-(40-1)-5103.

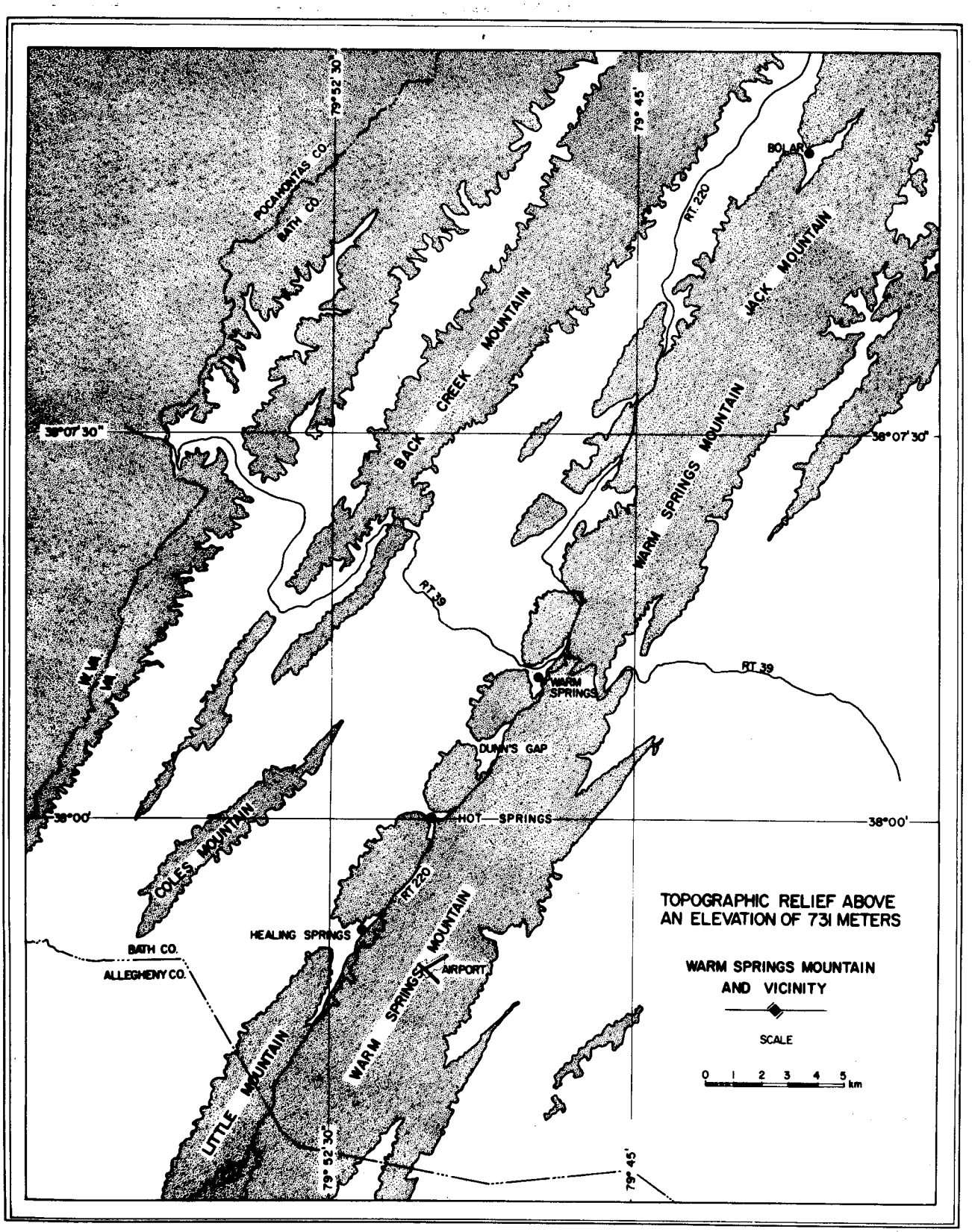

Figure 4. Shaded area shows topographic relief above an elevation of 731 meters. Water gaps at Healing Springs, Hot Springs, Dunn's Gap, and Warm Springs are prominent topographic features.

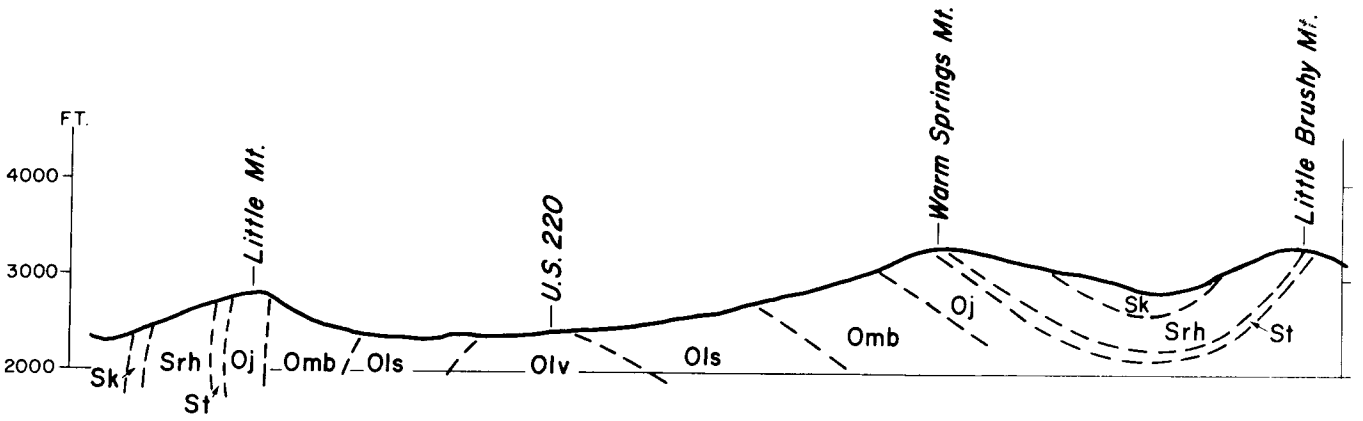

Section D-D', Dunns Gap

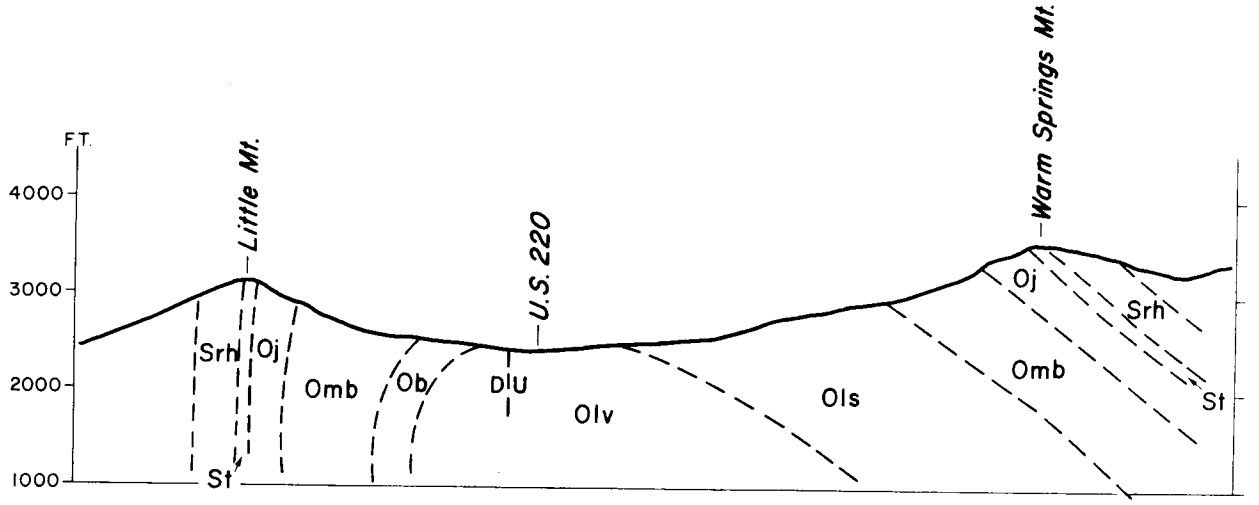

Section F-F', Thru Quarry, Hot Springs, Va.

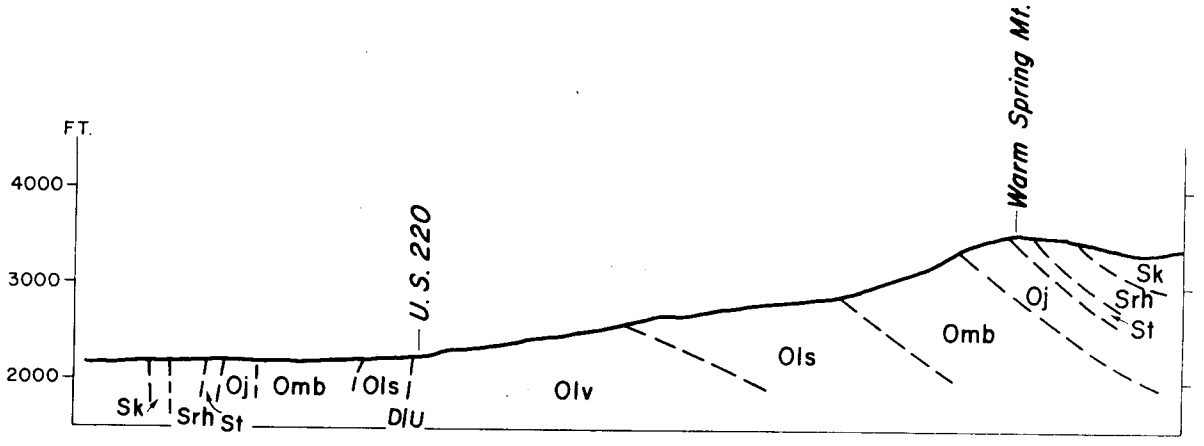

Section E-E', Thru Hot Springs Gap

Sk - Keefer
Srb - Rose Hill
St - Clinch ss.
Oj - Juniata
Omb - Martinsburg
Ols - Edinburg - Lincolnshine
Olv - Lurich
Ob - Beekmantown

Figure 5. Preliminary structure sections across the Warm Springs Anticline.

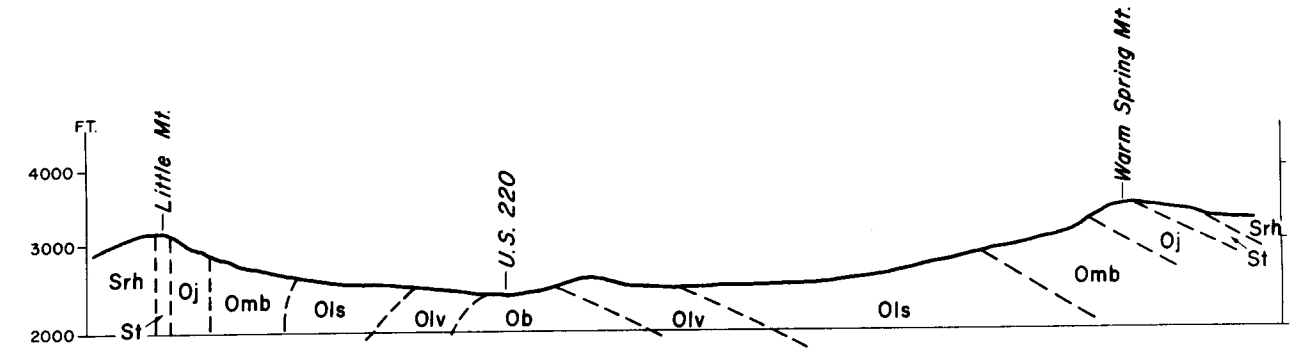

Section C-C', Bowen Farm

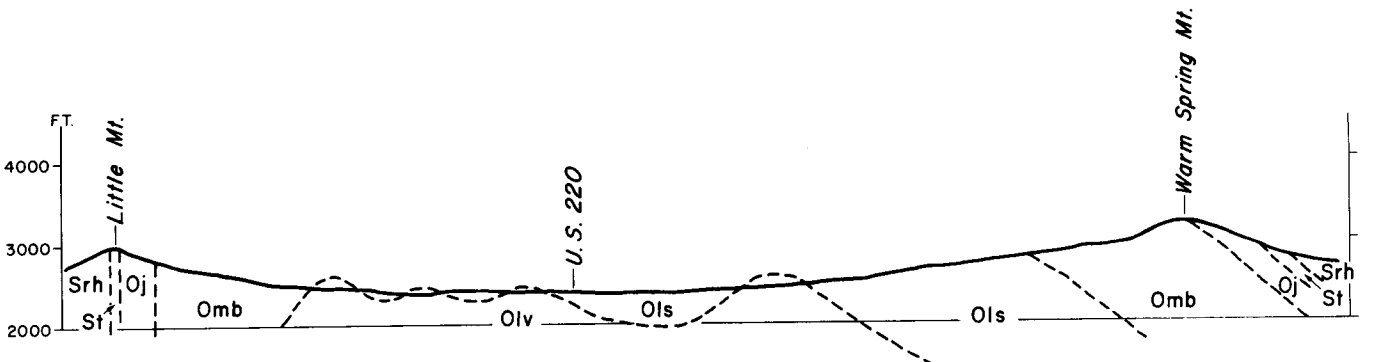

Section B-B', Falling Spring, Hollowrock Farm

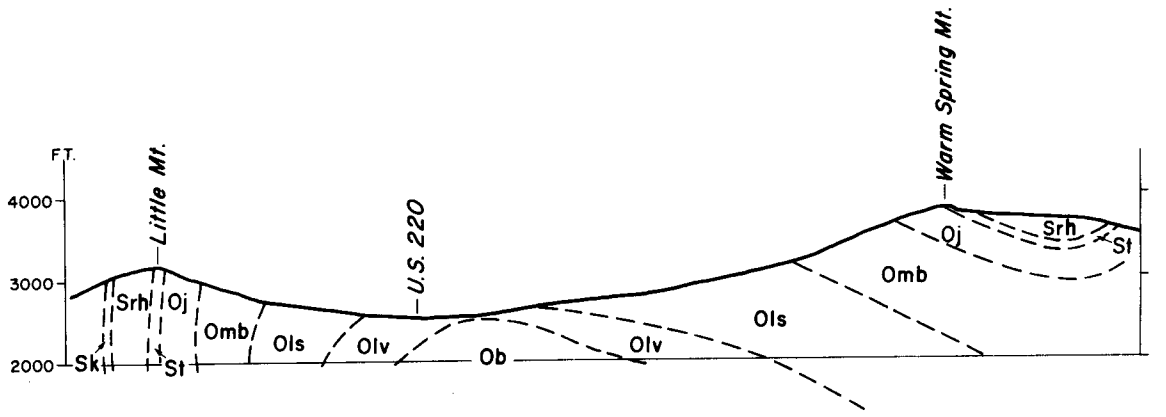

Section A-A', Ashwood

Figure 6. Preliminary structure sections across the Warm Springs Anticline. The drill site (see page 30) is located at the Bowen farm on Section C-C' at U. S. 220.

Electrical Resistivity Dipole Survey

Electrical methods of geophysical exploration have become a basic tool in prospecting for geothermal reservoirs. Such reservoirs usually have great size compared to the usual targets of electrical prospecting, and for this reason, the conventional electrical techniques have not been used with any degree of success. Rather, new methods of electrical prospecting which can be used on the scale required to examine geothermal reservoirs have had to be developed. Among these new methods are dipole or bipole-dipole and quadripole mapping surveys (Keller et al., 1975).

In bipole-dipole mapping, abbreviated dipole mapping, current flow is established in the earth by using a pair of source electrodes that are not necessarily closely spaced, and so they can be said to form a source "bipole". Current is fed to the ground through two widely separated electrodes. The electric field is then determined at many observation points by observing the voltage drop between two pairs of electrodes oriented approximately at right angles. The current flow pattern will be governed by the spatial variation in resistivity of the ground to a depth comparable to the distance from the source bipole. At each observation point the measured components of the electric field are added vectorially to determine the direction and magnitude of the electric field vector at the observation point. Each component of the electric

field at an observation point is measured using a pair of electrodes separated by a distance ranging from 10 meters to 100 meters. The larger separations are used at the greater distances from the source bipole, where the electric field is low. Signal levels as small as 10 to 20 microvolts are measured with an accuracy of ± 5%.

With a knowledge of the electric current put into the ground at the source bipole, and the direction and magnitude of the measured electric field vector at the observation site, the data obtained in a dipole mapping survey can be converted to values of apparent resistivity or of apparent conductance for the purpose of presentation and interpretation.

The vector sum of the measured components of the electric field at the observation point is given by:

$$E = \frac{\rho I}{2R1} \left[1 + \left(\frac{R1}{R2}\right)^4 - 2\left(\frac{R1}{R2}\right)^2 \cos d\right]^{1/2} \qquad (1)$$

where R1, R2, and d are defined by the geometry of the source-receiver configuration, I is the known total current flow at the source and ρ is apparent resistivity. The magnitude of the total electric field, E, is obtained from the vector sum of the field components, E_1 and E_2, measured at the observation point, where

$$E_1 = \frac{\rho I}{2R_1 2}$$

and

$$E_2 = \frac{-\rho I}{2R_2 2}$$

Inversion of equation (1) yields apparent resistivity, ρ, under the assumption of spherical symmetry in current flow for a uniform earth.

For many applications of the bipole mapping method, the distance from the source to an observation point is greater than the depth to crystalline rocks of the basement complex. The basement complex is generally composed of rocks of high electrical resistivity. Such rocks effectively prevent current from penetrating deeper into the earth. For those situations where a relatively conductive sedimentary section overlies rocks in the basement complex of relatively high resistivity, it is inappropriate to assume a spherical symmetry of current flow. Instead, a more meaningful way to present field results is through the use of a formula based on the assumption of cylindrical spreading of current through a thin conductive plate. For a current, I, at the source, the vector sum of the two measured electric field components is given by:

$$E = \frac{1}{2\pi S R_1}\left[1 + \left(\frac{R1}{R2}\right)^2 - 2\left(\frac{R1}{R2}\right)\cos D\right]^{1/2}$$

where S is defined as the conductance of the plate, and is the ratio of the thickness, h, of the plate, to its resistivity, ρ.

It is important to note that the apparent values computed for resistivity or conductance are equal to the actual values for a real earth only when the structure of the earth is as simple as that assumed for the derivation of the above formulae. Where

lateral changes in resistivity are present, the computed values of apparent resistivity and apparent conductance may be quite unlike the values actually existing in the ground. Therefore, it is necessary to evaluate the significance of the computed values of apparent resistivity or apparent conductance in order to interpret properly the cause of apparent resistivity patterns which depart from those expected on the basis of simple geometry.

One approach to the interpretation of the field data is to compute resistivity or conductance maps for various simple resistivity distributions for which calculations are possible. Such models include a sequence of horizontal layers, and vertical planes separating regions of different resistivities. Results of computations of apparent resistivity and conductance using such models are given by Keller et al., (1975), and Furgerson and Keller (1975).

Examination of bipole-dipole data reveals areas of apparent low resistivity that are not found for all source locations. Such false anomalies commonly occur along the boundary between an area of low resistivity and an area of high resistivity. In order to distinguish between false anomalies arising from the relative positions of the source with respect to resistivity contrasts, coverage of a suspected anomalous area is obtained with current

illumination from several bipole source locations. If the anomaly persists when an area is illuminated from several separate sources, it is probably a real anomaly.

Another approach to minimize the effect of source location and avoid false anomalies is the "rotating-field quadripole method", or more briefly, the "quadripole mapping method". A rotating-field quadripole survey actually consists of two dipole mapping surveys carried out with two bipole sources at the same location, but oriented approximately at right angles to one another. The two source bipoles are energized successively for periods of a few minutes each. Signals from each bipole source are recorded at a receiver site. Thus, apparent resistivity and apparent conductance can be computed either as a function of the direction of the bipole source, or as a function of the direction of the electric field at the receiver. The results of computations using simple models indicate that the most meaningful parameter for the interpretation of the resistivity data is the average of the maximum and minimum values of the apparent resistivity or conductance ellipse. A map of this average minimizes the false anomalies which are present on bipole maps obtained with single coverage.

Figure 10 is a composite apparent resistivity map derived from the data used at the three source locations. The composite map was prepared from maps obtained from three rotating-field

quadripole surveys which are shown in Figures 7, 8, and 9. Resistivity values on each map prepared from a quadripole survey represent the average of the maximum and minimum values of apparent resistivity at each recording location. The composite map is a linear average of the three quadripole maps.

Several resistivity lows are apparent on Figure 10. These are significant resistivity anomalies relative to the regions of high resistivity and are undoubtedly due to the presence of water at depth. With the present data, it is not possible to identify with certainty the cause of the resistivity lows evident on Figure 10 other than to say that they represent significant relative variations in apparent resistivity. The presence of a low southeast of Hot Springs is compatible with a model of deep artesian circulation of meteoric ground water. Further resistivity soundings should be made to determine the nature and depth of the source of the resistivity low. The resistivity lows might be a manifestation of slow downward percolation of ground water to a southeastward-dipping fault plane, followed by a relatively rapid upward movement of water along the fault plane and cross faults cutting the northwestern limb of the Warm Springs anticline.

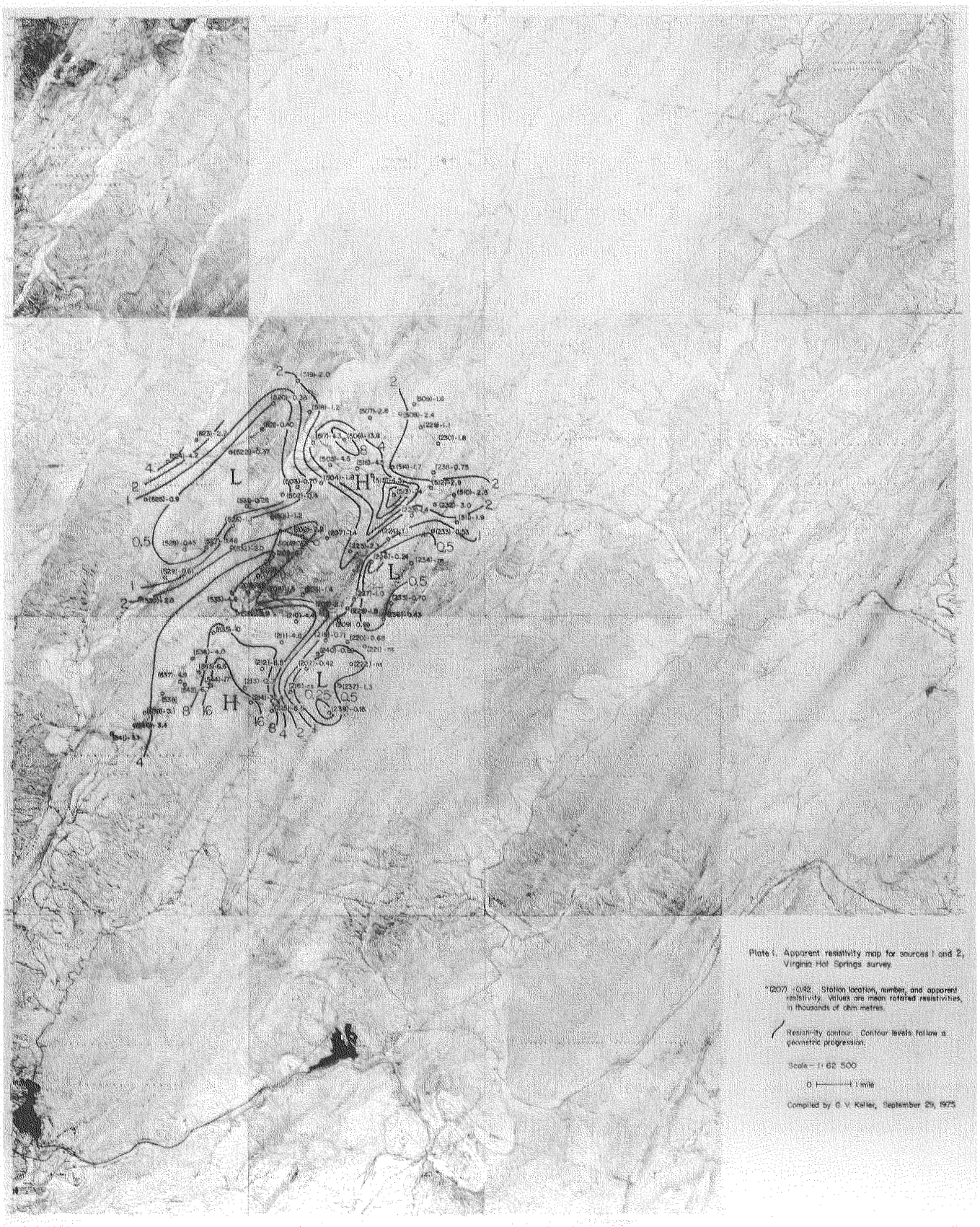

Figure 7. Apparent resistivity map for bipole sources 1 and 2.

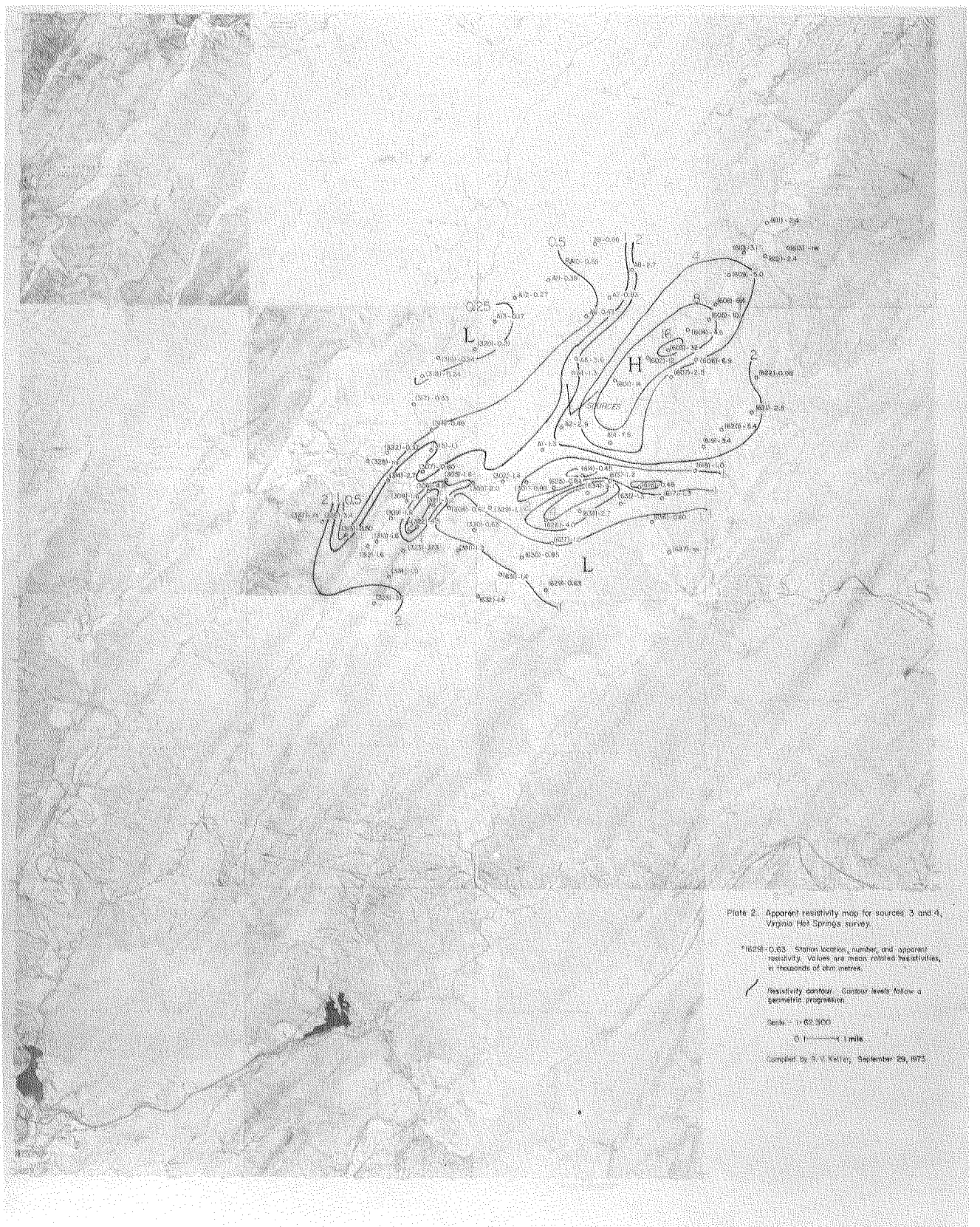

Figure 8. Apparent resistivity map for bipole sources 3 and 4.

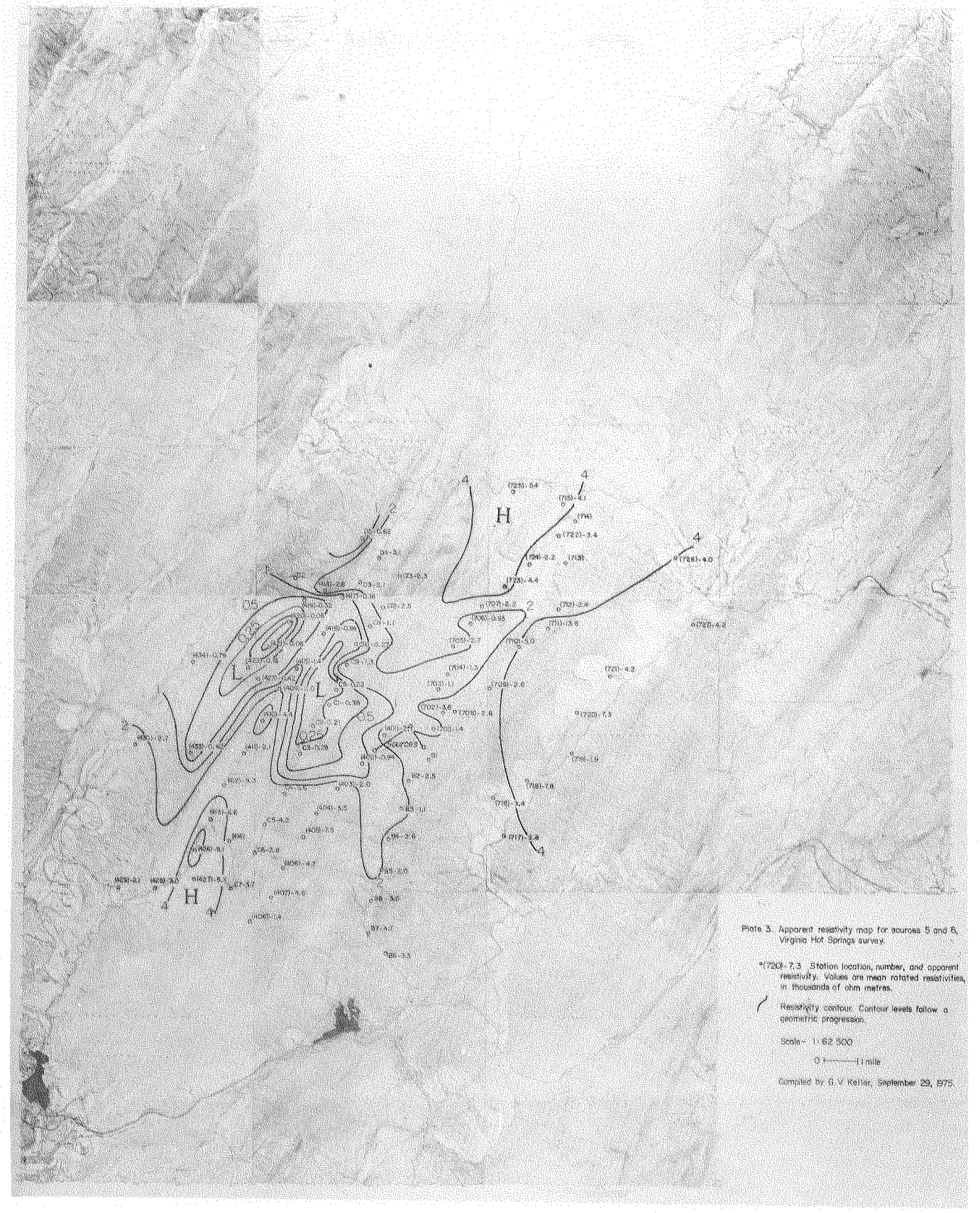

Figure 9. Apparent resistivity map for bipole sources 5 and 6.

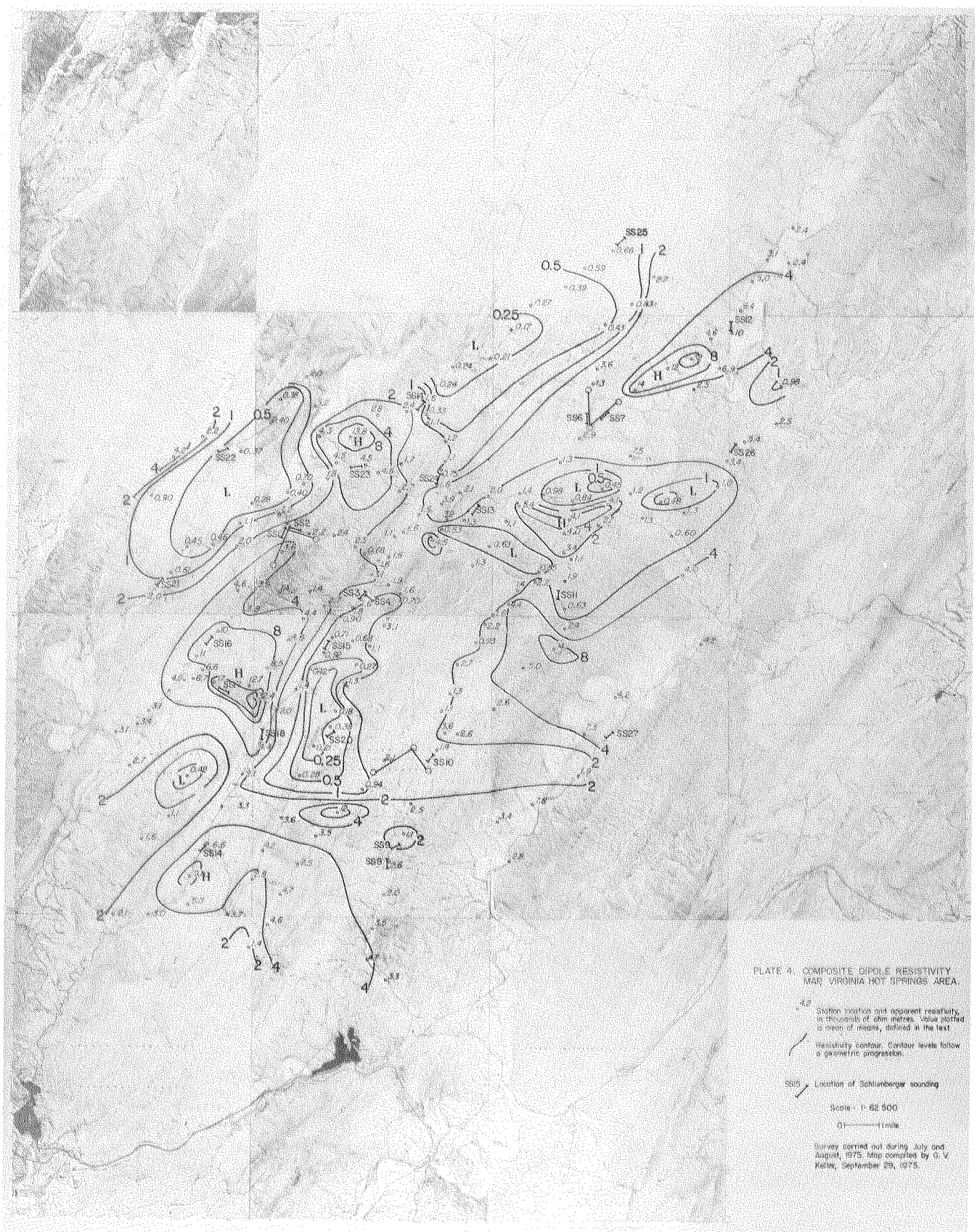

Figure 10. Composite resistivity map derived from the data shown on Figures 7, 8, and 9.

Geothermal Gradient and Heat Flow From Existing Holes in Bath County

We have obtained a reliable heat flow value of 1.23 ± 0.20 μcal/cm^2-sec from four holes at Back Creek at 38°13'N. Lat. 79°48'45"W. Long., about 25 km north of Hot Springs, Va. The temperature and gradient profiles are shown in Figure 11. The geothermal gradients over the parts of the holes not affected by moving ground water are approximately 14°C/km. The holes were drilled by others as part of a dam site investigation, and penetrate sandstones and shales of Devonian age.

We have also determined the heat flow at Hot Springs, Va. from a well drilled by the Homestead Corporation to a depth of about 230 meters. The temperature and gradient profiles are shown in Figure 12. The well penetrated limestone of Middle Ordovician age. No core was obtained from the hole; however, several specimens of limestone were collected from surface outcrops near the hole and thermal conductivity values were determined. The heat flow is 7.6 μcal/cm^2-sec. The geothermal gradient is approximately 100°C/km. This high gradient is probably not representative of the regional geothermal gradient because of the increase in the gradient at the bottom of the hole which appears to be in or probably close to a zone of ground-water circulation. The temperature at the bottom of the hole is approximately 32°C (90°F).

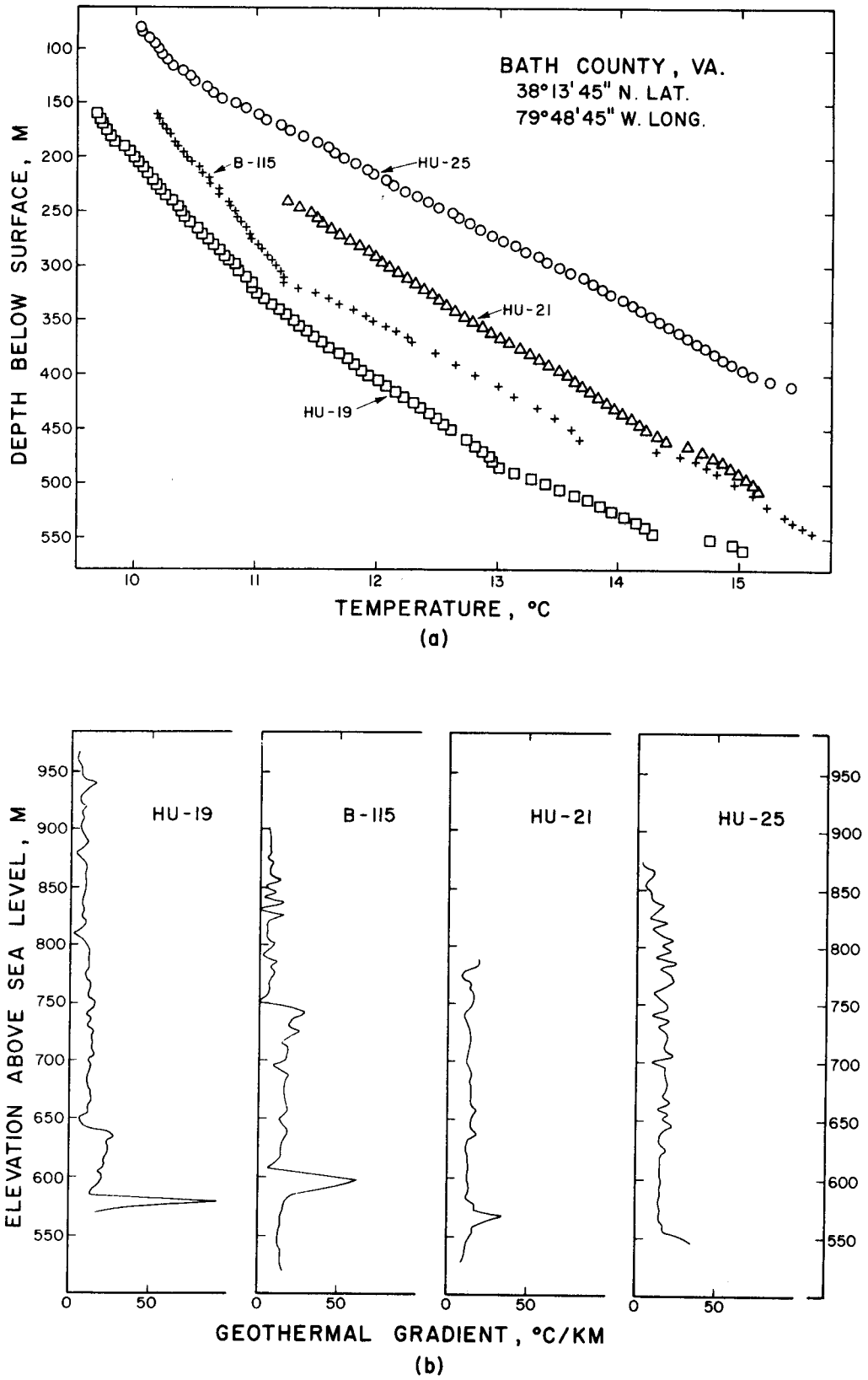

Figure 11. Temperature and geothermal gradients for the Back Creek holes, Bath County, Virginia.

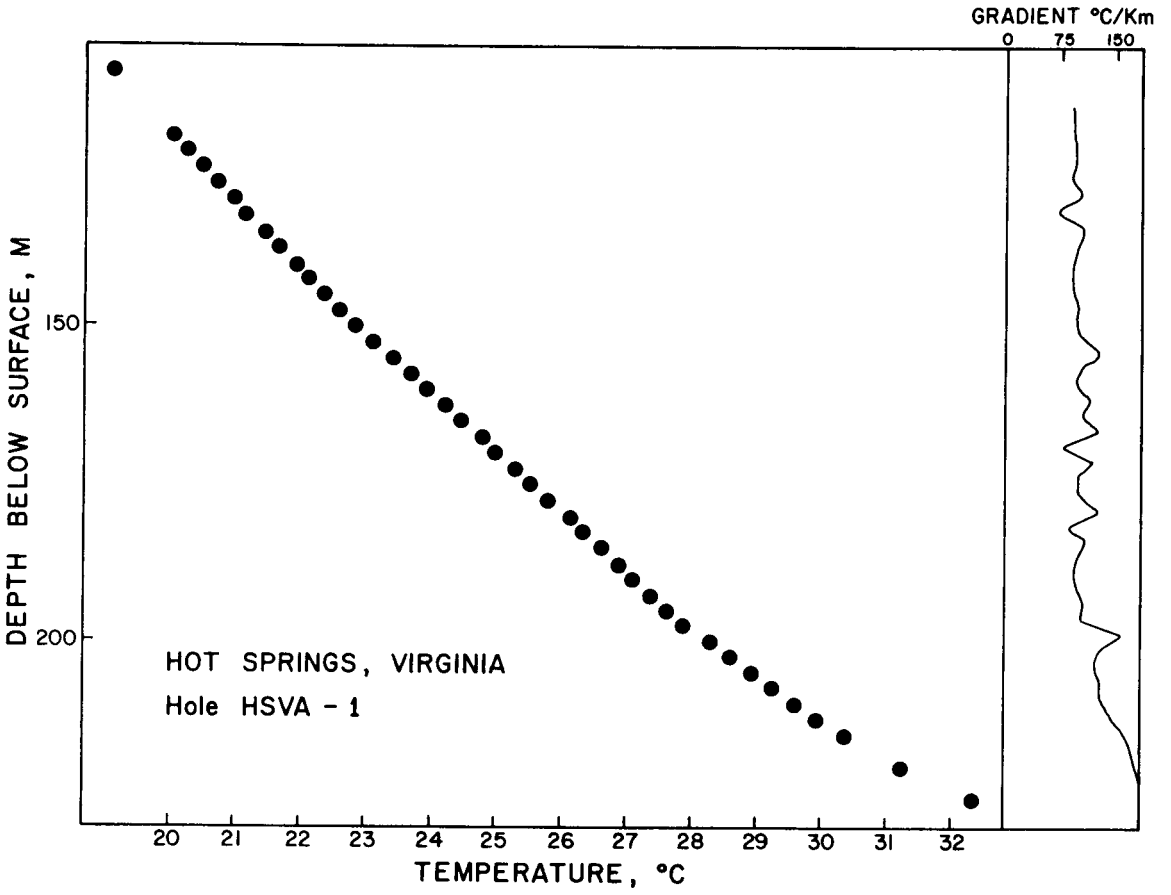

Figure 12. Temperature and geothermal gradient in the well on the Homestead at Hot Springs, Virginia.

Drilling Site in the Warm Springs Anticline

One hole approximately 305 m in depth was drilled in the Warm Springs anticline (Figure 2) specifically for the purpose of obtaining a reliable heat flow determination. Drilling began on December 16, 1975 and was completed on January 10, 1976.

Several factors entered into the selection of the drill site:

(1) The transverse faults that cut the northwest limb of the Warm Springs anticline (Figure 2) are not considered to be of regional tectonic significance; they are interpreted as extension fractures in a rigid, essentially vertical plate of quartzite. Such cross faults are common in anticlinal folds particularly where the anticlinal axis plunges (DeSitter, 1956, p. 206-211). While not of regional significance, they do appear to be important in controlling the locations of the warmest springs. The hottest springs are located next to the cross-faults and the faults may therefore provide the vertical permeability for the ascending warm water. Drilling sites near cross faults were avoided because convection in such zones might prevent the determination of a representative geothermal gradient.

(2) From the work of Reeves (1939) and from our own field work, most of the hot and warm springs appear to issue from limestones of Middle Ordovician age. The limestones unconformably overlie the Knox Dolomite of Early Ordovician age. It is generally accepted that limestone develops solution porosity and permeability at a considerably faster rate than dolomite. If bedding plane permeability is

preferentially developed in the Middle Ordovician limestones, then drilling in or above this part of the stratigraphic section should be avoided. The selected drilling site begins in the Knox Dolomite of Early Ordovician age and which lies stratigraphically beneath the limestone section. The outcrops of Knox Dolomite at the Bowen farm are the oldest rocks exposed in the Warm Springs anticline. Rocks as old or older are exposed at only one other locality on Figure 2 at Bolar, approximately 20 km to the north in the core of another anticline.

(3) The electrical resistivity survey showed the drill site to be an area of relatively high resistivity (Figure 10) and therefore hopefully free of significant subsurface water circulation.

The temperature profile and gradient for the drilled hole are shown in Figure 13. The hole was logged on three separate occasions. Repeated temperature measurements on February 10, 1976 and March 3, 1976 were in excellent agreement, indicating that the hole had reached thermal equilibrium. The gradient over most of the upper part of the hole is disturbed by ground-water circulation; however, the lower 50 meters of the hole appear to be undisturbed and the gradient there of 9.28 ± 0.046°C/km is believed to be a reliable equilibrium gradient in the Knox Dolomite. Thermal conductivity was determined on core from the hole. Values are given in Table 2. The mean and standard deviation of thermal conductivity of the Knox Dolomite based on 35 values is 12.4 ± 0.21 mcal/cm -sec-°C. The product of the gradient and thermal conductivity is 1.15 ± 0.02 μcal/cm^2-sec. This is believed to

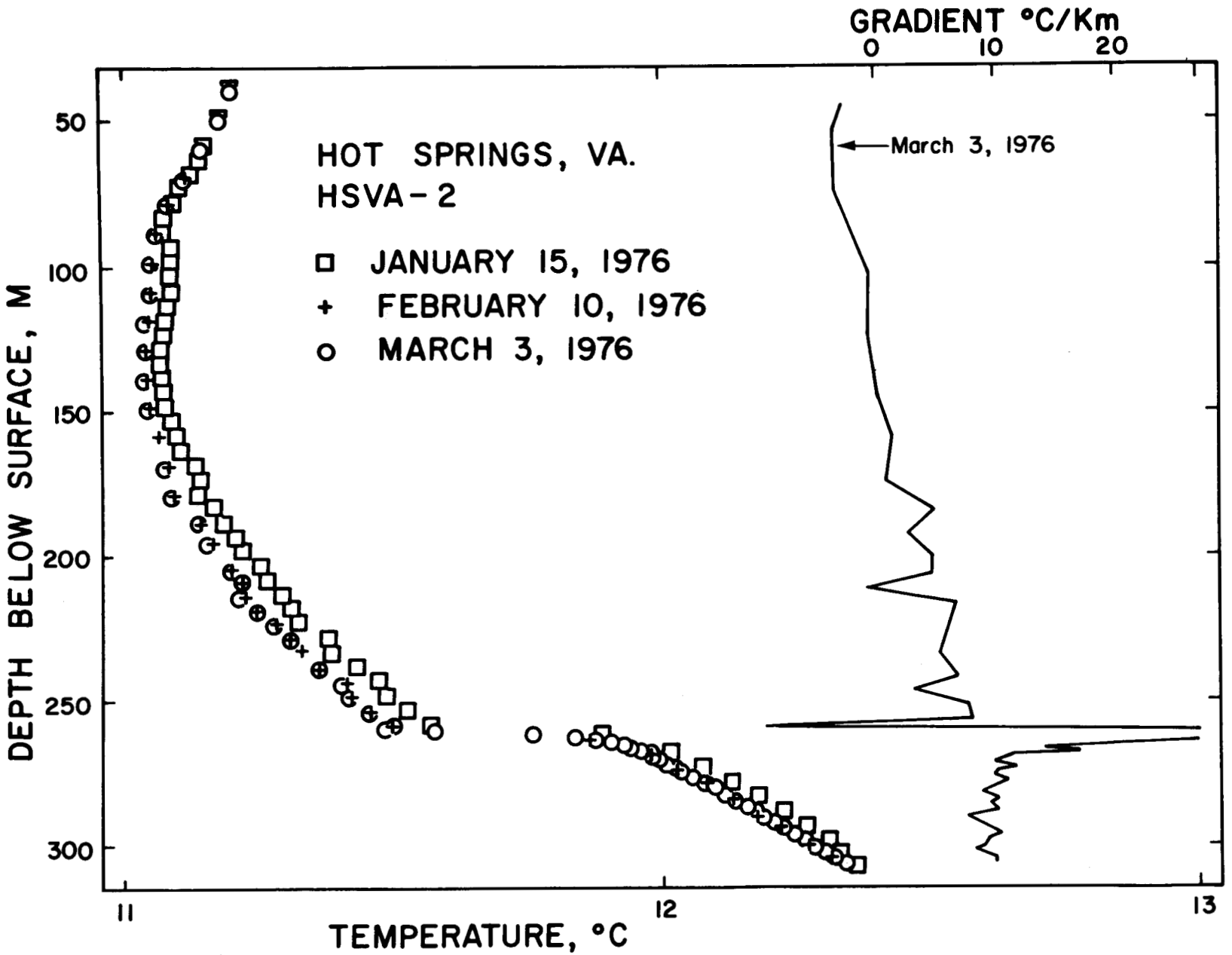

Figure 13. Non-equilibrium (Jan. 15, 1976) and equilibrium (Feb. 10 and Mar. 3, 1976) temperatures in the hole drilled on the Bowen Farm. See Figures 2 and 6 for hole location.

be a reliable regional heat flow value for the area in the vicinity of the Warm Springs anticline. The value of heat flow does not differ significantly from the value of 1.2 $\pm$ 0.1$_0$ found to the north at Back Creek.

Sample #	Depth, m	Thermal Conductivity mcal/cm-sec-°C 1" Samples	Thermal Conductivity mcal/cm-sec-°C 2" Samples	Percent Difference
887	270.4	12.86	12.67	-1.5%
892	271.9	13.12	13.16	+0.3%
897	273.4	10.29	11.04	+7 %
901	274.6	12.57	13.07	+4 %
907	276.5	11.92	12.07	+1 %
911	277.7	10.62	10.81	+2 %
914	278.6	9.81	10.58	+8 %
919	280.1	12.26	12.29	+0.2%
927	282.6	14.20	14.50	+2 %
934	284.7	12.88	13.13	+2 %
941	288.8	12.43	12.25	-1.5%
949	289.3	13.93	13.39	-4 %
959	292.3	12.37	12.36	0 %
968	295.0	12.82	10.05	-22 %
979	298.4	13.52	14.05	-4 %
985	300.2	13.58	13.26	-2 %
990	301.8		14.53	
1000*	304.8	11.66*	11.49	-1.5%
Average (all samples)		12.40 $\pm$ 0.30	12.48 $\pm$0.31	+0.65%
Average (omitting samples 914 and 1000)		12.62 $\pm$0.28	12.66 $\pm$0.32	

*epoxied

Table 2. Thermal conductivity values for Knox Dolomite from hole HSVA-2. Mean and standard error of 35 samples above is 12.44 $\pm$ 0.21 mcal/cm-sec-°c

Temperature Increase from Radiogenic Sources

Jaeger (1964) gives the temperature away from a buried cooling non-radioactive spherical pluton as:

$$T(r,t) = \frac{T_o}{2} \left[\text{erf}\left((r/a + 1)/2\,(\kappa t/a^2)^{1/2}\right)\right.$$
$$-\text{erf}\left((r/a - 1)/2\,(\kappa t/a^2)^{1/2}\right)$$
$$\left.-\exp\left(-(r/a + 1)^2/4\,(\kappa t/a^2)\right)\right]$$

where r = the distance from the center of the pluton, a = radius of pluton, κ = thermal diffusivity of intruded rock, t = time since intrusion, T_o = original temperature of intrusion. For values of T_o = 1200 °C, t = 47 m.y., κ = 0.01 cm^2/sec, and a = 5.0 km there is essentially no influence remaining from the original temperature of the intrusion (Perry, 1975).

An increase in temperature due to radioactive disintegration of uranium and thorium in a radiogenic source can be significant. Estimates of the heat generated can be obtained by a solution from Carslaw and Jaeger (1959) for a continuous spherical surface source. Their solution for a spherical surface source is

$$T(r,t) = \frac{q}{8\pi\kappa rr'}\left\{2(\kappa t/\pi)^{1/2}\left[e^{-(r-r')^2/4\kappa t} - e^{-(r+r')^2/4\kappa t}\right]\right.$$
$$\left. - |r-r'|\ \text{erfc}\left(\frac{r-r'}{2(\kappa t)^{1/2}}\right) + (r+r')\ \text{erfc}\left(\frac{r+r'}{2(\kappa t)^{1/2}}\right)\right\}$$

where

q = heat liberated per unit time divided by the density and specific heat of the material

r' = radius of the spherical source

κ = thermal diffusivity

A more general approach to modelling anomalies from buried heat-producing sources is obtained by summing contributions from arbitrary distributions of point sources and using image theory. The temperature,

v, at a distance, r, from a continuous point source of heat is given by Carslaw and Jaeger (1959, p. 261):

$$v = \frac{q}{4\pi\kappa r} \quad \text{erfc} \quad \frac{r}{\sqrt{4\kappa t}}$$

where t = time since existence of the point source, and q is the quantity of heat instantaneously generated at t = 0. The two approaches to modelling spherical intrusions gave identical results.

Results of the above equations indicate that for the same values of k and κ used previously, a time of 47 m.y., a pluton with a radius of 5 km with its top at a depth of 4.8 km (at the base of the sedimentary section) and with heat production of 10 to 30 HGU, the temperature at depth can be raised significantly, thus requiring shallower circulation. For example, for 10 HGU the temperature at a depth of 3 km is raised approximately 3°C, and for 20 HGU it is raised approximately 6°C. Values for a larger pluton are given in Table 3.

TEMPERATURE INCREASE (^{o}C) FROM RADIOGENIC HEAT PRODUCTION

Radius of pluton, km	Depth to top of pluton, km	Heat generation, HGU (10^{-13}cal/cm^{3}-sec)	Temperature increase, 2 km	Temperature increase, 3 km
5	4.8	10	2	3
5	4.8	20	4	6
5	4.8	30	6	9
15	4.8	10	13	19
15	4.8	20	25	39
15	4.8	30	38	58

Table 3. Temperature increase from a radiogenic source with a spherical distribution of heat-producing elements.

Relationship of the 38th Parallel Fracture Zone to Resistivity Anomalies

From the data now available, it cannot be stated unambiguously that the 38th parallel fracture zone has any manifestation in the study area; however, the resistivity data suggest several east-west trending anomalies as shown on Figure 10. Since this trend is certainly not representative of structural trends in the area, but is representative of the trend of the approximately east-west 38th parallel fracture zone, there may be a causal relationship between the fracture zone and the east-west resistivity lows. Figure 3 shows the location of the Warm Springs anticline with respect to the 38th parallel fracture zone. It is noteworthy that the igneous intrusions of Eocene age are directly in line with the projection of the 38th parallel fracture zone. Further deep resistivity studies will help to define the extent of east-west resistivity anomalies to the north in the vicinity of the exposed intrusive rocks of Eocene age, and to the east and west to determine if resistivity anomalies are characteristically found along the projection of the 38th parallel fracture zone.

Conclusions

Studies made to date by V.P.I. & S.U. do not support the suggestion of a still-cooling pluton (Dennison and Johnson, 1971) as the source of heat of the warm springs in the Warm Springs anticline. This was, however, an attractive hypothesis because of the proximity of the 38th parallel fracture zone, the regional Bonguer gravity anomaly described by Dennison and Johnson, and the exposed alkalic igneous rocks to the north in Highland County. The heat flow values we have obtained appear to be representative of normal heat flow. The possibility still remains, however, that cool alkalic plutonic rocks buried at depth are contributing sufficient radiogenic heat to raise subsurface temperatures by a few degrees Centigrade. As shown by the data of Table 3, a buried spherical pluton of reasonable size and heat generation could easily increase the gradient by a few C/km. If deep circulation of meteoric water in sedimentary rocks is the correct model to explain the origin of the thermal springs, then the addition of radiogenic heat from buried plutonic sources would permit circulation to shallower depths than would otherwise be required. As yet, we have no compelling evidence to suggest that such plutonic rocks are present at depth. It should be noted that Diment et al. (1972, Fig.3) predicted heat flow values of less than 0.8 HFU for this general area; their predictions were necessarily based on only a few available heat flow values. If their contours are assumed to be approximately correct, however, then the heat flow values we obtained at Back Creek and in the warm springs anticline are indeed significantly above regional values, and a value of 1.2 HFU would be quite appropriate

for a source of radiogenic heat from buried plutonic rocks. We do not yet have enough data to confirm the regional low postulated by Diment et al.

At the present time the model favored to explain the origin of the warm springs is as follows. Meteoric water percolates slowly downward through topographically high exposures southeast of the Warm Springs anticline in the vicinity of the relatively low resistivity anomalies (see Figures 4 and 10). At depth, say about 3 km, the descending water encounters one or more thrust faults dipping gently southeastward and passing beneath the Warm Springs anticline. No direct evidence for the thrust faults is available; however, extensive thrust faulting dipping gently to the southeast is known from seismic data in nearby areas (Snelson, 1972). Water is assumed to rise relatively rapidly along cross-faults which cut the northwest limb of the Warm Springs anticline and intersect one or more of the gently-dipping thrust faults at depth. The cross-faults are believed to play an important part in the hydrology and origin of the warm springs. Probably the most likely location to encounter warm or hot water in the Warm Springs anticline is by drilling into the transverse fracture zones. Detailed structural mapping in the vicinity of these cross-faults is planned for the summer of 1976 under ERDA Contract No. E-(40-1)-5103.

The warm springs certainly constitute a geothermal resource for low temperature application such as space heating. A study is presently underway by the Homestead, Inc. to investigate the feasibility of using 300 gpm of warm water (30 °C) for non-electric applications in the immediate area (personal communication, Ray Rogers, Chief Engineer for The Homestead, Inc.)

Acknowledgements

Mr. J. R. T. Bowen, Route 2, Hot Springs, Va., gave permission to have a 305-meter hole drilled on his property for the purpose of obtaining a heat flow value.

The cooperation and assistance of Mr. Ray Rogers, Chief Engineer of the Homestead, Inc., was also very much appreciated. The permission granted by the Homestead, Inc. to carry out studies on their land was essential to the success of this study.

Dr. C. G. Tillman spent several days in the field and made critical identifications of key stratigraphic units.

The electrical resistivity survey was done under the supervision of Dr. G. V. Keller of the Colorado School of Mines, with the assistance of Mr. R. A. Crewdson. Most of the reconnaissance geologic mapping was done by Dr. C. E. Sears with the assistance of Mr. L. N. Ford.

References

Bollinger, G. A., and M.C. Gilbert, 1974, A reconnaissance microearthquake survey of the Hot Springs area, Va., Bull. Seism. Soc. Amer., v. 64, p. 1715-1720.

Carslaw, H. S. and J. C. Jaeger, 1959, Conduction of Heat in Solids, Oxford University Press, 510pp.

De Sitter, L. U., 1956, Structural Geology, McGraw Hill, 552 pp.

Dennison, J. M. and R. W. Johnson, 1971, Tertiary intrusions and associated phenomena near the thirty-eighth paralled fracture zone in Virginia and West Virginia, Bull. Geol. Soc. Amer., v. 82, p. 501-507.

Diment, W. H., T. C. Urban, and F. A. Revetta, Some geophysical anomalies in the eastern United States, in The Nature of the Solid Earth, edited by E. C. Robertson, 544-572, McGraw-Hill, New York, 1972.

Fullagar, P. D. and M. L. Bottino, 1969, Tertiary felsite intrusions in the Valley and Ridge province, Virginia, Bull. Geol. Soc. Amer., v. 80, p. 1853-1858.

Furgerson, R.B., and G.V. Keller, 1974, Computed dipole resistivity effects for an earth model with vertical and lateral contrasts in resistivity, Off. Naval Res. Rep. of Investigations, Colorado School of Mines.

Hall, S.T., 1975, Mineralogy, chemistry and petrogenesis of some hypabyssal intrusions, Highland County, Virginia (thesis), Virginia Polytechnic Institute and State University.

Heyl, A. V., M. R. Brock, J. L. Jolly, and C.E. Wells, 1965, Explosive igneous activity along an Illinois-Kentucky mineral districts, U.S.G.S. Bull. 1202-8.

Jaeger, J. C., 1964, Thermal effects of intrusions, Rev. of Geophys., 2, 443.

Keller, G. V., R. Furgerson, C. Y. Lee, Harthill, J. J. Jacobson, 1975, The dipole mapping method, Geophysics, v. 40, no. 3, p. 451-472.

Perry, L. D., 1975, New heat flow values from Virginia, M.S. thesis in Geophysics, Virginia Polytechnic Institute and State University, Blacksburg, Virginia, 46 pp.

Reeves, F., 1932, Thermal Springs of Virginia, Bull. 36, Virginia Geological Survey.

Rogers, W. B., 1884, On the connection of thermal springs in Virginia with anticlinal axes and faults, Assoc. Am. Geologists and Naturalists, Report of 1st, 2nd, and 3rd meetings, p. 328-330, 1840-1842. A reprint: Geology of the Virginias, p. 577-597, New York.

Snelson, S., 1972, Subsurface data bearing on the tectonic style of the Valley and Ridge province (abstract), Am. Assoc. Pet. Geol., Eastern Sec. Ann. Mtg., Columbus, Ohio, Program of Abstracts, p. 15.

Snyder, F.G. and P. E. Gerdemann, 1965, Explosive igneous activity along an Illinois-Missouri-Kansas axis, Amer. J. Sci., v. 263, p. 465-493.

Sweeting, M. M., 1972, Karst Landforms, Macmillan, New York, 362 pp. See especially Chapter 3, The Solution of Limestones.

Watson, T. L., 1924, Thermal springs of the southeast Atlantic States, Journ. Geology, v. 32, no. 5.

Zartman, R. E., M. R. Brock, A. V. Heyl, and H. H. Thomas, 1967, K-Ar and R6-Sr ages of some alkalic intrusive rocks from central and eastern United States, Amer. Jour. Sci., v. 265, p. 848-870.

Personnel of Project

Dr. John K. Costain	Principal Investigator Professor of Geophysics Department of Geological Sciences Virginia Polytechnic Institute and State University Blacksburg, Virginia 24061
Dr. George V. Keller	Professor of Geophysics Department of Geophysics Colorado School of Mines Golden, Colorado
Robert A. Crewdson	Department of Geophysics Colorado School of Mines Golden, Colorado
Dr. C. E. Sears	Associate Professor of Geology Department of Geological Sciences Virginia Polytechnic Institute and State University Blacksburg, Virginia 24061
Field Assistants:	L. N. Ford J. Ligon L. Perry R. Hart

A P P E N D I X

Report of Investigations

January 20, 1976

ELECTRICAL RESISTIVITY SURVEY OF THE VIRGINIA HOT SPRINGS AREA, BATH COUNTY, VIRGINIA

George V. Keller and Robert A. Crewdson

ELECTRICAL RESISTIVITY SURVEY OF THE VIRGINIA HOT SPRINGS AREA, BATH COUNTY, VIRGINIA

Introduction

An investigation of the possible geothermal potential in the Virginia Hot Springs area of west central Virginia is being carried out by the Department of Geological Sciences, Virginia Polytechnic Institute and State University, with support from the Energy Research and Development Administration. As part of this investigation, an electrical resistivity survey of an area of approximately 500 square miles in Bath county and adjacent parts of Allegheny county has been carried out. This survey was done using deep investigation techniques being developed at the Colorado School of Mines specifically for use in geothermal exploration.

Over the last few years, the measurement of electrical resistivity has become one of the principal geophysical methods used in exploration for geothermal resources. This use is based on the fact that the resistivity of rock is strongly temperature dependent. For example, the resistivity of a water-bearing rock will change by about 1.5 percent per degree C. change in temperature. This amount of temperature dependence is enough to cause a nearly three-fold reduction in resistivity if the temperature of a water-bearing rock is raised from 20° C. to 100° C.

Because ground water at any significant depth beneath the earth's surface is under sufficient hydrostatic pressure to prevent boiling, water may exist in the liquid state at temperatures far above the atmospheric boiling point. Geothermal systems now being produced commercially at places such as Wairaki, New Zealand, and Cerro Prieto, Mexico, contain pore water in place at temperatures ranging from 220° C. to 350° C. When pressure is applied to prevent boiling of water, the electrical resistivity of a rock will continue to decrease with increasing temperature, even above 100° C., and will reach a minimum value at temperatures in the vicinity of 325° C. The relationship between resistivity and temperature for a water-bearing rock is shown graphically in Figure 1. The maximum decrease in resistivity caused by change in temperature alone is approximately by a factor of seven.

Under normal circumstances, hot ground water will take more salt into solution than cold ground water. In geothermal systems this tendency for anomalously large amounts of solids to dissolve in the water also contributes to the reduction in the electrical resistivity of the rock. It has been demonstrated in every known geothermal field that the electrical resistivity of the reservoir is lower than that in the surrounding rock by a factor of 5 to 10. Moreover, the resistivity of the heated rock is usually quite low in an absolute sense, with most geothermal reservoirs having resistivities below 10 ohm-meters. As a consequence, the measurement of electrical resistivity is an effect means of prospecting for geothermal systems.

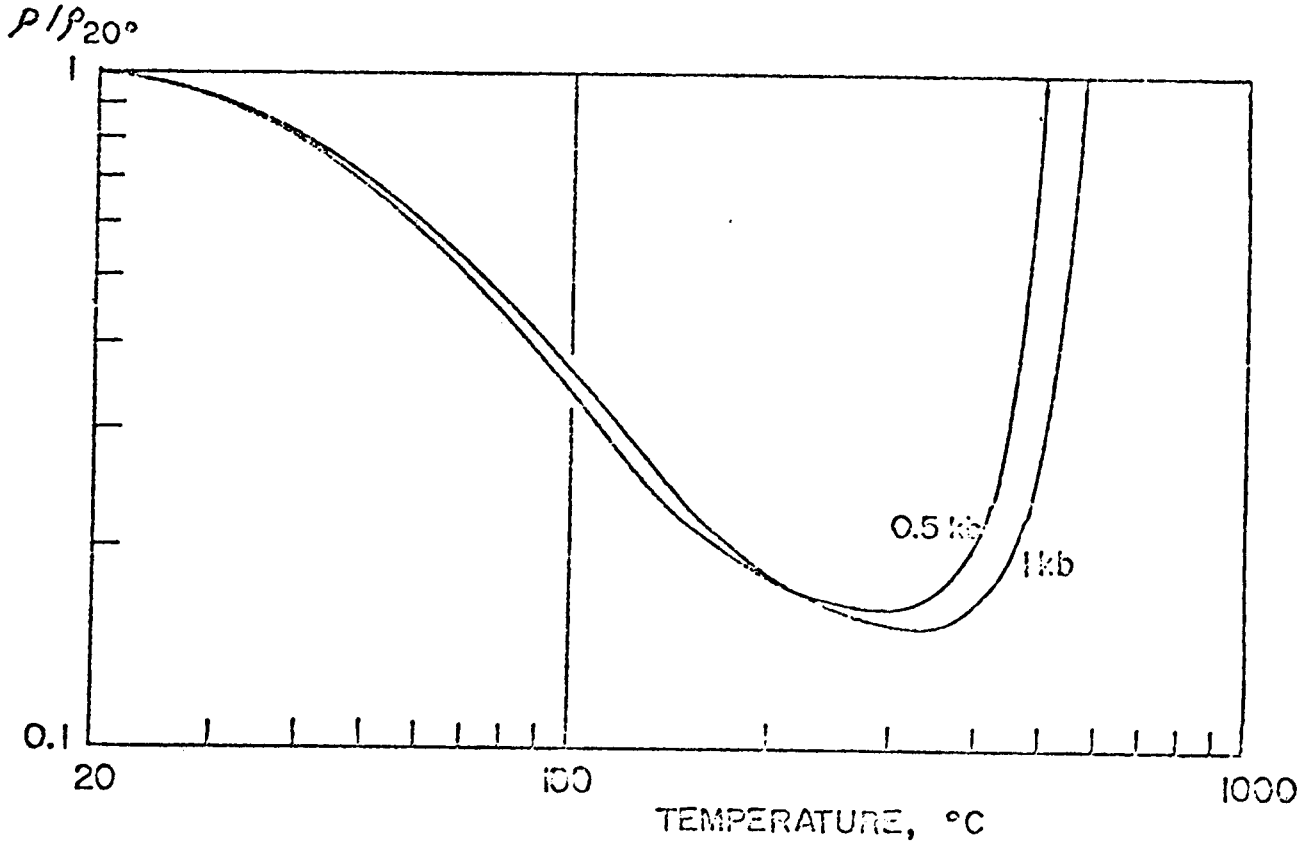

Figure 1. Variation in the resistivity of an acqueous solution of sodium chloride, under pressure. The resistivity of a rock containing the same solution will behave similarly.

Because known geothermal systems are of considerable size and extend to depths of several kilometers, the development of electrical surveying methods for the purpose of geothermal prospecting has been concentrated on extending the penetration capabilities of standard methods, and on organizing surveys in ways in which large areas can be covered at relatively low costs. One of several basically new resistivity techniques that is being used in geothermal exploration is the dipole mapping method, sometimes also called the roving dipole method. This method, which is described in more detail in a later section of this report, was used as the basic exploration technique for the study of electrical resistivity in Bath County.

In dipole mapping, a long grounded wire is used to drive an intense current into the ground. The flow pattern of this current is then mapped by exploring around the grounded wire source with pairs of electrodes to determine the electric field intensity caused by the current. The flow pattern of the current will be determined by the electrical structure of the earth, so mapping the current flow pattern provides a means for mapping the electrical structure.

Experience has shown that the dipole method is rapid, and effective in locating the boundaries of areas with low resistivity such as are usually associated with the presence of heated ground water. However, the precision with which the results can be interpreted is considerably poorer than in the case of several of the more conventional electrical surveying methods. Therefore, dipole mapping should be considered as serving primarily in the

reconnaisance phase of an exploration program. More definitive electrical sounding methods should be used in a followup program to study areas of anomalously low resistivity in detail. Only very limited followup surveying was done in the Virginia Hot Springs area as part of the work described in this report.

The Dipole Mapping Survey

The area surveyed around the Virginia Hot Springs comprised approximately 500 square miles, covering most of Bath county, and a small part of Allegheny county, to the south. (See Figure 2 for locations). A total of six dipole sources was used, sited in pairs at three locations, as shown in Figure 3. These particular source locations were selected to provide overlapping coverage of the valley extending from Warm Springs in the north, through Hot Springs, to Healing Springs in the south from all six sources. Each source cable was 1 to 2 kilometers in length, grounded usually at metal road culverts to obtain good contact with the ground. The primary power source was a gasoline-engine motor-generator set capable of providing 27 KVA at 235-volt 60-Hz output. Normally, the output of this generator is stepped up to 660 or 880 volts to drive a maximum amount of current into the ground, but for the Virginia Hot Springs survey, the 235-volt output was used directly for reasons of safety. Because of this low voltage, currents of only 5 to 12 amperes were driven into the ground.

Before being supplied to the grounded cable, power from the generator supply was rectified to form direct current. This current was alternately switched to cause current to flow first one way

Figure 2. Sketch-map of Bath county, Virginia showing locations of electrical surveys.

and then the other in the cable connecting the power supply to the electrode contacts. The period of reversal of the current flow was 28 seconds, so that the frequencies contained in the waveform of the current would be sufficiently low to avoid problems with electromagnetic attenuation of the current field and lack of penetration because of skin-depth limitations. The current waveform was asymmetrical, with the duration of current flow in one direction being about 40 percent greater than the duration in the other; this provides a means for assigning a polarity to the voltage detected at the receiving sites. The amplitude of the current steps was recorded with an analog recorder and monitored visually with an indicating meter.

The current field from a source dipole was mapped by measuring voltages between electrode pairs at many points around a source bipole. Because the direction of current flow at a measurement point is quite unpredictable, the total voltage drop must be determined by making measurements with two electrode pairs oriented roughly at right angles to one another and adding these voltages vectorially. The electric field is then assumed to be the ratio of voltage drop to the separation between the measuring electrodes. Measurements were made with electrode separations of 30 meters. The receiver consisted of a sensitive DC amplifier and filter, with a battery-operated analog recorder. The deflection of the trace on the stripchart as current flow in the ground reversed was taken as the signal. The least signal that could be detected with the recording system was approximately 5 microvolts.

The primary data recorded for the six bipole sources are reproduced in Appendix C, as copies of the field notes.

The measurement of two components of the electric field at each receiver site from each of two sources provides a redundant set of data for computing apparent resistivity. As a result, there is an infinite variety of ways to define apparent resistivity for a dipole mapping survey. We have made use of two relatively standard definitions of apparent resistivity in processing the measurements made from the six bipole sources; in one, we have treated the six sources independently, while in the other, resistivities have been computed by combining measurements made from pairs of sources.

The usual definition of apparent resistivity is based on the behavior of current flow and voltage in a completely uniform earth. In this special case, current spreads out from a single electrode with spherical symmetry. The electric field on the surface of the earth at a distance R_1 from the electrode is:

$$E_1 = \frac{\rho I}{2\pi R_1^2}$$

where I is the current and ρ is the resistivity of the earth. When the return current to the second electrode is considered, a second component of electric field caused by this return current must be added to E_1:

$$E_2 = \frac{-\rho I}{2\pi R_2^2}$$

where R_2 is the distance from the observation point to the second current electrode.

The electric fields E_1 and E_2 are vector quantities, and so, must be added vectorially. The vector sum is:

$$E_T = \frac{\rho I}{2\pi R_1^2}\left[1 + \left(\frac{R_1}{R_2}\right)^4 - 2\left(\frac{R_1}{R_2}\right)^2 \cos D\right]^{\frac{1}{2}}$$

Solution of this equation for ρ provides the means for computing apparent resistivity under the assumption of spherical symmetry in current flow. Values for apparent resistivity computed with this expression are given in Appendix A.

When resistivity surveys are conducted on the scale necessary in exploration for geothermal systems, a somewhat different basic model of the earth may be more appropriate than a completely uniform model. An alternative definition of apparent resistivity can be obtained by assuming the earth consists of a plate of conductive rock resting on a perfectly insulating substratum. Such a model can be used to characterize the usual sedimentary veneer covering crystalline basement rocks. For current spreading through a plate, the electric field depends on the ratio of plate thickness to resistivity, h/ρ. This quantity is termed the conductance of the plate, and is designated by the symbol, S. The electric field caused by a current I passing through a single electrode on the surface of a plate is:

$$E_1 = \frac{I}{2\pi S R_1}$$

where R_1 again is the distance from the first current electrode to the observation point. With the addition of a second electrode to complete the bipole current source, the contribution of a second electric field at the observation point must be considered:

$$E_2 = \frac{-I}{2\pi S R_2}$$

The vector sum of these two electric fields is:

$$E_T = \frac{I}{2\pi S R_1}\left[1 + \left(\frac{R_1}{R_2}\right)^2 - 2\left(\frac{R_1}{R_2}\right) \cos D\right]^{1/2}$$

where, as before, D is the angle formed between the two lines R_1 and R_2. Solution of this expression for S provides a definition for "apparent conductance". Values for apparent conductance are also listed in Appendix A.

It should be stressed that these two ways for convert observed data are not essentially different. The use of apparent conductance is to be preferred in presenting data where there is a strong effect from basement, causing apparent values of resistivity to increase with distance from the source. If such is not the case, results should be presented as values of apparent resistivity. Individual maps showing the locations of the stations along with the values of apparent conductance and apparent resistivity are included in Appendix A. These are not the principal presentation of results and are included for completeness only.

Since the use of dipole mapping has become fairly commonplace in recent years, one significant problem in the use of single dipole sources has been recognized. In an earth with complex electrical structure, regions with high resistivity may divert the current flow in the earth, and cause shadow zones where current does not penetrate. Without current, the electric field is low, and the computed resistivity will be low. This will cause false lows to appear on a contour map of apparent resistivity values measured from a single source. An effective

method for reducing the ambiguity found in single dipole coverage is the use of several dipole sources which illuminate the prospect area with current flowing in different directions. The particular approach to multiple coverage used in the survey in Bath County was that of a "rotating" source bipole. At each of the three source locations, two bipole sources were energized sequentially, with measurements being made at every observation point for each of the two sources. The two bipole sources were oriented roughly at right angles to one another, so that for most observation points, the direction of current flow for each of the two sources was significantly different. The data could be used to compute two resistivity values for an observation point, corresponding to the two directions of current flow. If lateral changes in resistivity near an observation point cause distortion in current flow, then these two values are likely to differ, providing evidence for that distortion.

The use of two bipole sources in this manner permits the computation of apparent resistivity values for any direction of current flow at the observation point. The computation is carried out by adding together the effects of the two sources in varying proportions. This addition is analytically equivalent to the physical rotation of a single source about its midpoint, and so, it is possible to obtain the same results by computations based on two sets of measurements as would be obtained in the field by making many measurements with many source orientations.

In processing, the electric fields observed at a single observation point from the two sources were added together with weights corresponding to rotations of 5° over a range of 180°, or a range adequate to determine the apparent resistivity for current flow in any direction. It can be shown analytically and may be verified experimentally that these resistivity values form an ellipse when plotted as a function of direction. This ellipse can be characterized by a maximum semi-diameter and a minimum semi-diameter, or by an average. Each of these three parameters is listed in Appendix B.

Modelling of simple earth structures has indicated that the parameter most simply related to actual resistivity distributions in the ground is the arithmetic average of the maximum and minimum resistivity values calculated on rotation. For this reason, the primary presentation of results consists of contour maps of this value, presented on Plates I-IV. The first three plates are presentations of the data individually from the three pairs of sources, while Plate IV is a composite of the first three. On Plate IV, where overlapping coverage provides two or three values of average resistivity at an observation point, the value plotted is the average of these averages. No good justification for this averaging can be proposed, and evaluation of Plate IV should be combined with careful consideration of the individual dipole maps.

Schlumberger Soundings

One concern in evaluating the dipole maps described in the preceeding section is that the current may not have penetrated beneath the weathered layer, and that as a consequence, the patterns of apparent resistivity may be determined only by the depth and extent of weathering. This problem is of particular concern in areas where the bedrock has a very high resistivity, such as is the case in Bath County. For example, if the bedrock resistivity is a hundred times greater than the resistivity in the weathered zone, current flow will be confined largely to the more conductive surface layer, and appreciable currents will penetrate the bedrock only at distances equal to 100 times the thickness of the weathered layer. In order to evaluate whether or not such a large contrast in resistivity might exist between the weathered layer and the bedrock, a number of shallow Schlumberger soundings were carried out, at locations indicated on Figure 2. These soundings are shown graphically on Figures 3- .

The Schlumberger sounding method is a standard electrical sounding method in which an array of four electrodes is expanded about its midpoint. The four electrodes are all inline, with the outer two serving as current electrodes, and the inner two, located at the middle of the array, being used to detect the voltage caused by this current. As the array is expanded, the

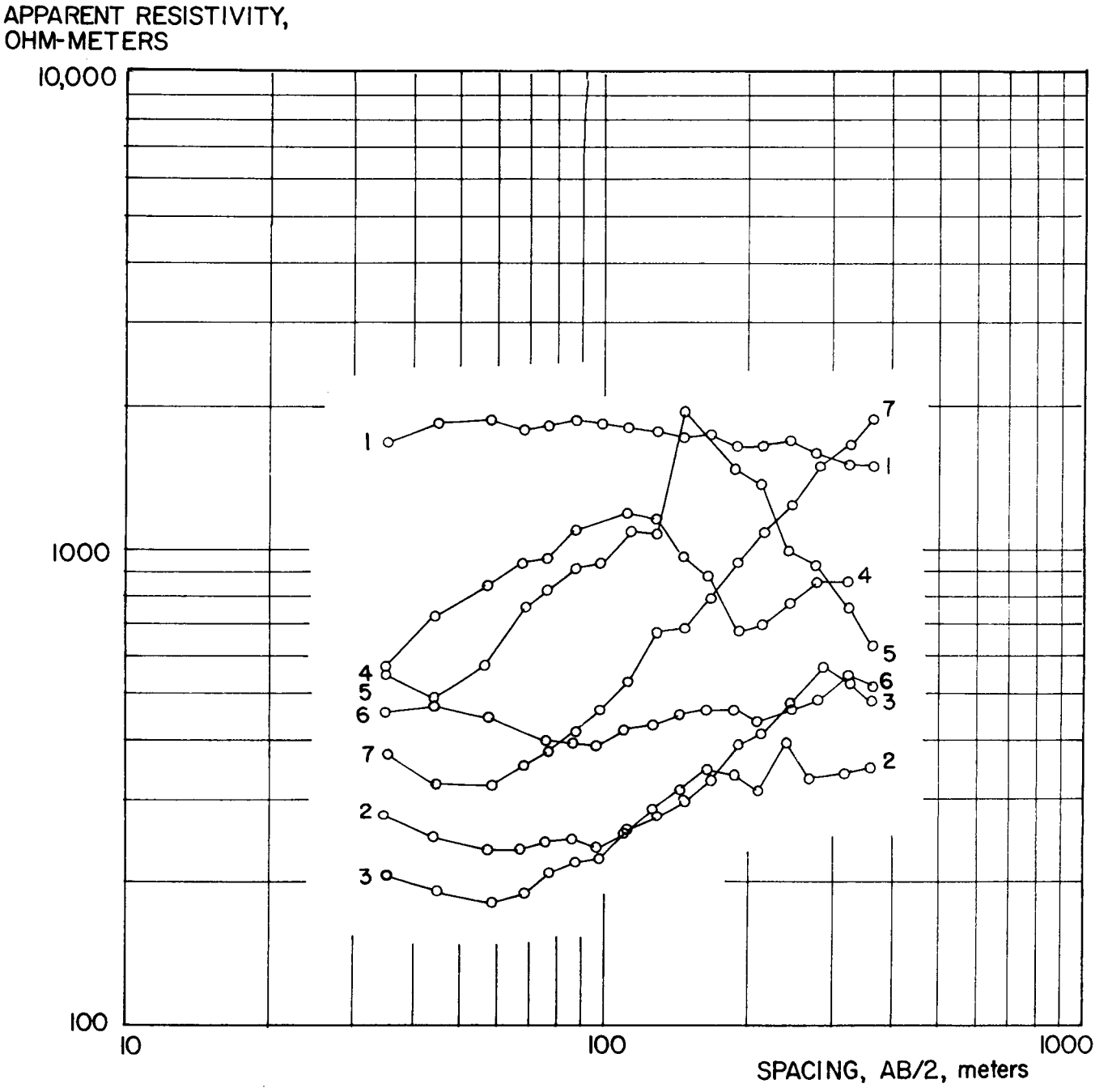

Figure 3. Apparent resistivities measured for Schlumberger soundings 1-7, at locations indicated on Figure 2.

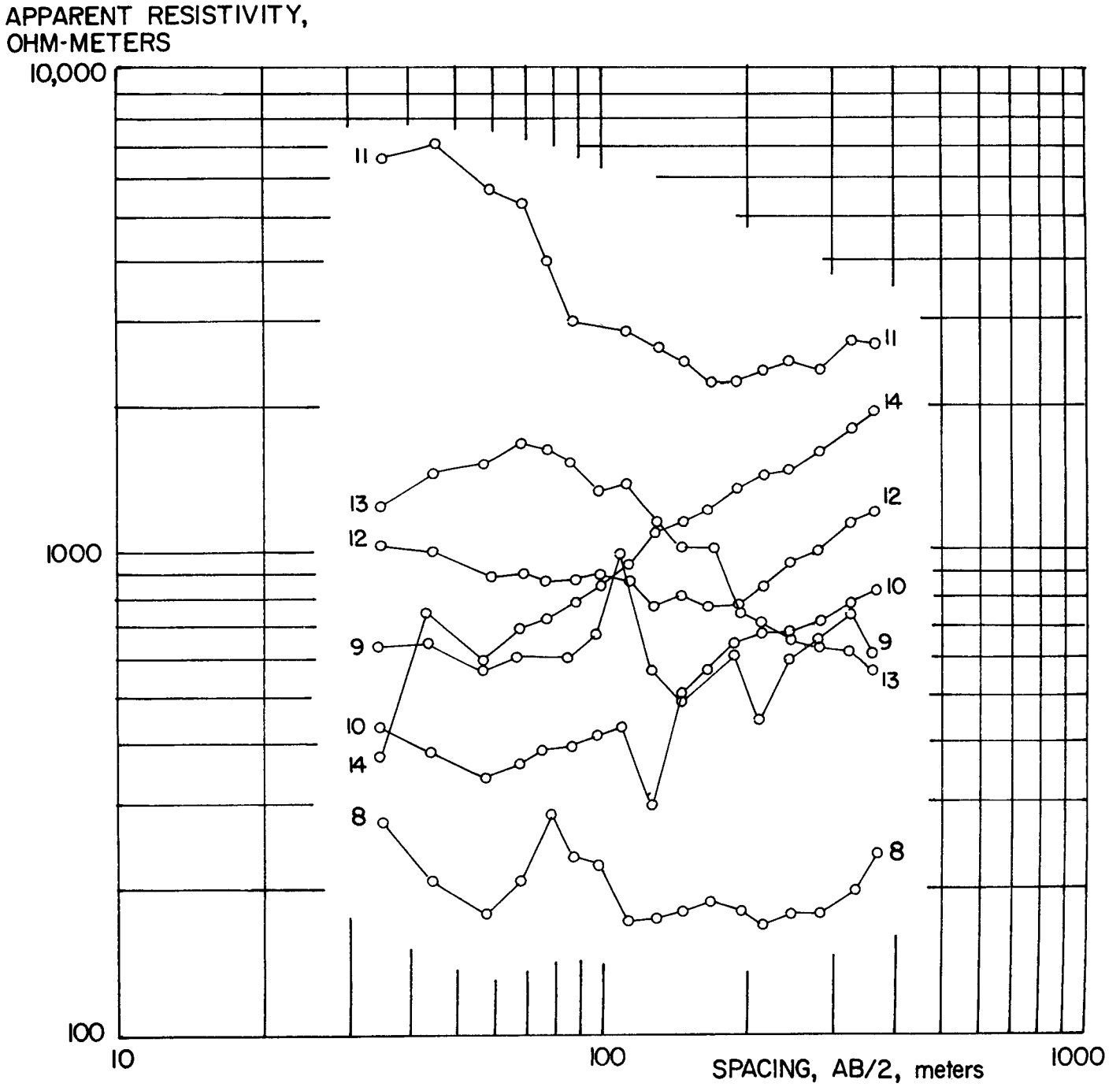

Figure 4. Apparent resistivities measured for Schlumberger soundings 8-14.

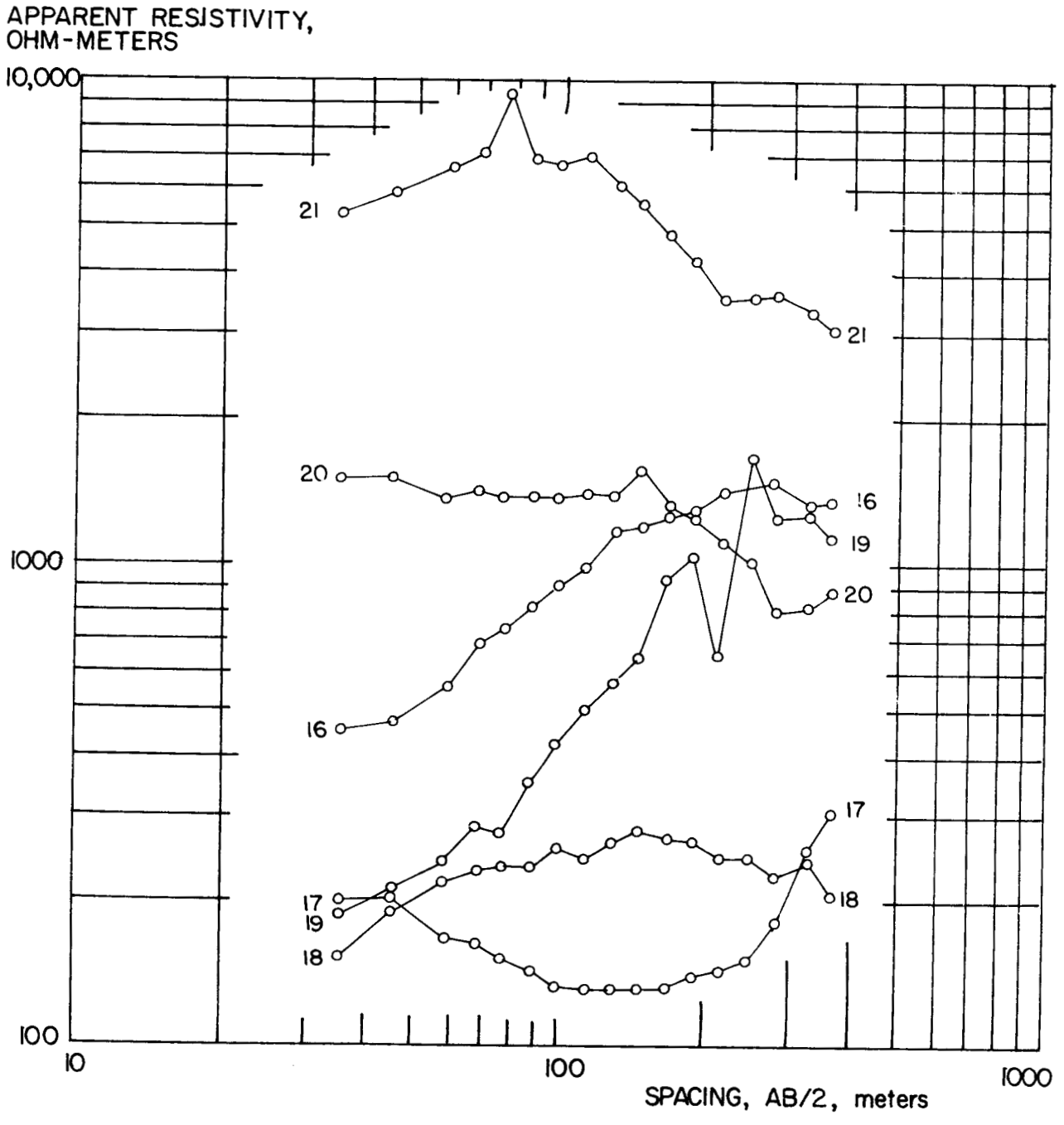

Figure 5. Apparent resistivities measured for Schlumberger soundings 16-21.

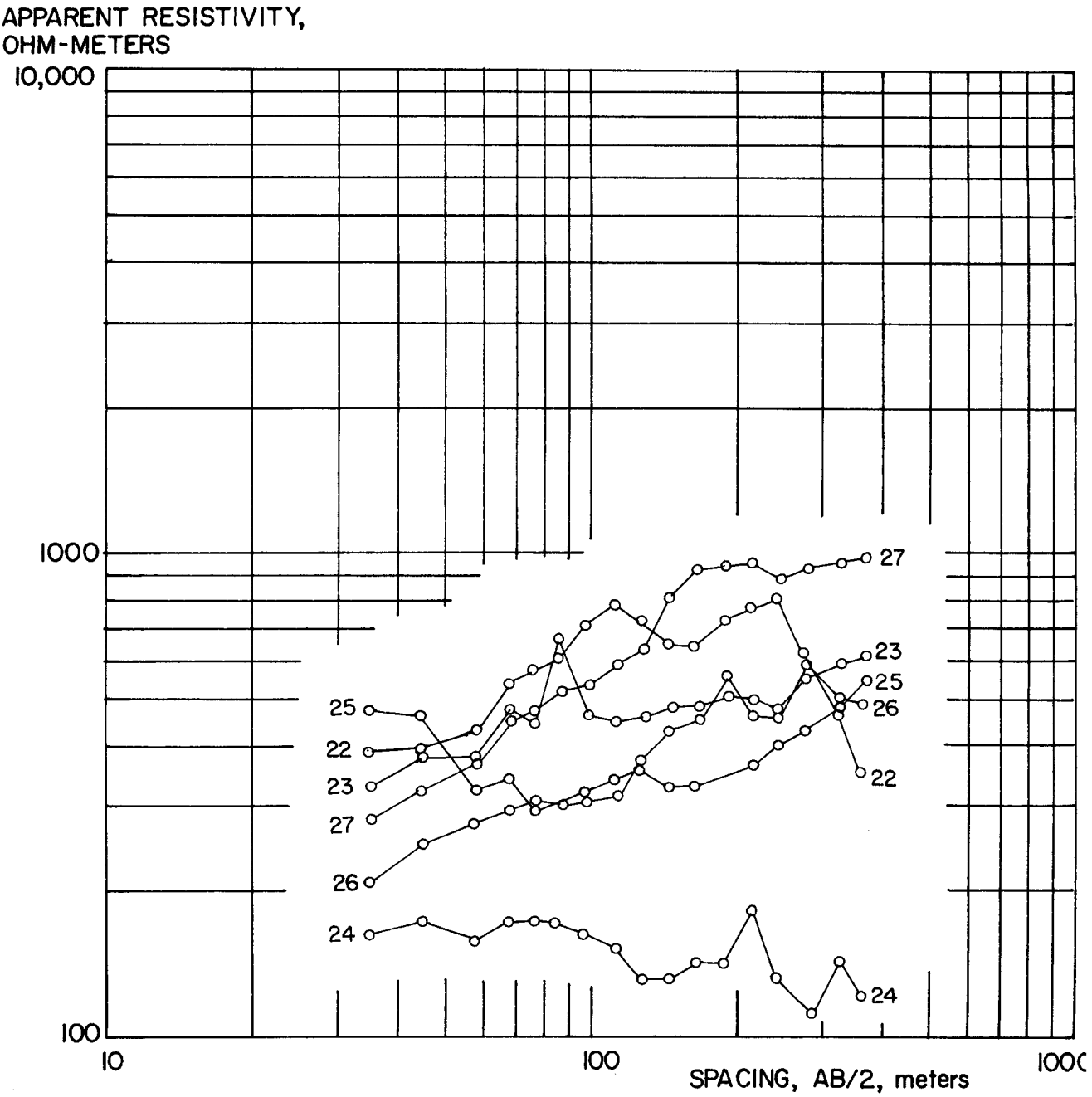

Figure 6. Apparent resistivities measured for Schlumberger soundings 22-27.

apparent resistivity values reflect greater penetration of current into the earth. If the surface layer has a much lower resistivity than the subsurface, characteristically, the apparent resistiviity will increase linearly with spacing (spacing is measured as half the distance between current electrodes in the Schlumberger array).

In the shallow soundings, the spacing factor was increased incrementally from 35 meters to 370 meters, with the larger spacings being great enough to detect the presence of a marked resistivity contrast at depths up to about 200 meters. Examination of the 26 soundings shown in Figures 3-6 indicates that very few of them show a rapid increase in apparent resistivity with spacing. Many show a gradual increase, while a good number show no change or a decrease in apparent resistivity with spacing. It appears that there is no serious problem with current being confined to a near-surface conductive zone.

This may be confirmed to some extent by considering the average behavior of apparent resistivity as a function of spacing. Figure 7 shows an average "sounding curve", obtained by combining all measurements, both Schlumberger and dipole, into a small set of average values. The points to the left in Figure 7, for spacings of 370 meters and less, are averages derived from the Schlumberger soundings; each point is the geometric average of the values obtained at that spacing for the 26 soundings. The values to the right are averages derived from the single dipole calculations. Each point represents the geometric average of 50 to 150 values measured over a small range of distances from a source. The distance used is the distance from an observation point to the nearer end

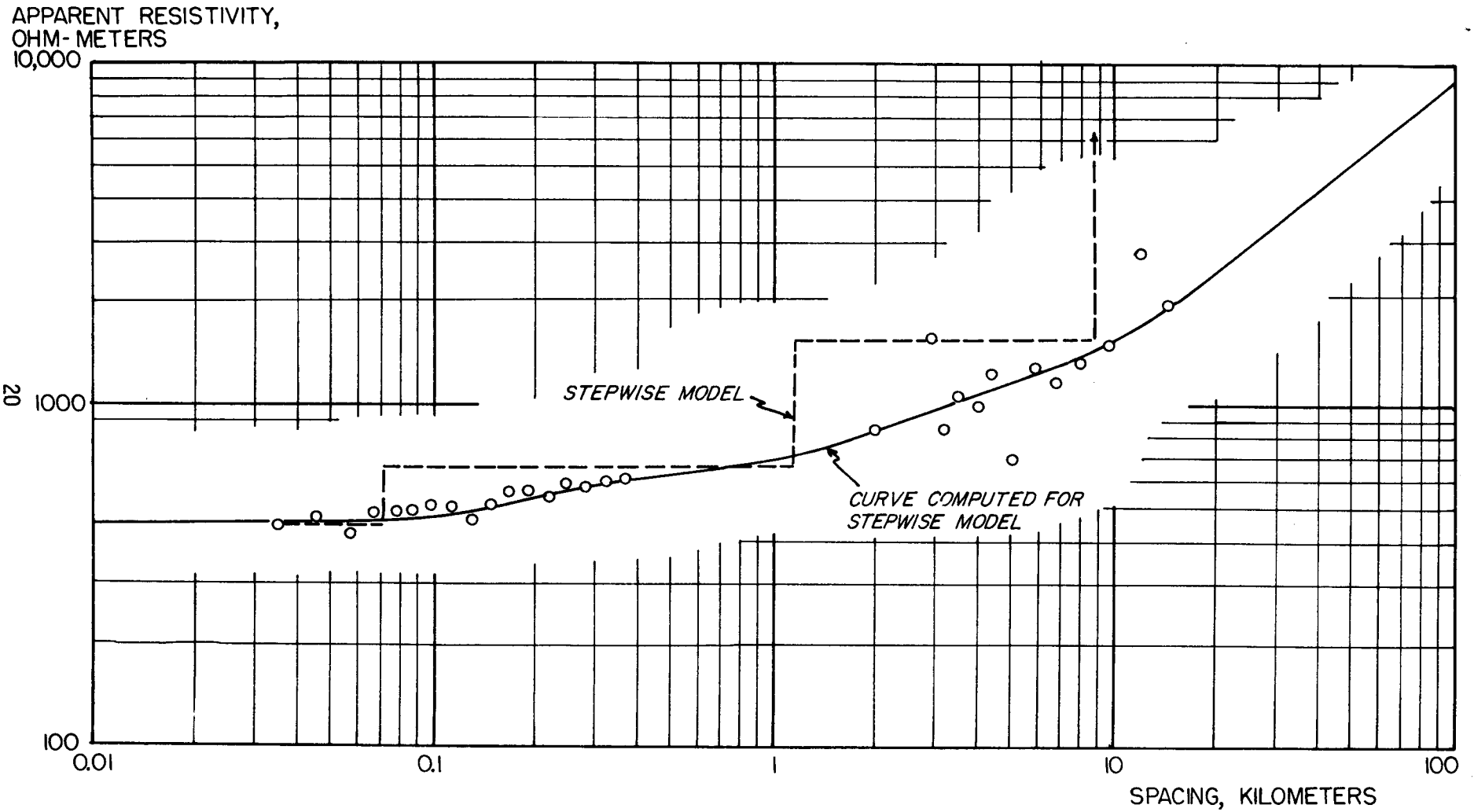

Figure 7. Average resistivities for all Schlumberger and dipole data plotted as an equivalent sounding curve.

of the source bipole.

The equivalent sounding curve in Figure 7 characterizes a section in which the resistivity increases very gradually with depth, up to a depth of 8.8 kilometers. The solid curve which passes through the data was computed for a three-layer-plus-basement stepwise resistivity model. This model suggests that the strongest rate of increase in resistivity occurs at a depth of about 1 kilometer, and that if the change is concentrated at that depth, the contrast in resistivity is about 3;1. These data confirm that there is no strong tendency for the current used in dipole mapping to be confined to a thin, conductive surface layer. For the dipole mapping measurements, it would be expected that the apparent resistivity values represent penetration of singificant amounts of current to depths comparable to the offset distance from the source at which measurements are made.

Dipole-Dipole Pseudosection

In addition to the dipole mapping and Schlumberger soundings, a short dipole-dipole sectioning survey was done along Highway US-220, south of Hot Springs, as indicated on Figure 2. The purpose was to provide detailed information on resistivity variations to a depth of a few hundred meters in areas under consideration as sites for drilling a thermal gradient test hole. In dipole-dipole sectioning, a colinear array of four electrodes is used, but in contrast to the symmetric positioning of electrodes in

the Schlumberger array, in the dipole-dipole array, the two electrodes at one end of the array are used to drive current into the ground, while the two electrodes at the other end of the array are used to measure voltage. In making a set of measurements, the current pair of electrodes is fixed at one location on a traverse, while the measuring pair is moved away from the current pair incrementally along the traverse. As the array is expanded, resistivity is measured to greater depth, but the center of the array also moves laterally along the traverse line. Because of this, in presenting the data, values are plotted on a section at points midway between the current and measuring electrode pairs, at lines dropped at 45° from the centers of the two dipoles (see Figure 8). In the survey along US220, the unit dipole lengths were 100 meters, with separations between dipoles being 100, 200 and 300 meters during incremental expansion.

The data obtained in the dipole-dipole survey are shown contoured as a pseudosection in Figure 8. The individual resistivity values were plotted as described above, and then contoured (in this case, as in all others, resistivity contours were spaced in a logarithmic progression). Such pseudosections commonly give a graphic semi-quantitative picture of resistivity variations both laterally and vertically, and the method is widely used for mineral exploration. The section given in Figure 8 shows very marked changes in apparent resistivity along the traverse. Very high values were measured at the south end of the traverse, just across the county line in Allegheny county. To the north, the

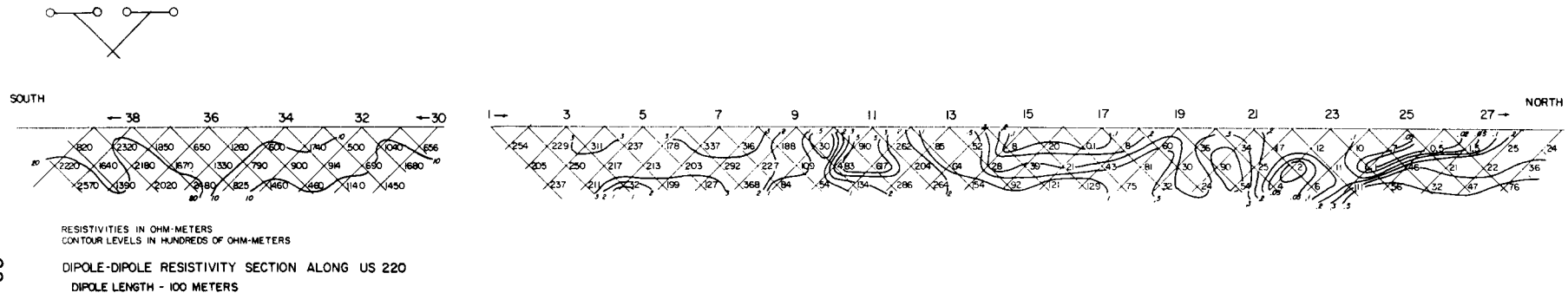

Figure 8. Pseduosection of apparent resistivity values measured with the dipole-dipole array along highway US 220.

resistivities decrease markedly, with values of one ohm-meter being recorded at the south edge of Hot Springs. Unfortunately, cultural effects prevented the traverse from being extended further to the north, where the Hot Springs are present. Some of the very low resistivity values on this traverse may also be a result of cultural effects, but even discarding such values, there is clearly a strong reduction of resistivity in the surface layers in the area between Healing Springs and Hot Springs.

Evaluation of Results

Dipole mapping, the principal surveying method used in this study, is primarily a reconnaisance tool, with the results not being suitable for a highly detailed interpretation. Dipole mapping surveys provide information on the location of areas of anomalously low electrical resistivity which are worthy of further detailed study with other electrical methods, as well as other geophysical and geological methods.

In the case of the dipole mapping survey of Bath county, a major factor to consider in evaluation of the resistivity patterns which were mapped is the possible effect of anisotropy. A model study, described in Appendix D, indicates that anisotropy in the horizontal plane can produce very strong effects. In particular, anisotropy can cause apparent resistivity to decrease across the strike direction of anisotropy, and increase along the strike direction, even though the medium may be uniformly anisotropic. This tendency is evident in many of the apparent resistivity maps presented here; low apparent resistivities are observed to the northwest and southeast of the various sources,

while high resistivities are observed to the southwest and northeast. Careful examination of the individual dipole maps presented in Appendix A indicates that the scale of the linear structures in the survey area is not small enough for the structures to be considered uniformly anisotropic. For example, the maps showing direction of the electric field vectors show that the directions are preferentially oriented along strike in the valleys and across the strike on the ridges. Despite the fact that the structures are too large to be lumped together to form a uniform anisotropic medium, the generalizations about increases or decreases in resistivity along or across strike should still hold. Resistivity lows located along the northwestern edge of the survey area should be viewed with suspicion.

The most striking feature of the dipole resistivity maps is the area of low apparent resistivity between Warm Springs and Healing Springs, and apparently extending to the east beneath Warm Springs Mountain. This low is bounded to the north and to the south by east-west striking bands of moderately low resistivity, which appear to be associated with windgaps and other topographic expressions of east-west striking structural features. This area is structurally high, so one would expect a relatively thin section. The composite sounding shown in Figure 7 indicates that as the section thins by removal of the younger Paleozoic formations, the average resistivity should increase slightly, by factors amounting to 2 or so. The decrease in apparent resistivity must then be explained by some

method. In the anomalous block, resistivities are low by factors ranging from 1.5 to 6(apparent resistivities in this block range from less than 250 ohm-meters up to 1000 ohm-meters, while the average resistivities for the section given in Figure 7 are about 1500 ohm-meters). The lower resistivity in this area could be explained by any of a number of factors, including an increase in average porosity over the section by a factor of 1.2 to 2.5, an increase in average salinity of groundwater over the whole section by a factor of 1.5 to 5, or an increase in temperature over the whole section by 100° to 200° C. There is no surface evidence for highly saline groundwaters, and so, it is likely that the low resistivity is caused by fracture-induced porosity in the section and/or elevation of temperatures.

Recommendations

The results of the reconnaisance electrical survey of Bath County have defined an area of interest for further study, bounded on the west by highway US 220, on the north by an east-west line passing through Warm Springs, and on the south by an east-west line passing through Bald Knob. This region should be studied in more detail to determine what part of the section is responsible for the low apparent resistivities. Among the methods which might be used effectively is the Schlumberger sounding method, carried to spacings of 3 to 5 kilometers. Consideration should be given to the use of other geophysical techniques which may yield information about the structural controls for this anomalous block.

A second recommendation is that reconnaisance dipole mapping surveys be extended to the north of the area already surveyed. The objective would be to locate possible areas of low resistivity associated with similar structural settings along the strike of the geology north of Bath County.

APPENDIX A: Apparent resistivities and apparent conductances computed for each of the six sources.

N. Receiver station identifier number, keyed to the various maps and plates.

X. The x coordinate of an observation point, measured in kilometers east of the common point of a pair of source bipoles.

Y. The y coordinate of an observation point, measured in kilometers north.

ANG. The bearing angle of the electric field vector at a receiver station, computed in degrees clockwise from north.

RES. The apparent resistivity, computed from the magnitude of the electric field vector observed at a receiver station. Ohm-meters.

CON. The apparent conductance, in mhos.

APPENDIX A1; Single-coverage dipole resistivities measured from source 1.

N	X	Y	ANG	RES	CON
201	-0.93	0.42	-47.	3298.4	0.27
202	-1.35	-1.87	-152.	952.5	0.46
203	-1.53	-2.73	-18.	339.5	3.02
204	2.88	0.09	45.	1235.5	1.84
205	0.96	-2.84	17.	202.4	8.93
206	1.00	0.08	-22.	4059.6	0.20
207	2.12	0.37	-172.	1925.7	0.85
208	1.66	-3.53	163.	1443.1	1.81
209	2.43	-4.08	128.	357.8	9.69
210	0.67	-4.13	134.	678.7	3.10
211	-0.03	-5.14	66.	417.1	5.65
212	-0.93	-6.37	100.	294.0	9.80
213	-1.90	-7.18	87.	349.8	9.44
214	-1.56	-7.80	89.	1522.7	2.37
215	-2.62	-8.30	-83.	32838.3	0.12
217	2.99	-6.47	68.	181.3	18.84
218	2.43	-4.08	-142.	357.8	9.69
219	2.01	-5.03	136.	721.2	4.67
220	2.96	-5.17	131.	396.5	12.64
223	6.11	0.57	109.	1085.6	4.29
224	5.01	-0.45	127.	725.9	5.85
225	3.09	-0.84	106.	3063.4	0.96
226	4.14	-1.52	144.	265.4	16.03
227	3.33	-3.24	-177.	359.3	11.96
228	2.94	-3.66	158.	809.2	4.86
229	6.52	4.81	-34.	1073.5	4.45
230	7.28	4.02	154..	1806.8	2.84
231	7.12	2.72	144.	717.5	6.97
232	7.11	1.11	-153.	552.3	9.55
233	7.10	-0.08	146.	342.5	16.77
235	5.12	-3.35	144.	1076.2	5.66
236	4.61	-4.19	140.	646.0	8.93
237	2.67	-7.25	112.	427.5	11.02
238	2.13	-8.41	57.	112.6	43.61
239	2.01	-5.03	72.	320.7	10.51
240	1.87	-6.64	52.	141.0	27.95

APPENDIX A1: Continued

N	X	Y	ANG	RES	CON
501	-0.54	-0.52	133.	501.6	1.66
502	0.30	1.63	82.	566.3	1.97
503	2.56	2.03	123.	508.9	2.68
504	1.83	2.18	63.	2461.7	0.72
505	2.28	3.13	-83.	8241.3	0.28
506	2.83	4.18	-12.	2322.4	1.25
507	4.27	5.20	-85.	1971.8	1.59
508	5.51	5.31	-171.	1014.6	4.31
509	6.35	5.70	-128.	1414.9	3.45
510	7.97	1.67	-122.	340.2	16.99
511	8.18	0.34	128.	771.6	8.32
512	6.95	1.91	45.	593.3	8.37
513	5.22	1.68	151.	24795.7	0.15
514	5.23	2.95	-134.	3125.9	1.20
515	4.18	2.55	-143.	7528.8	0.41
516	3.54	2.86	-43.	8518.2	0.33
517	1.43	4.16	-24.	2126.6	1.20
518	1.41	5.63	125.	634.5	5.17
519	2.85	6.95	74.	571.0	6.93
520	-0.25	5.97	86.	335.6	10.54
521	-0.79	4.78	82.	314.3	9.59
522	-2.17	3.54	103.	355.7	8.47
523	-3.58	4.23	132.	2720.6	1.69
524	-5.23	3.33	88.	10453.3	0.55
525	-6.33	1.52	156.	1089.7	5.91
526	-2.23	0.29	108.	1347.8	1.73
527	-3.53	-0.72	-152.	556.0	4.89
528	-4.68	-0.79	-156.	370.5	9.72
529	-5.43	-1.98	-172.	595.6	6.10
530	-6.71	-3.00	138.	303.5	14.38
531	-1.67	1.19	145.	323.3	5.62
532	-2.36	-0.75	-162.	628.1	2.85
533	-2.36	-2.78	41.	196.7	7.25
534	-2.12	-3.77	-39.	336.4	4.96
535	-3.32	-4.67	62.	3426.9	0.72
536	-4.30	-5.84	45.	5613.9	0.58
537	-4.86	-6.85	-124.	207.8	18.44
538	-3.55	-7.40	-166.	334.2	12.85
539	-6.52	-8.23	-163.	104.2	47.64
540	-7.24	-8.89	-26.	158.2	34.12
541	-8.12	-9.22	-118.	293.1	20.36
542	-4.44	-6.87	-22.	1903.4	1.94
543	0.28	7.55	-14.	3158.8	1.37
544	-3.55	-7.02	-27.	444.5	7.84

APPENDIX A2: Single-coverage dipole resistivities measured from source 2

N	X	Y	ANG	RES	CON
201	-0.83	0.42	-54.	1306.5	0.50
202	-1.05	-1.87	56.	********	0.00
203	-1.53	-2.73	33.	6535.7	2.45
204	2.88	0.09	89.	1044.4	1.20
205	0.96	-2.84	-124.	2334.8	0.86
206	1.30	0.08	-43.	321.4	1.99
207	2.12	0.37	-100.	369.0	2.80
208	1.66	-3.53	157.	5937.7	0.39
209	2.43	-4.08	-132.	1437.9	1.81
210	0.67	-4.13	159.	10772.0	0.33
211	-0.03	-5.14	137.	8743.5	0.52
212	-0.93	-6.37	124.	17050.6	0.36
213	-1.90	-7.18	-41.	27939.6	0.26
214	-1.56	-7.80	98.	58874.6	0.13
215	-2.62	-8.30	-83.	68482.8	0.11
217	7.99	-6.47	131.	656.1	7.59
218	2.43	-4.08	-133.	1439.4	1.81
219	2.21	-5.03	71.	744.4	4.56
220	2.96	-5.17	144.	1117.9	3.00
223	6.11	0.57	-84.	1576.6	1.97
224	5.21	-3.45	-143.	1017.8	2.25
225	3.89	-0.84	-125.	544.8	2.27
226	4.14	-1.52	-99.	215.5	8.58
227	3.33	-3.24	-125.	225.5	9.59
228	2.94	-3.66	-147.	1388.2	1.69
229	6.52	4.81	99.	1099.4	5.57
230	7.28	4.02	-9.	2291.4	2.46
231	7.12	2.72	-16.	490.4	9.43
232	7.11	1.11	-94.	4456.9	0.85
233	7.10	-2.08	-62.	900.1	3.85
235	5.12	-3.35	-126.	255.5	10.85
236	4.61	-4.19	157.	517.2	5.73
237	2.67	-7.25	156.	2168.2	2.28
238	2.13	-8.41	-73.	171.5	35.26
239	2.21	-5.03	121.	1510.5	2.24
240	1.67	-6.64	-9.	1631.4	2.89

APPENDIX A2: Continued

N	X	Y	ANG	RES	CON
501	-3.54	-3.52	135.	892.1	0.71
502	3.20	1.63	89.	633.3	2.10
503	3.66	2.03	137.	1038.7	1.94
504	1.83	2.18	69.	3458.6	0.80
505	2.28	3.13	-59.	1344.6	2.82
506	2.83	4.18	-66.	5657.0	0.88
507	4.07	5.20	58.	4592.4	1.35
508	5.51	5.31	19.	4180.7	1.55
509	6.35	5.70	52.	2782.5	2.51
510	7.97	1.67	-68.	6403.5	1.31
511	8.18	0.34	83.	2600.7	1.59
512	6.95	1.91	-21.	3060.5	1.33
513	5.22	1.68	-32.	15285.8	0.21
514	5.23	2.95	41.	2631.9	1.56
515	4.18	2.55	12.	2379.5	1.46
516	3.54	2.86	-16.	2580.7	1.42
517	1.43	4.16	-24.	6038.8	0.71
518	1.41	5.63	137.	2083.9	2.63
519	3.85	6.95	113.	2234.9	2.77
520	-0.25	5.97	103.	551.2	8.63
521	-3.79	4.78	93.	533.2	6.72
522	-2.17	3.54	114.	342.2	7.59
523	-3.88	4.23	147.	3502.3	0.95
524	-5.23	3.33	89.	11409.8	0.30
525	-6.33	1.52	147.	982.1	3.63
526	-2.23	3.29	111.	1121.7	1.24
527	-3.53	-2.72	-143.	845.6	2.66
528	-4.68	-3.79	-148.	816.4	3.52
529	-5.43	-1.98	-161.	927.4	4.00
532	-6.71	-3.00	-146.	2893.1	1.67
531	-1.67	1.19	152.	374.2	3.41
530	-2.36	-0.75	-117.	3079.7	0.54
533	-2.36	-2.78	27.	8746.9	0.35
534	-2.12	-3.77	61.	7424.6	0.55
535	-3.32	-4.67	48.	24545.5	0.21
536	-4.33	-5.84	12.	11312.3	0.58
537	-4.86	-6.85	32.	6385.8	0.91
538	-5.55	-7.40	-25.	137631.6	0.06
539	-6.92	-3.23	32.	6034.7	1.54
540	-7.24	-8.69	-129.	6862.4	1.46
541	-8.12	-9.22	-132.	5378.9	1.96
542	-4.44	-6.87	47.	13239.2	0.75
543	8.28	7.55	34.	6629.4	0.74
544	-3.55	-7.22	95.	7217.1	1.07

APPENDIX A3: Single-coverage dipole resistivities measured from source 3.

N	X	Y	ANG	RES	CON
301	-2.15	-3.15	-117.	1029.2	2.22
302	-3.30	-3.15	-65.	2722.2	0.97
303	-4.74	-3.21	171.	2166.4	1.50
304	-5.87	-4.36	126.	1176.4	3.43
305	-5.98	-3.13	142.	2131.5	1.78
306	-6.71	-3.61	146.	6586.6	0.66
307	-7.17	-2.69	74.	1001.0	4.35
308	-7.89	-4.12	104.	2112.2	2.33
309	-8.65	-4.91	141.	2238.3	2.67
310	-9.39	-6.01	138.	1732.8	3.37
311	-9.43	-7.24	163.	2786.2	2.27
312	-9.91	-6.10	172.	1956.5	3.20
313	-13.95	-5.48	-119.	793.4	9.37
314	-8.32	-2.97	128.	3578.5	1.47
315	-6.76	-1.63	152.	1658.6	2.47
316	-6.73	-0.65	-179.	628.9	6.60
317	-7.59	0.46	97.	232.7	21.21
318	-7.14	1.84	22.	289.9	18.18
319	-6.38	2.64	54.	274.1	19.52
320	-4.60	3.10	114.	250.5	19.33
321	-6.66	-4.26	-69.	7262.3	0.62
322	-7.36	-5.27	-113.	73137.0	0.07
323	-8.08	-6.23	-107.	2658.7	2.37
324	-8.81	-7.69	-98.	1559.5	4.00
325	-9.56	-9.11	-123.	2458.3	2.84
326	-11.39	-5.07	-126.	5291.1	1.39
329	-3.69	-4.41	-144.	1882.9	1.77
330	-4.73	-5.56	-123.	1184.3	3.43
331	-5.51	-6.48	-111.	2398.3	1.95
332	-5.22	-1.80	85.	236.5	22.25
601	2.09	1.63	-138.	145.3	4.86
602	3.57	2.68	-138.	3669.6	0.46
604	5.93	4.01	-95.	258.4	11.39
605	6.54	4.23	-171.	5153.2	0.67
606	5.99	2.65	-86.	4069.1	0.72
607	4.78	1.73	16.	213.3	10.52
608	6.92	5.29	-128.	2973.6	1.31
609	7.54	6.65	-87.	1536.0	2.97
610	5.24	7.66	49.	4828.4	1.07
611	9.42	9.07	-170.	4603.1	1.72
612	9.23	7.45	-6.	732.1	7.48
614	3.58	-2.91	-61.	213.5	10.51
615	1.86	-3.13	72.	749.7	4.42

APPENDIX A3: Continued

N	X	Y	ANG	RES	CON
616	3.23	-3.49	35.	399.3	11.86
617	4.33	-4.24	-167.	2499.4	2.37
618	5.79	-2.98	-8.	630.4	9.10
619	6.32	-1.60	-22.	388.7	12.37
620	7.18	-0.71	67.	3409.5	1.33
621	8.67	0.13	119.	2725.3	1.83
622	8.86	1.86	146.	1828.7	2.54
625	-3.06	-3.48	37.	411.5	5.64
626	-1.26	-5.02	79.	2374.6	1.37
627	-2.92	-6.17	-41.	1078.9	3.72
628	-1.17	-7.15	-134.	268.6	17.09
629	-1.24	-8.46	-62.	1241.7	4.36
630	-2.51	-6.77	-63.	167.6	25.57
631	-3.43	-7.58	-72.	849.7	5.65
632	-4.59	-8.69	-112.	2094.7	2.76
633	0.38	-4.57	32.	931.2	3.54
634	2.77	-3.69	2.	917.3	3.15
635	2.34	-4.26	110.	1214.6	3.61
636	3.79	-5.08	-47.	236.1	26.11
801	-1.42	-1.68	56.	2346.9	2.60
***	-2.49	-2.57	12.	3968.9	2.14
803	-2.12	2.64	85.	146.7	4.86
804	3.19	1.90	15.	570.5	2.60
805	3.27	2.57	-21.	480.4	3.44
806	3.66	4.65	-11.	233.2	11.74
807	1.88	5.59	-38.	312.2	9.56
808	2.92	6.86	-134.	1955.3	1.88
89	3.99	8.04	-95.	813.2	5.95
810	-3.11	7.24	-123.	710.9	6.83
811	-1.25	6.36	3.	390.8	12.75
812	-2.54	5.55	91.	490.7	12.65
813	-3.66	4.45	45.	315.5	16.14
14	1.85	-1.40	31.	2219.5	1.17

APPENDIX A4: Single-coverage dipole resistivities measured from source 4.

N	X	Y	ANG	RES	CON
301	-2.15	-3.15	-160.	837.5	4.17
302	-3.30	-3.15	178.	101.6	44.81
303	-4.74	-3.21	174.	2972.5	1.91
304	-5.87	-4.36	161.	3035.7	2.39
305	-5.98	-3.13	117.	1723.4	3.62
306	-6.91	-3.61	131.	3696.9	1.93
307	-7.17	-2.69	122.	739.3	8.61
308	-7.89	-4.12	103.	1862.7	4.34
309	-8.65	-4.91	125.	1772.4	5.19
310	-9.39	-6.01	124.	2241.8	4.72
311	-9.40	-7.24	137.	2819.6	4.14
312	-9.91	-6.10	147.	1568.7	6.96
313	-12.95	-5.48	91.	428.6	25.21
314	-8.82	-2.97	115.	1496.5	4.95
315	-6.76	-1.63	121.	676.0	7.67
316	-6.73	-0.65	54.	349.1	12.68
317	-7.59	0.46	49.	235.0	18.25
318	-7.14	1.84	49.	94.5	38.33
319	-6.38	2.64	54.	152.9	27.27
320	-4.63	3.10	-4.	117.8	18.17
321	-6.66	-4.26	-67.	2504.9	3.94
322	-7.36	-5.27	-54.	16236.7	7.55
323	-8.28	-6.23	-126.	650.7	15.48
324	-8.31	-7.69	82.	738.2	15.82
325	-9.56	-9.11	164.	4077.4	2.71
326	11.89	-5.07	62.	4860.2	2.23
329	-3.39	-4.41	-152.	1538.6	3.74
330	-4.73	-5.56	-123.	756.4	9.45
331	-5.51	-6.48	-111.	1495.5	5.58
332	-8.82	-1.80	74.	354.3	18.29
601	2.29	1.63	144.	14178.1	0.17
602	3.57	2.68	-142.	9698.2	0.42
604	5.53	4.21	-122.	43869.2	0.14
605	6.54	4.23	122.	1898.1	3.63
606	5.99	2.65	-74.	6667.7	0.79
607	4.78	1.73	-135.	8476.3	0.46
608	6.92	5.29	102.	4921.1	1.65
609	7.54	6.65	-146.	11389.0	0.85
610	8.24	7.66	13.	5149.7	2.13
611	9.42	9.07	14.	3112.7	4.13
612	9.23	7.45	-85.	3105.0	3.61
614	1.50	-2.91	-174.	439.7	4.60
615	1.86	-3.13	-34.	623.4	3.65

APPENDIX A4: Continued.

N	X	Y	ANG	RES	CON
616	3.23	-3.49	-18.	542.5	5.20
617	4.32	-4.04	175.	1209.3	2.62
618	5.79	-2.98	-98.	1157.7	3.16
619	6.32	-1.60	-123.	4437.3	0.89
620	7.18	-2.71	61.	4961.1	0.92
621	8.87	0.13	25.	1182.8	4.94
622	8.86	1.86	-27.	1263.5	5.10
625	-2.86	-3.48	-34.	897.9	3.89
626	-1.28	-5.02	-155.	713.3	5.58
627	-3.98	-6.17	-111.	299.0	15.17
628	-1.17	-7.15	-129.	1786.4	2.97
629	-1.24	-8.46	-53.	377.8	16.33
630	-2.51	-6.77	-28.	764.9	7.68
631	-3.43	-7.58	162.	366.2	19.33
632	-4.59	-8.69	187.	713.1	12.22
633	3.38	-4.57	-115.	1520.9	2.23
634	2.77	-3.69	-119.	525.2	4.75
635	2.34	-4.26	-122.	241.6	12.18
636	3.79	-5.08	-27.	1007.2	3.64
801	-1.42	-1.68	63.	2174.5	0.96
***	-2.49	-9.57	11.	3619.6	2.23
803	-2.12	3.64	-26.	49962.9	0.02
804	1.10	1.97	-65.	964.0	1.89
805	3.27	2.57	-142.	752.7	2.99
806	3.66	4.65	-179.	652.9	5.53
807	1.93	5.59	-112.	1136.1	4.62
808	2.92	5.86	-121.	4733.2	1.45
80	3.99	8.04	-75.	925.6	6.28
810	-3.11	7.24	130.	612.4	7.47
811	-1.35	6.36	-62.	378.5	9.38
812	-2.64	5.55	-49.	93.8	28.96
813	-3.66	4.45	12.	36.1	62.19
14	1.35	-1.40	-95.	2647.6	0.58

APPENDIX A5. Single-coverage dipole resistivities measured from source 5.

N	X	Y	ANG	RES	CON
401	-1.29	-2.55	-126.	739.6	1.07
402	-2.27	-1.81	-122.	850.8	0.84
403	-3.44	-2.99	172.	1468.5	1.11
404	-4.62	-4.05	33.	4184.2	0.58
405	-5.22	-5.33	41.	5263.7	0.64
406	-5.98	-6.79	62.	2706.6	1.52
407	-6.56	-8.14	47.	3819.1	1.28
408	-7.66	-9.04	79.	962.6	5.80
409	-6.41	-1.08	-57.	367.9	8.29
410	-7.24	2.30	-32.	3343.7	1.15
411	-7.86	-1.18	-39.	1711.4	2.26
412	-8.77	-2.78	-33.	2425.9	1.77
413	-9.45	-4.43	-5.	4939.2	0.96
414	-8.62	-5.30	46.	1634.7	2.76
415	-5.09	-1.37	-58.	357.1	7.58
416	-4.68	3.59	-32.	1503.7	3.52
417	-3.29	6.07	-113.	645.7	10.20
418	-4.92	6.57	63.	975.3	7.72
419	-5.21	5.98	-12.	151.3	51.67
420	-5.77	4.93	-165.	37.6	193.54
421	-6.73	3.73	-176.	86.5	73.72
422	-7.73	2.88	-72.	85.2	69.58
423	-7.25	2.28	-86.	511.4	12.24
424	-3.74	5.07	-161.	695.7	9.03
425	-2.75	4.97	-115.	827.8	6.53
426	-10.33	-5.85	64.	2972.5	1.82
427	-10.37	-7.16	33.	2992.5	1.93
428	-12.22	-7.65	7.	4386.2	1.52
429	-13.92	-7.59	81.	278.3	26.72
430	-13.77	-2.81	114.	682.1	12.19
431	-11.25	-3.14	14.	209.1	26.81
432	-12.51	-4.21	23.	512.6	12.29
433	-13.43	-1.22	8.	127.3	41.99
434	-13.34	3.06	-98.	715.2	12.16
701	1.13	-2.06	96.	314.9	2.77
702	1.48	0.69	143.	1798.2	2.63
703	1.27	1.74	144.	578.6	2.49
704	1.69	2.66	-94.	813.4	2.44
705	2.05	3.84	-105.	812.7	3.34
706	2.95	4.93	3.	672.6	5.12
707	3.32	5.73	72.	353.4	11.13
708	2.27	2.75	119.	639.7	2.39
709	3.73	1.88	24.	4030.4	2.62
710	5.27	3.74	-6.	2157.8	3.09
711	5.39	4.54	-152.	16934.3	3.26
712	6.93	5.50	-146.	3175.8	1.54
713	7.24	7.74	122.	4736.3	1.23
714	7.76	9.73	113.	37311.7	2.18
715	7.13	10.55	-35.	1974.4	3.60

APPENDIX A5. Continued.

N	X	Y	ANG	RES	CON
716	3.93	-3.38	-52.	530.9	9.24
717	4.44	-5.15	63.	5638.8	1.15
718	5.58	-2.53	-62.	2828.2	1.60
719	7.65	-1.23	-36.	2255.2	2.24
720	7.87	2.74	106.	6227.3	2.76
721	9.59	2.73	-43.	6933.7	2.62
722	6.57	9.12	113.	2652.7	2.39
723	4.34	6.66	174.	1656.1	2.78
724	5.55	7.77	135.	2386.6	2.26
725	4.77	11.21	91.	913.8	7.89
726	12.43	8.24	153.	7002.2	1.12
727	13.30	4.51	-39.	559.7	13.73
901	0.98	-1.55	-4.	7097.9	0.25
902	-3.26	-2.54	-61.	151.3	14.47
903	-3.43	-3.92	-29.	240.2	11.28
904	-1.84	-5.18	-126.	191.9	16.77
905	-1.34	-6.69	-151.	228.5	18.17
906	-1.95	-8.24	-147.	472.2	10.69
907	-2.10	-9.62	-166.	597.4	9.95
908	-1.26	-10.57	-147.	499.6	13.91
909	-3.07	1.00	92.	67.9	40.24
910	-4.65	0.12	-68.	223.7	12.04
911	-5.23	-1.26	-125.	183.7	12.62
912	-6.70	-3.20	21.	2341.5	1.22
913	-6.96	-4.73	107.	1672.7	2.25
914	-7.36	-6.09	47.	1696.8	2.52
915	-8.52	-7.57	53.	1943.7	2.68
916	-3.53	1.68	-99.	411.7	8.03
***	-3.20	2.85	-114.	1715.8	2.43
918	-2.99	3.85	-152.	507.8	8.95
919	-2.71	4.74	161.	847.7	5.47
920	-1.25	5.65	-168.	420.7	11.21
921	-2.42	7.09	143.	773.2	6.84
922	1.43	9.82	144.	37207.6	0.18
923	-5.43	7.09	96.	100.6	88.89
924	-2.41	6.84	165.	799.1	7.97
926	-1.50	7.96	-145.	517.5	13.87
927	-2.23	8.98	-163.	479.5	16.87

APPENDIX A6. Single-coverage dipole resistivities measured from source 6.

N	X	Y	ANG	RES	CON
421	-1.29	-7.55	-129.	213.2	5.63
422	-2.27	-1.81	-145.	1137.4	2.55
423	-3.44	-2.90	62.	22872.8	0.20
424	-4.42	-4.85	-139.	5390.8	1.12
425	-5.22	-5.33	-134.	7251.4	1.02
426	-5.96	-6.79	-137.	4744.4	1.80
427	-6.56	-8.14	-132.	6438.4	1.48
428	-7.66	-9.04	-173.	1713.0	6.43
429	-6.41	-1.08	61.	2394.8	2.16
412	-7.24	2.30	153.	5338.5	2.92
411	-7.66	-1.18	142.	3967.1	1.58
412	-8.77	-2.78	166.	5622.9	1.43
413	-9.45	-4.43	-173.	13835.6	2.99
414	-9.62	-5.30	-132.	9533.2	1.05
415	-5.89	-1.37	142.	2104.9	2.38
416	-4.66	3.59	115.	685.3	4.81
417	-3.29	5.27	125.	958.6	3.92
418	-4.92	6.57	-128.	3628.5	1.13
419	-5.21	5.98	-142.	368.5	11.33
420	-5.77	4.93	-127.	92.8	44.61
421	-6.73	3.73	119.	61.9	72.81
422	-7.72	2.88	-158.	187.6	27.19
423	-7.25	2.28	-139.	322.7	14.41
424	-3.74	5.87	148.	4772.9	0.71
425	-2.75	4.97	125.	1824.5	1.78
426	-13.33	-5.85	-63.	13039.6	2.69
427	-13.37	-7.16	-133.	6764.3	1.86
428	-12.22	-7.65	-166.	6916.6	2.27
429	-13.92	-7.59	-94.	3323.0	4.69
430	-13.47	-8.81	-58.	3647.3	2.67
431	-11.25	-3.14	-129.	1673.2	6.30
432	-12.31	-4.21	-152.	3187.2	3.69
433	-13.43	-1.23	-169.	719.2	11.25
434	-13.34	3.06	172.	766.4	9.32
701	1.19	-2.26	-63.	2679.2	2.49
702	1.48	2.69	-34.	3524.3	2.47
703	1.27	1.74	-22.	915.6	1.96
704	1.99	2.68	117.	795.5	3.15
705	2.15	3.84	87.	1582.9	2.13
706	2.65	4.93	-63.	730.3	6.43
707	3.32	5.73	28.	3231.2	1.73
708	2.07	0.75	-47.	4961.8	2.44
709	3.73	1.88	-143.	3245.6	1.30
710	5.17	3.74	-32.	9237.8	0.68
711	6.39	4.54	79.	19593.9	2.74
712	6.93	5.50	143.	1816.6	4.79
713	7.24	7.74	-54.	29467.5	2.33
714	7.76	9.73	-6 .	72598.3	2.15
715	7.13	10.55	-45.	7182.8	1.48

APPENDIX A6: Continued.

N	X	Y	ANG	RES	CON
716	3.93	-3.38	134.	5452.2	0.43
717	4.44	-5.15	60.	606.1	5.13
718	5.50	-2.53	123.	4997.2	0.32
719	7.55	-1.23	150.	3415.7	1.44
720	7.87	0.74	79.	4085.4	1.53
721	9.59	3.73	136.	8266.1	0.89
722	6.57	9.10	-45.	5525.9	1.78
723	4.34	6.66	6.	5380.9	1.21
724	5.55	7.77	-25.	4329.9	1.86
725	4.77	11.21	30.	7717.2	1.15
726	12.43	6.04	-26.	4899.4	3.02
727	13.32	4.81	-177.	3959.5	3.32
901	0.98	-1.55	154.	2873.4	0.17
902	-0.76	-2.54	-76.	2943.2	2.45
903	-2.43	-3.92	114.	1893.7	1.26
904	-1.74	-5.15	54.	3534.7	7.86
905	-1.34	-6.69	54.	3697.2	1.16
906	-1.35	-8.24	55.	6388.8	8.86
907	-2.12	-9.62	54.	8497.6	8.75
908	-1.26	-13.57	54.	4222.3	1.51
909	-3.87	1.80	-99.	1027.4	2.54
910	-4.65	2.12	-124.	85.3	35.67
911	-5.20	-1.26	-124.	739.2	6.26
912	-6.58	-3.20	-139.	7668.3	2.85
913	-5.96	-4.73	-61.	7355.8	1.13
914	-7.36	-6.29	-115.	5334.6	1.78
915	-8.52	-7.97	-112.	5991.2	1.38
916	-3.53	1.68	73.	138.6	17.45
***	-3.02	2.85	75.	748.4	3.13
918	-2.59	3.85	178.	153.5	16.75
919	-2.11	4.74	113.	479.1	5.97
920	-1.25	5.65	132.	2662.2	1.24
921	-0.42	7.29	78.	2496.5	1.67
922	1.33	9.80	141.	33892.4	0.29
923	-5.43	7.29	96.	55.3	85.57
924	-2.41	6.84	141.	2733.8	1.45
926	-1.92	7.96	123.	3469.9	1.31
927	-2.23	8.98	65.	619.1	8.23

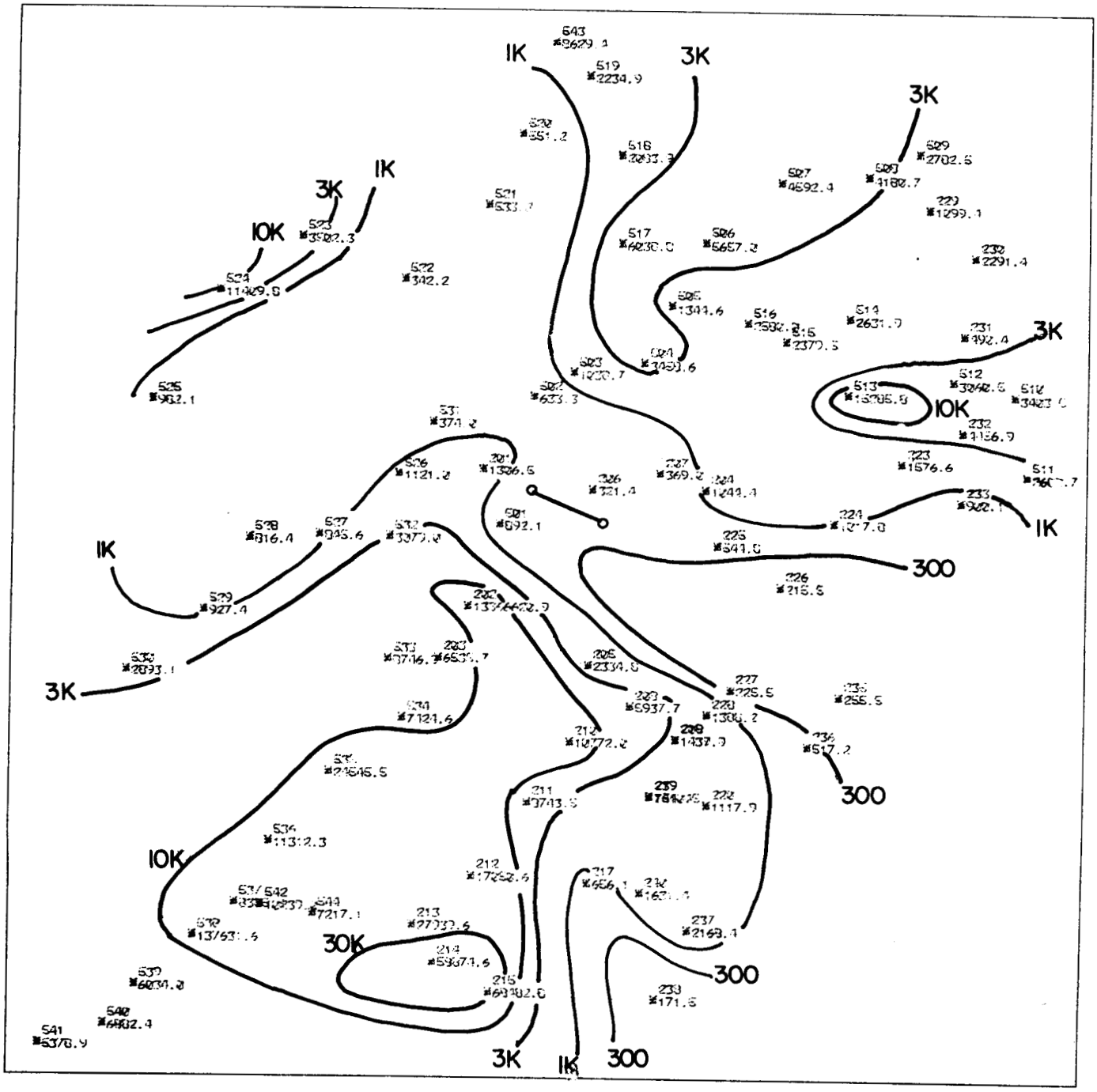

Figure A1. Apparent resistivities measured from source 1.

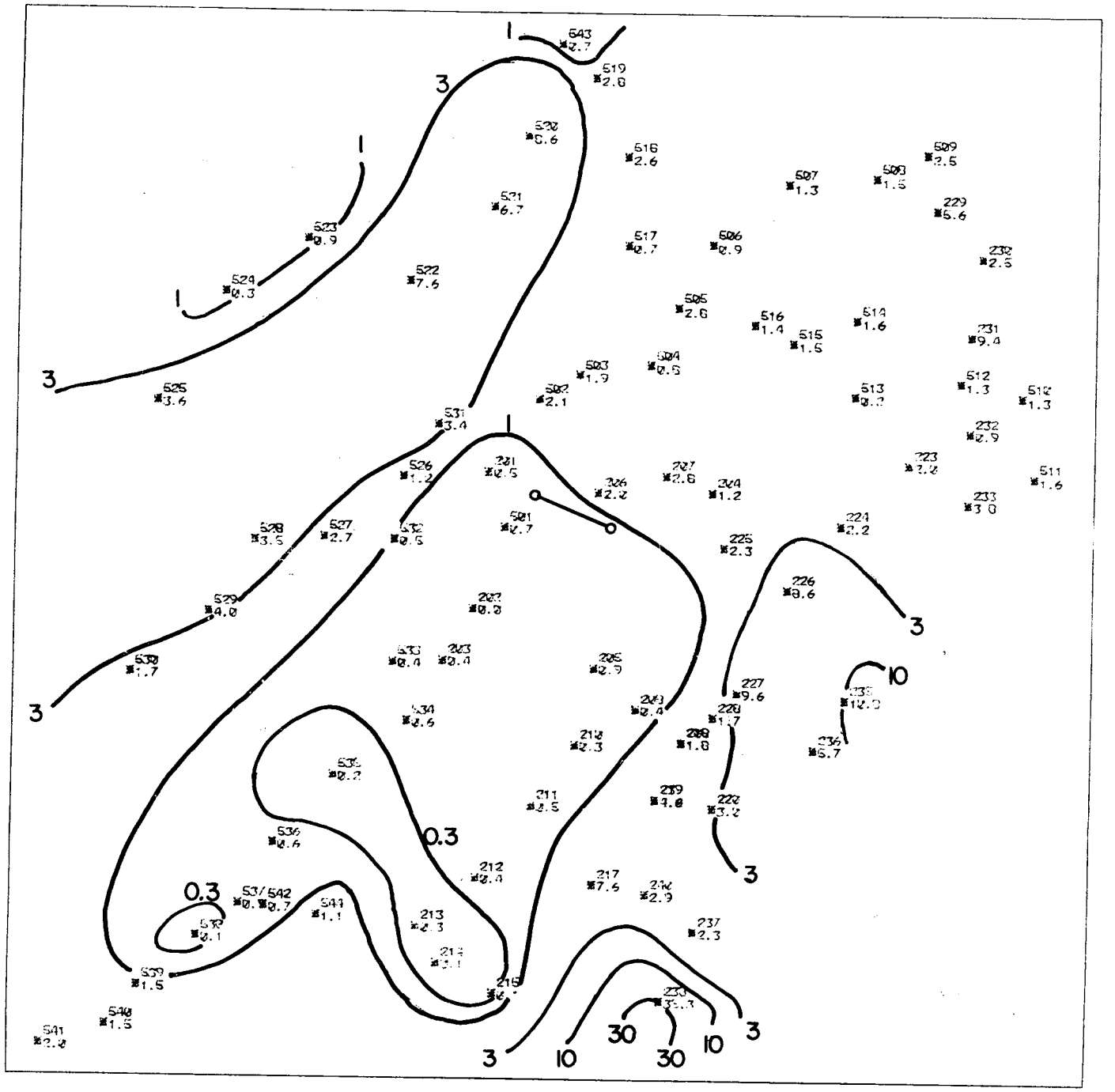

Figure A2. Apparent conductances measured from source 1.

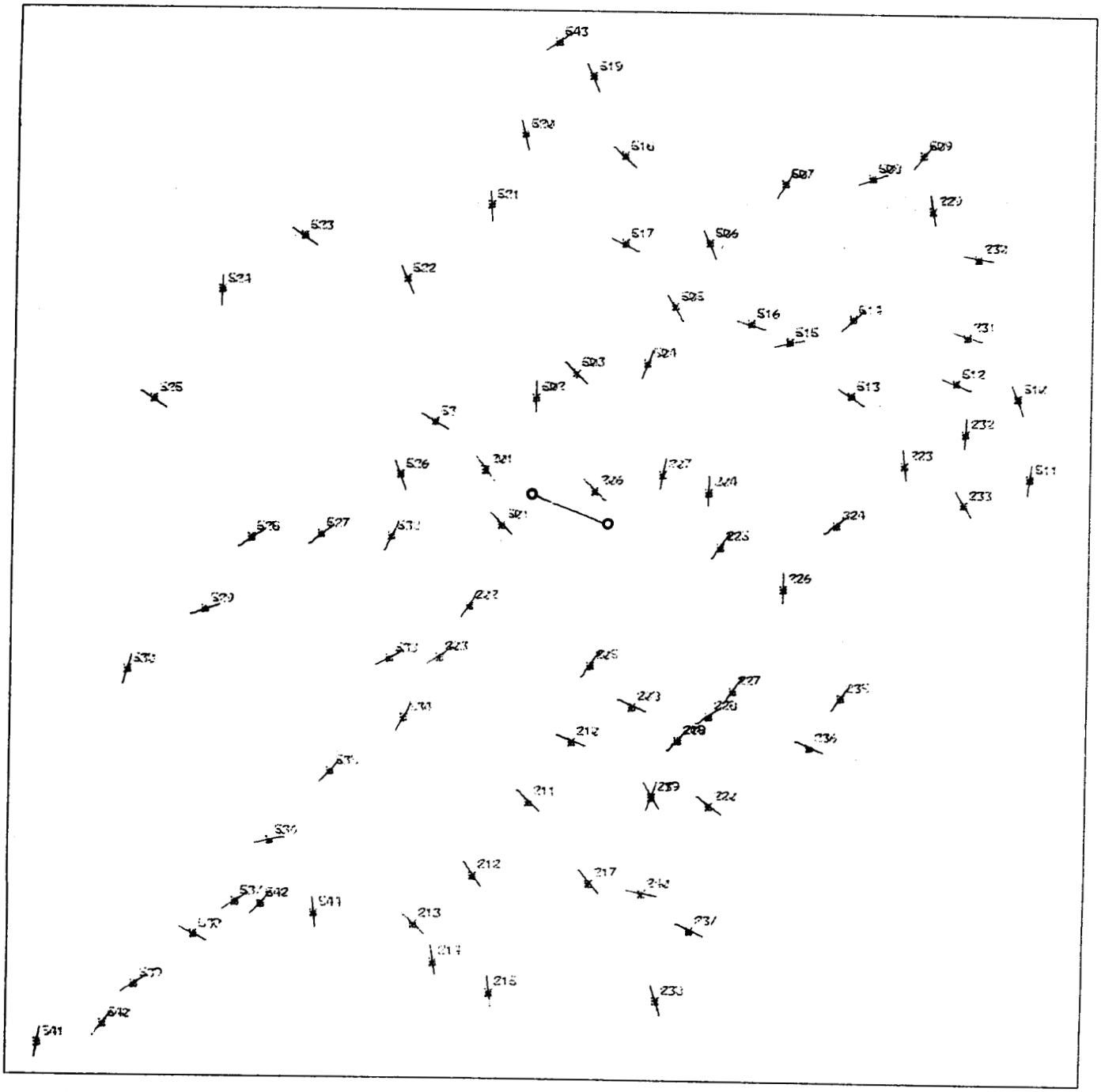

Figure A3. Directions of electric fields measured from source 1.

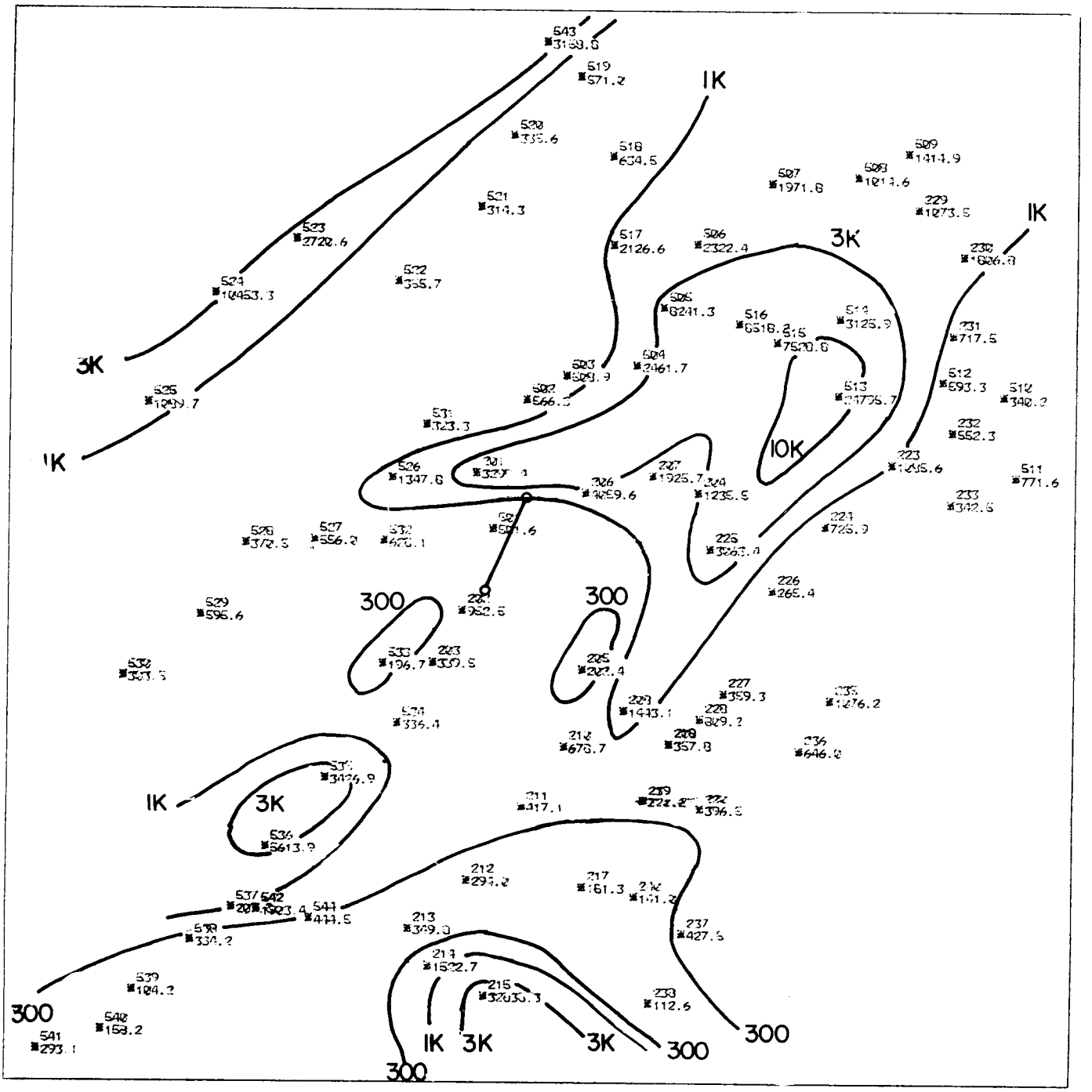

Figure A4. Apparent resistivities measured from source 2.

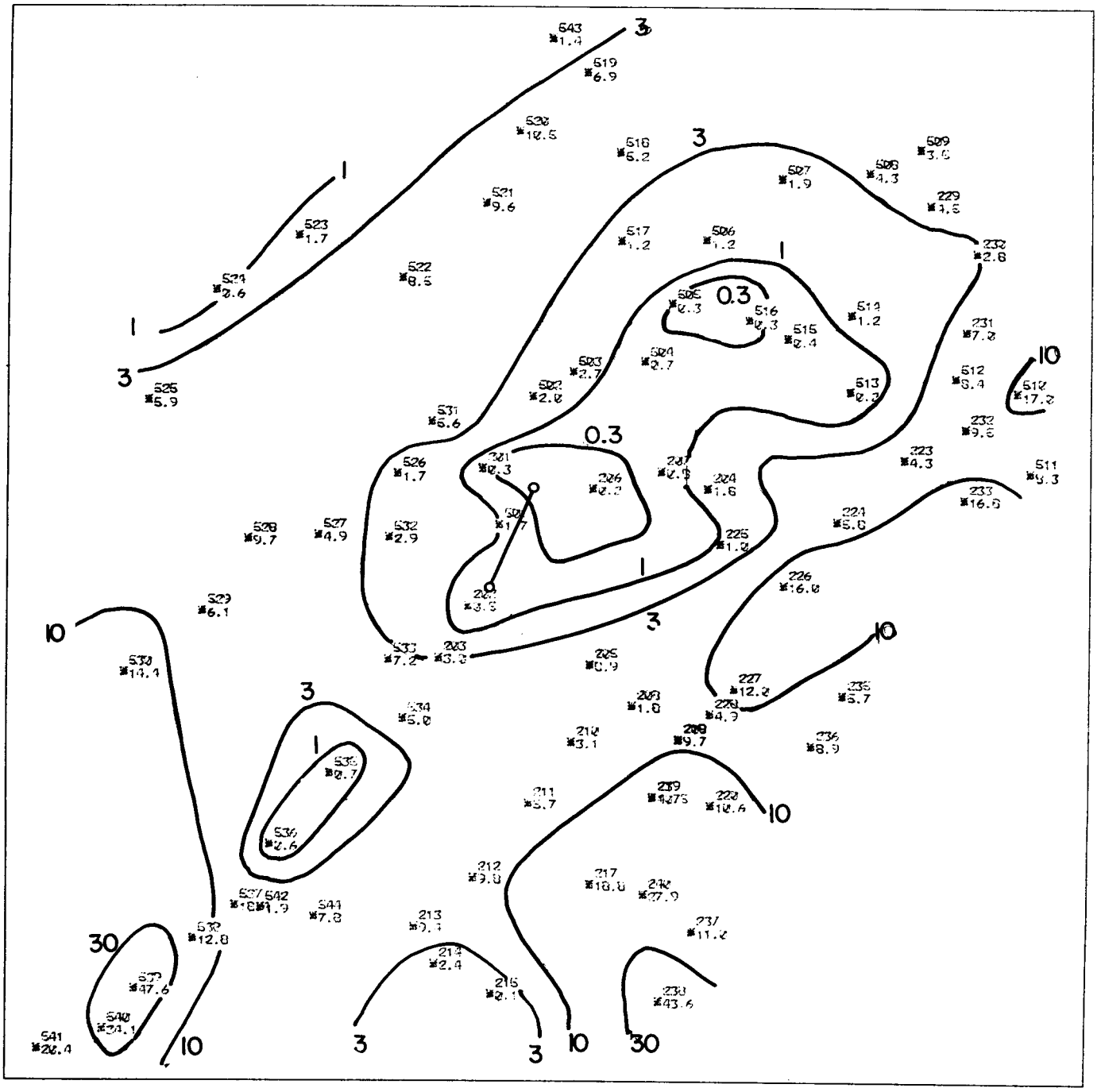

Figure A5. Apparent conductances measured from source 2.

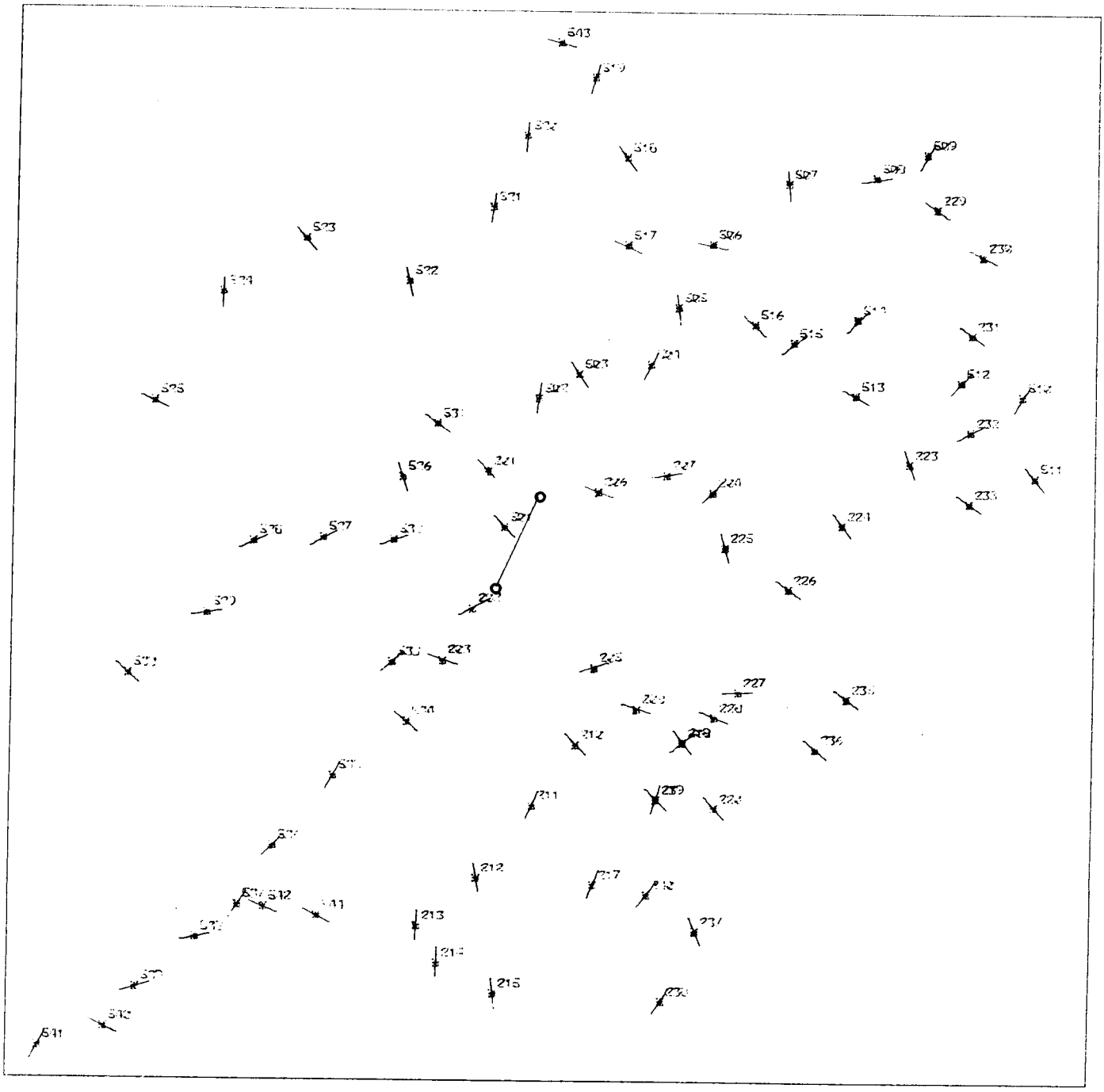

Figure A6. Directions of electric fields measured from source 2 .

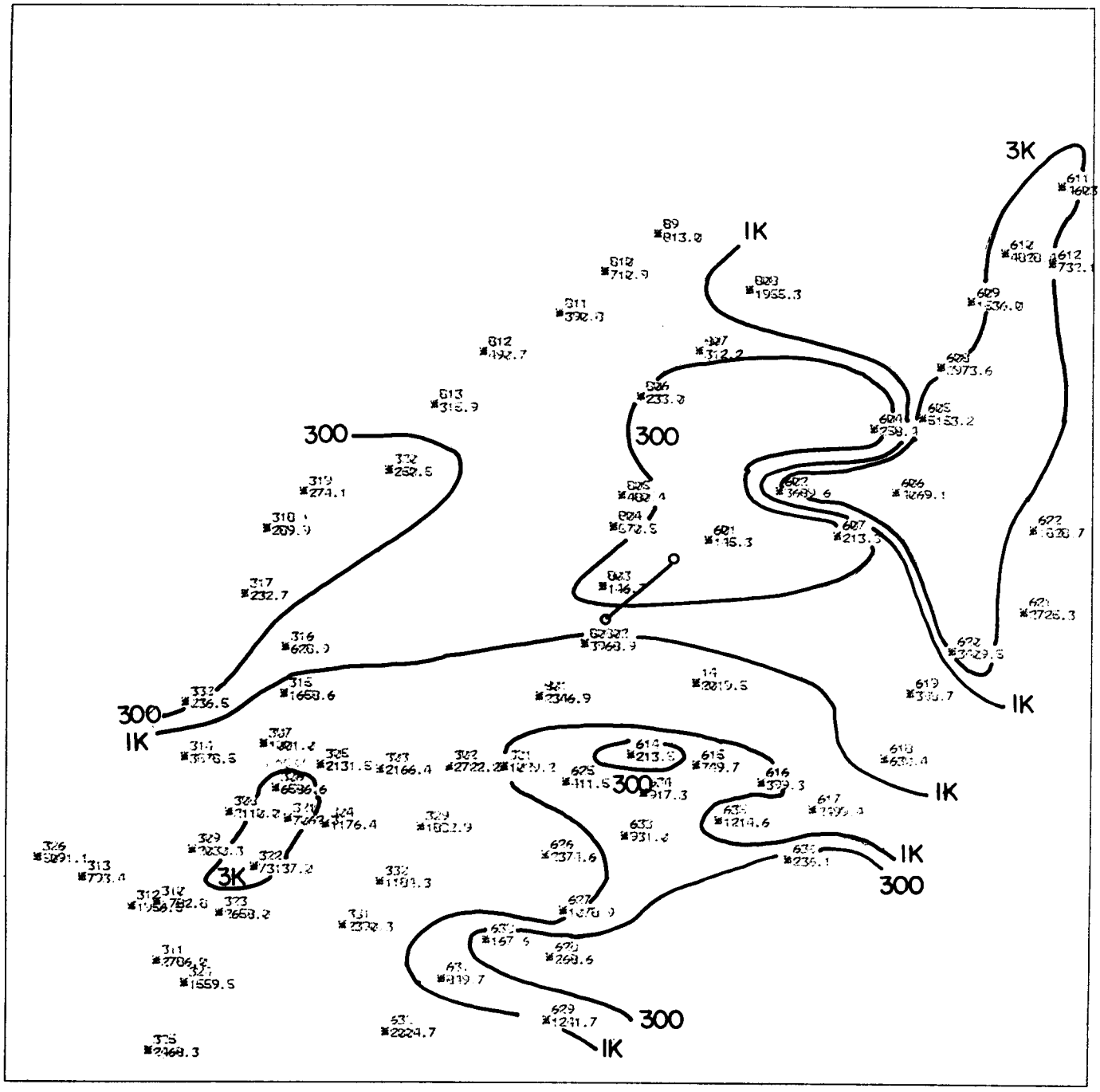

Figure A7. Apparent resistivities measured from source 3.

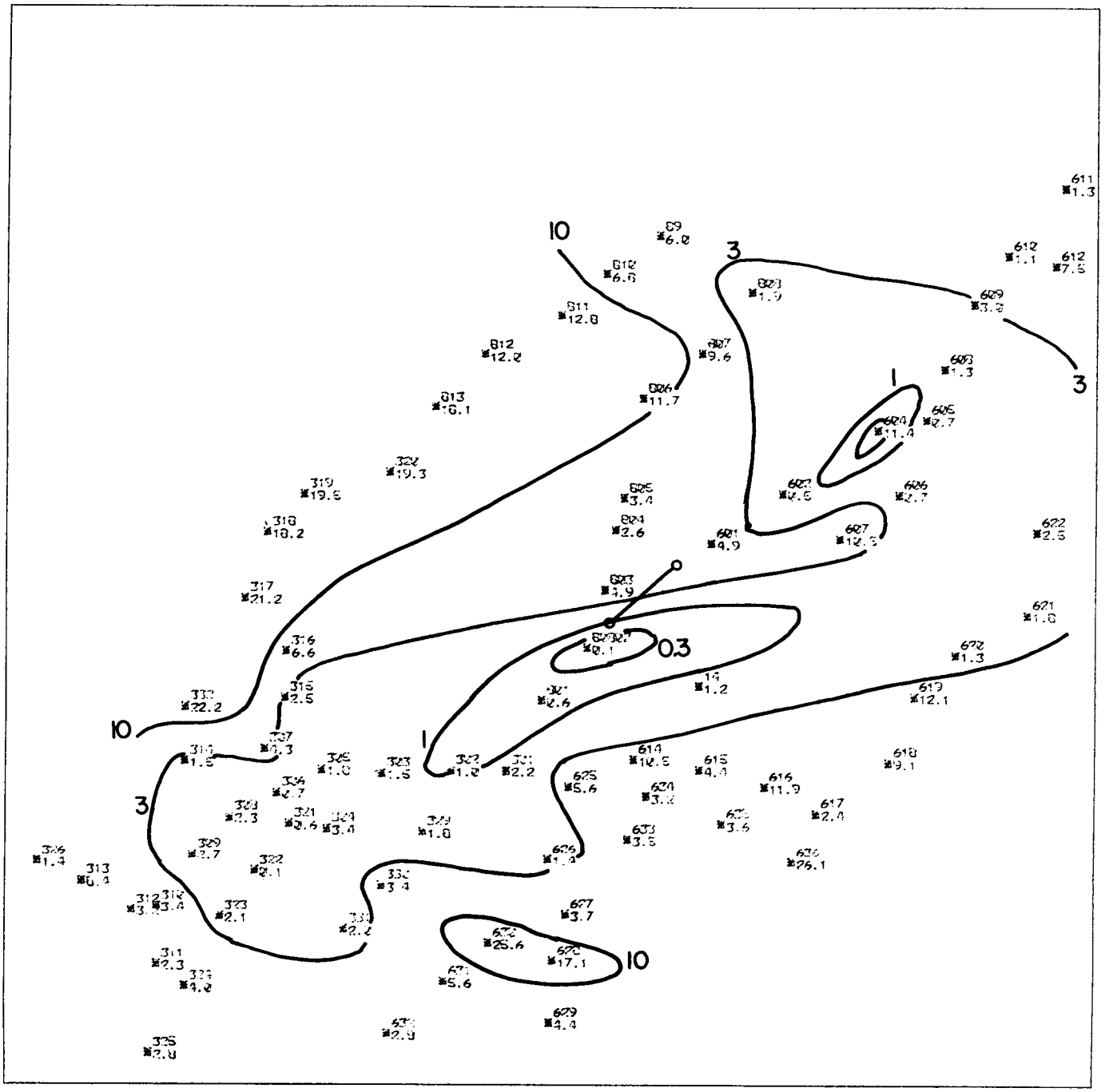

Figure A8. Apparent conductances measured from source 3.

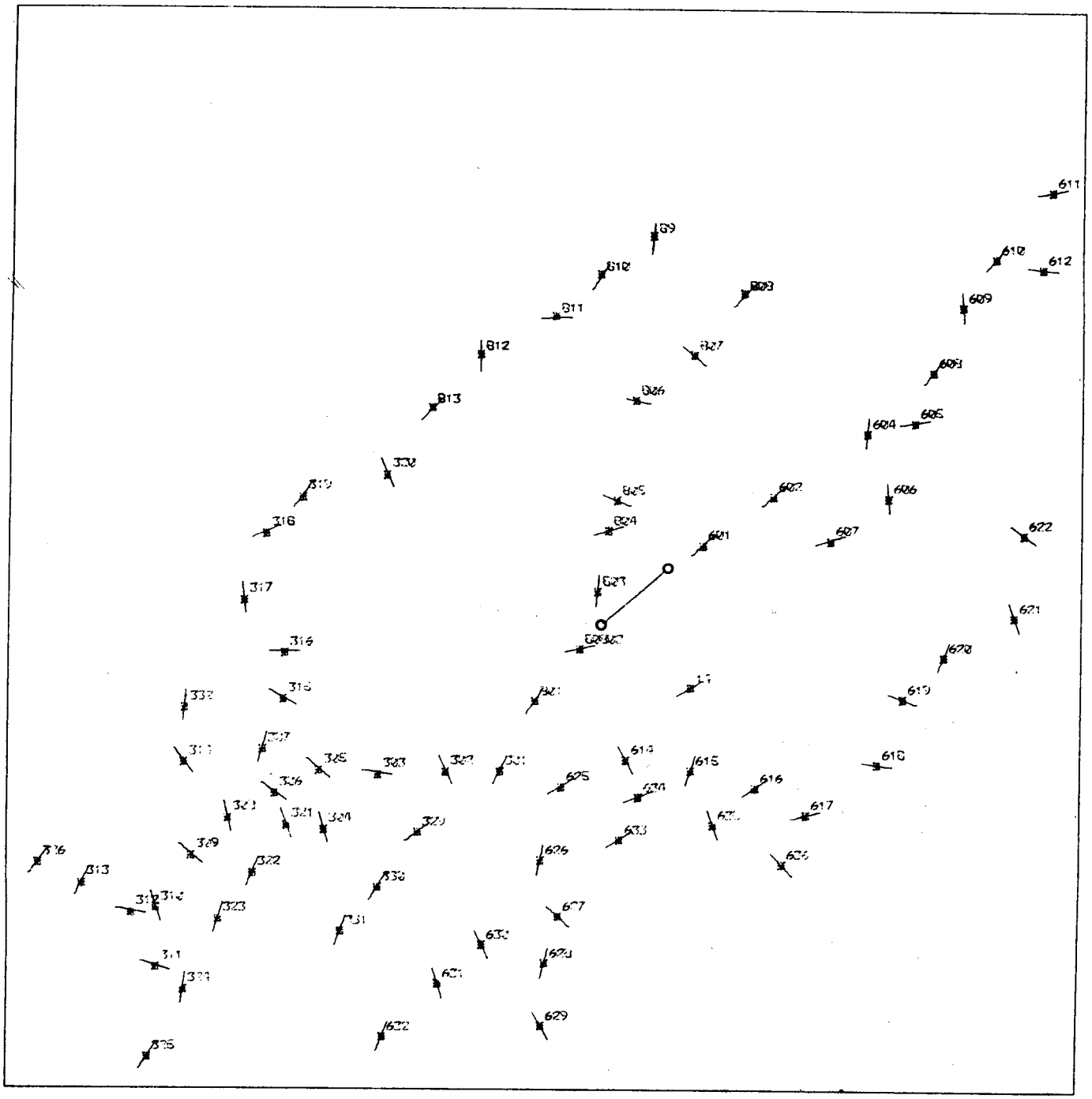

Figure A9. Directions of electric fields measured from source 3.

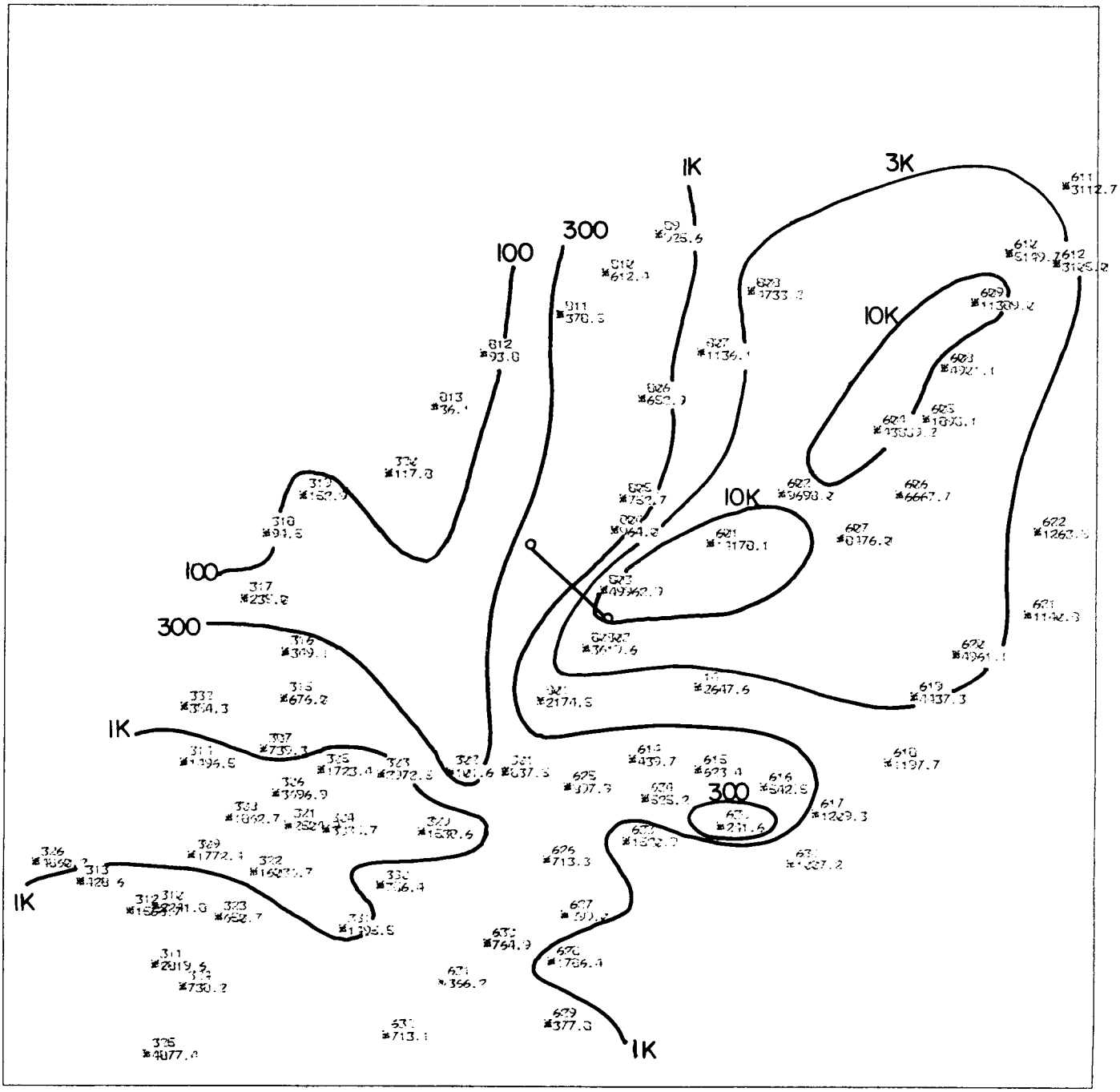

Figure A10. Apparent resistivities measured from source 4.

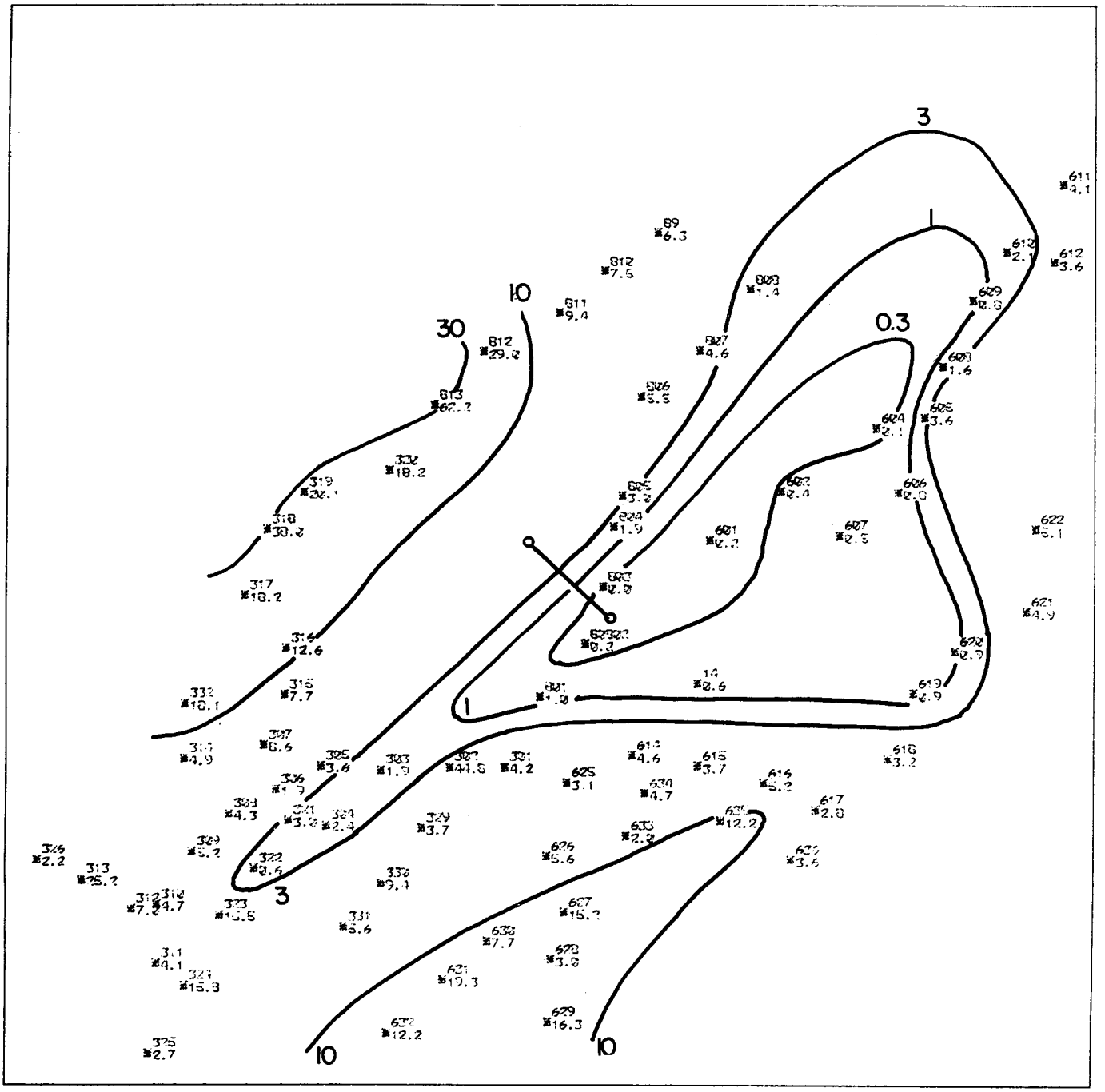

Figure A11. Apparent conductances measured from source 4.

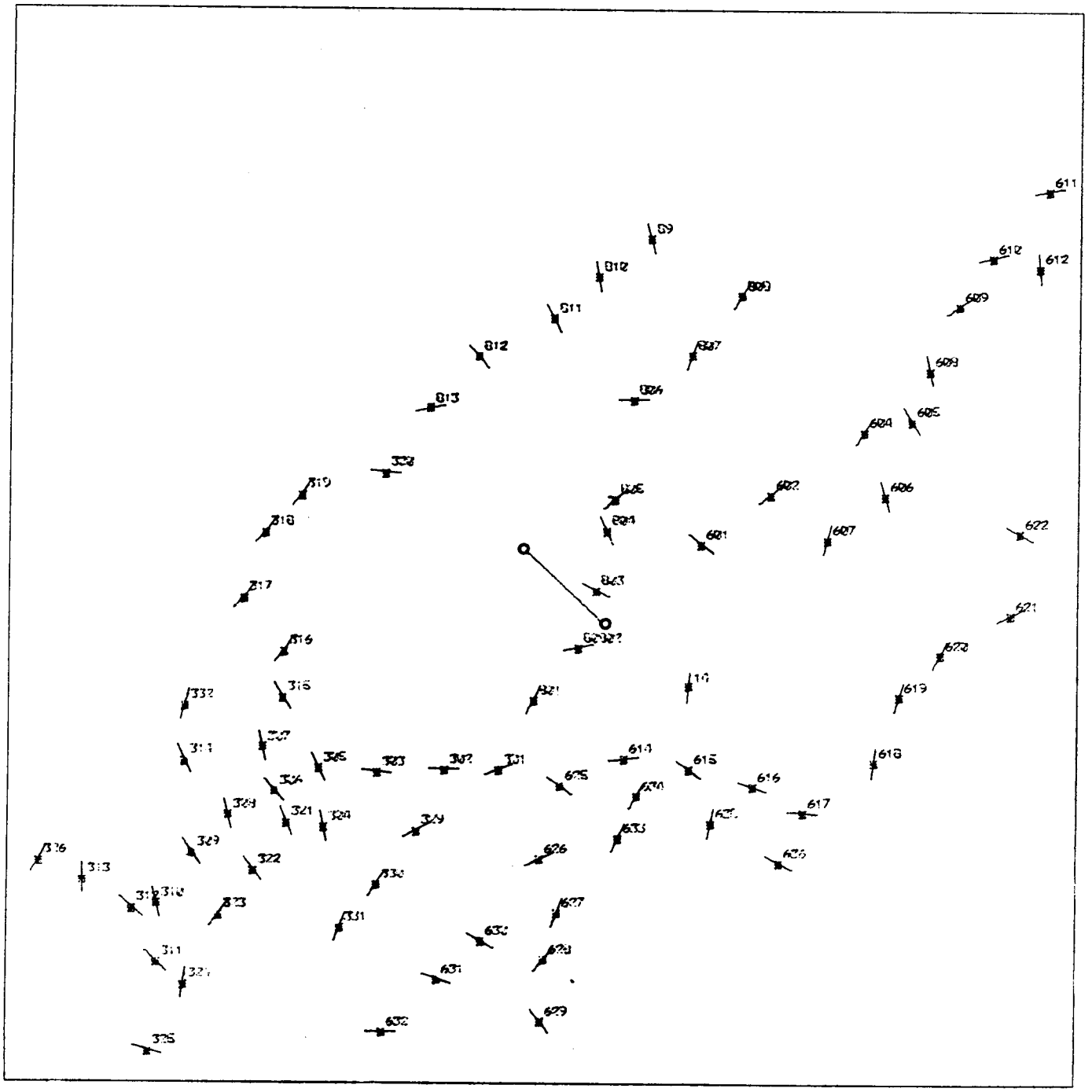

Figure A12. Directions of electric fields measured from source 4.

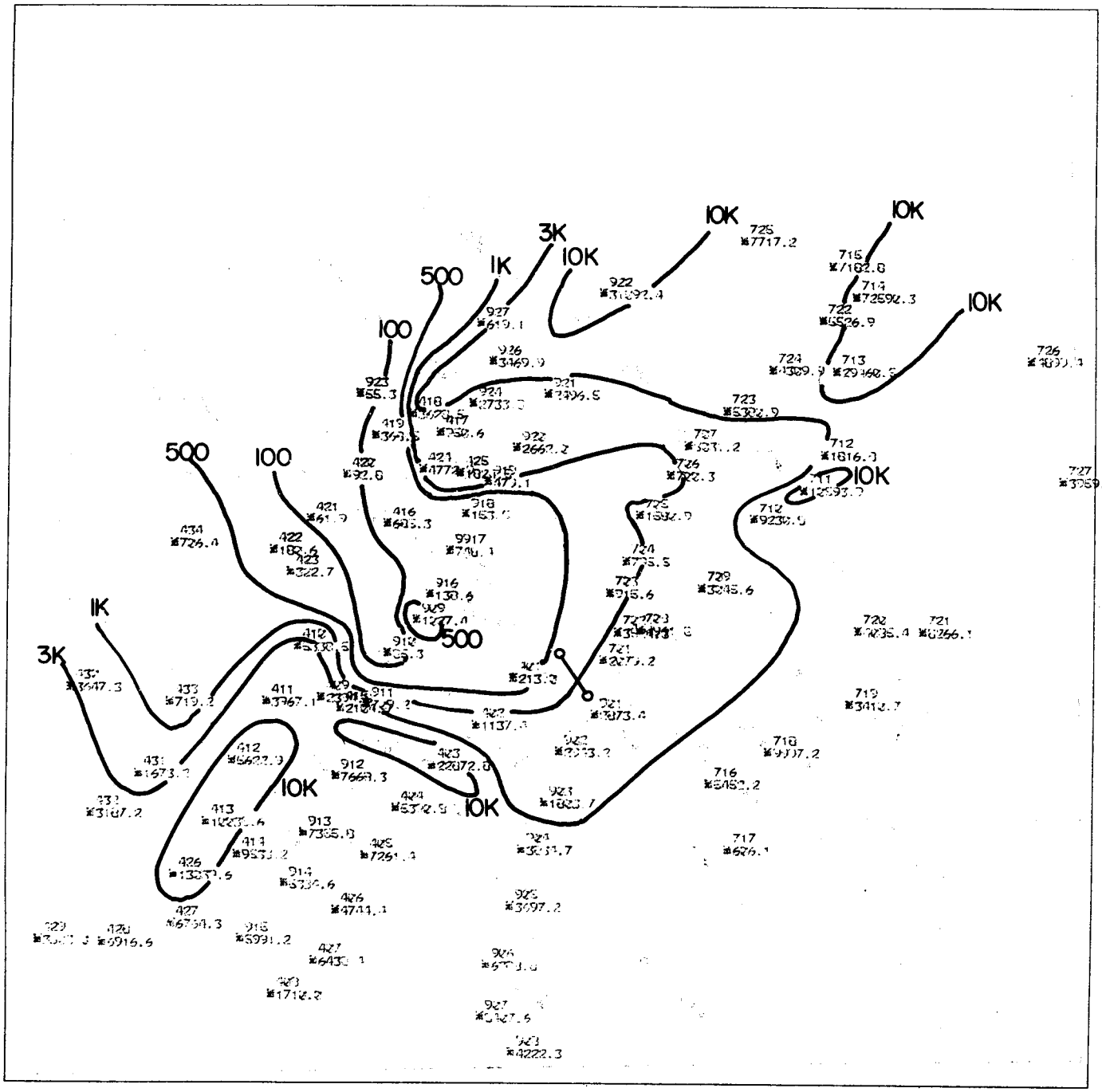

Figure A13. Apparent resistivities measured from source 5.

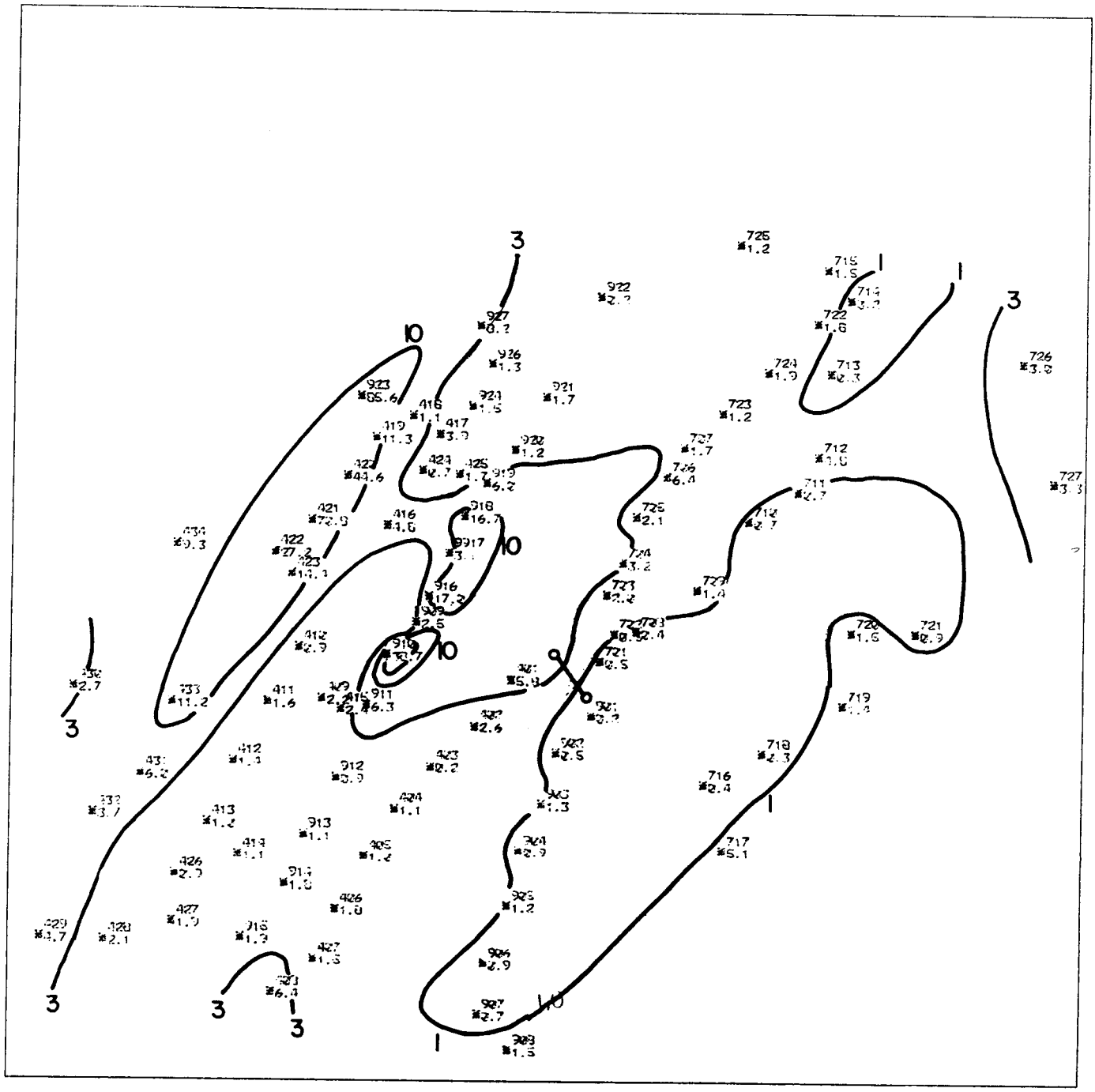

Figure A14. Apparent conductances measured from source 5.

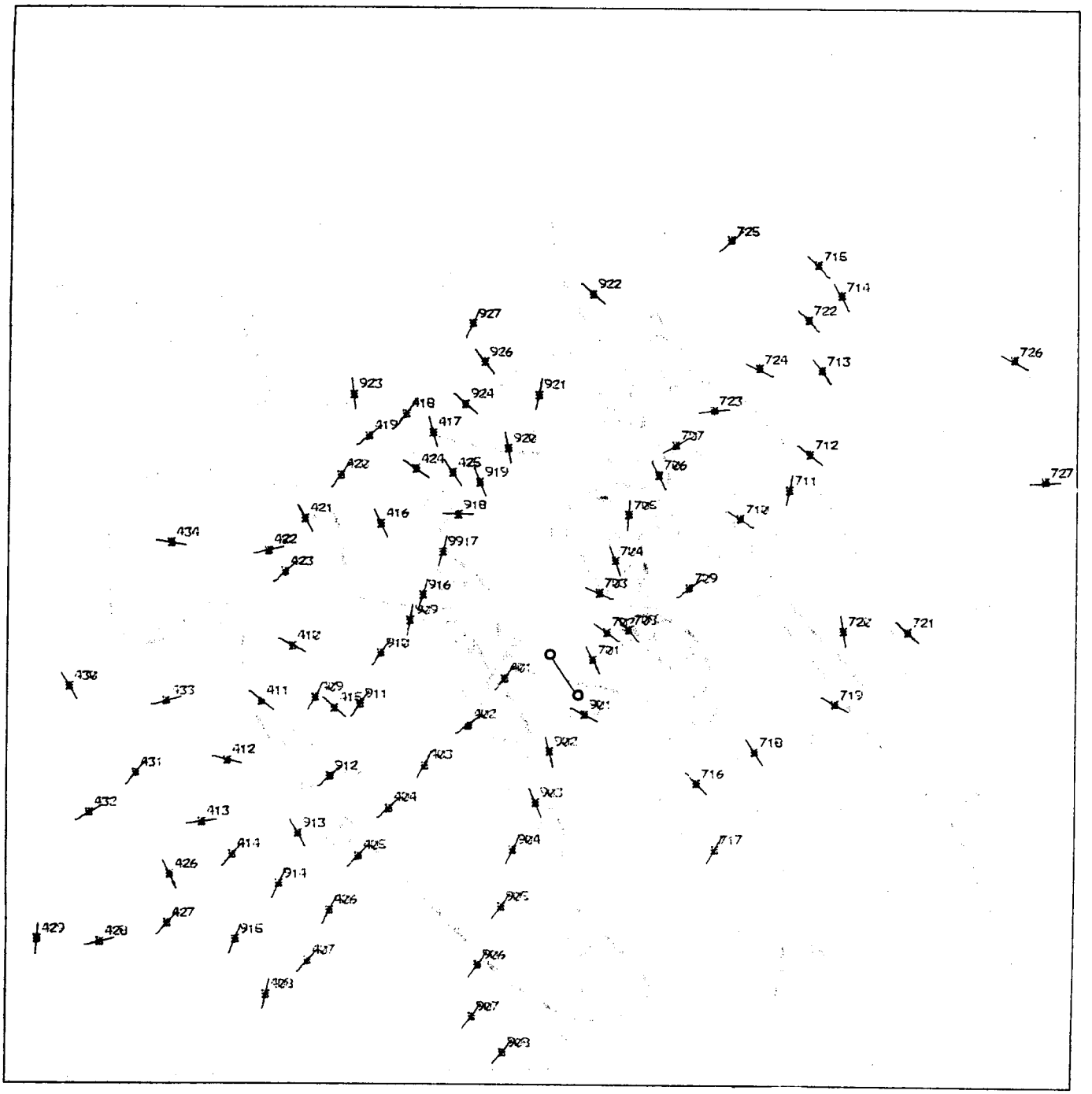

Figure A15. Directions of electric fields measured from source 5.

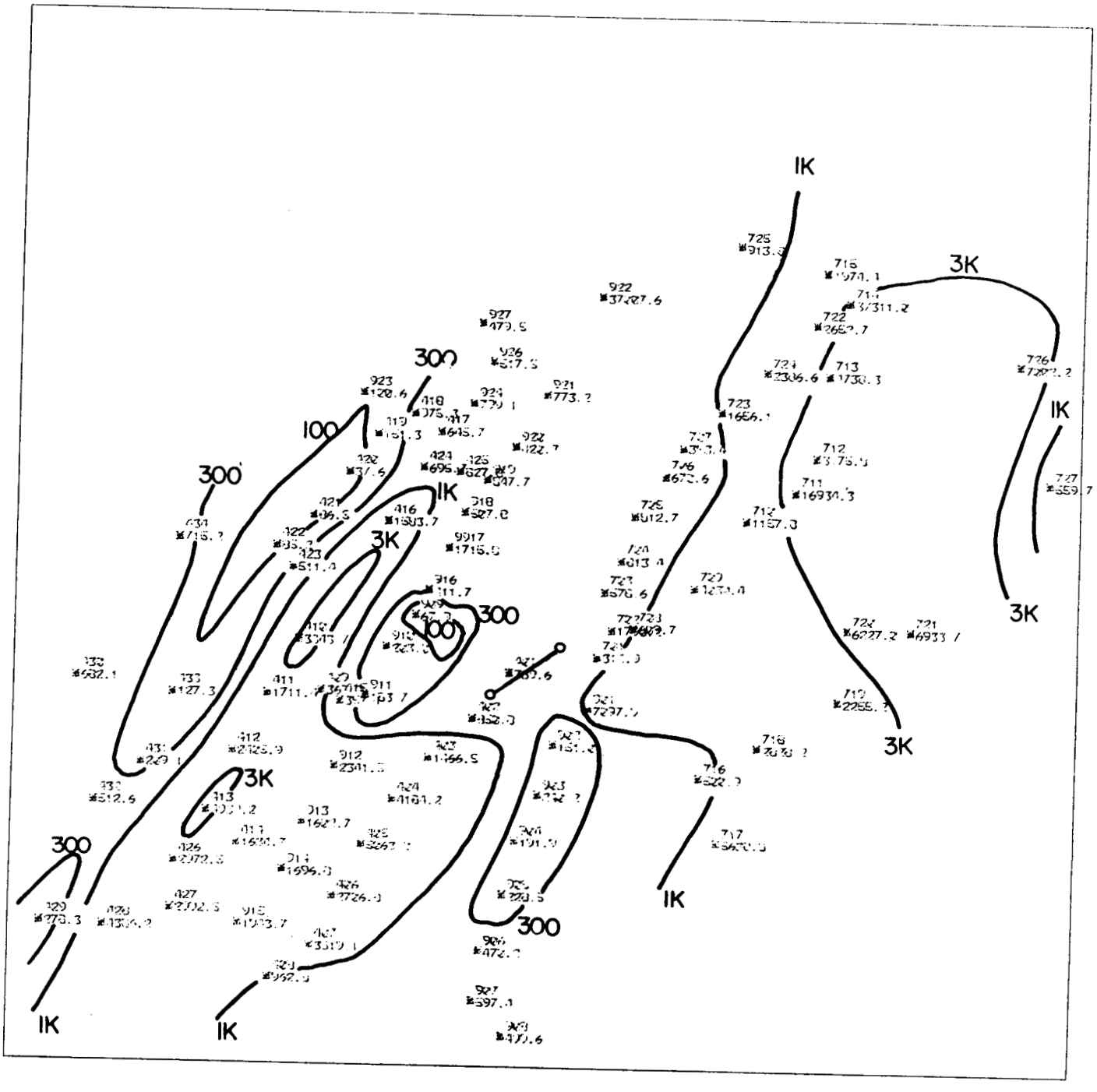

Figure A16. Apparent resistivities measured from source 6.

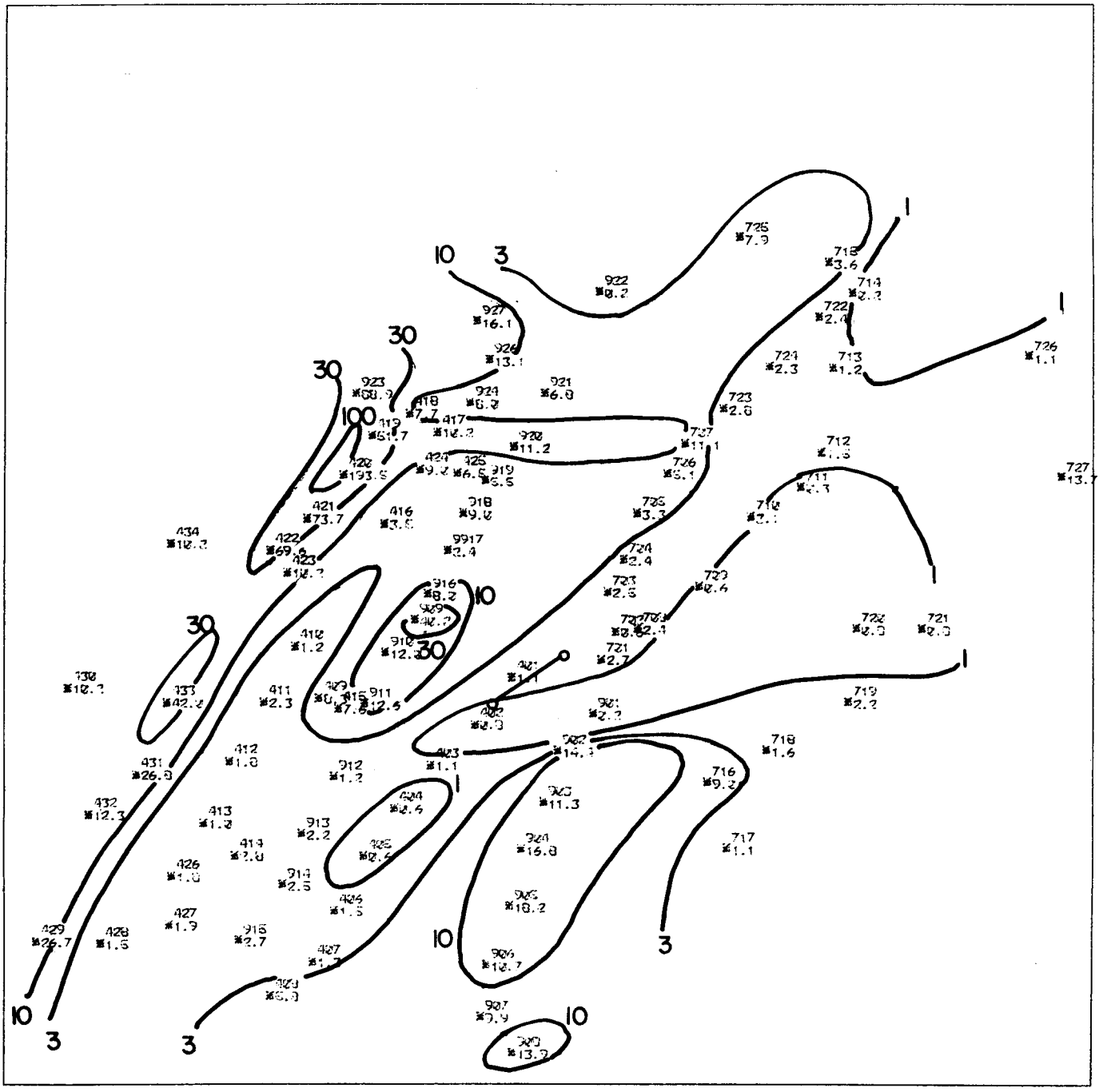

Figure A17. Apparent conductances measured from source 6.

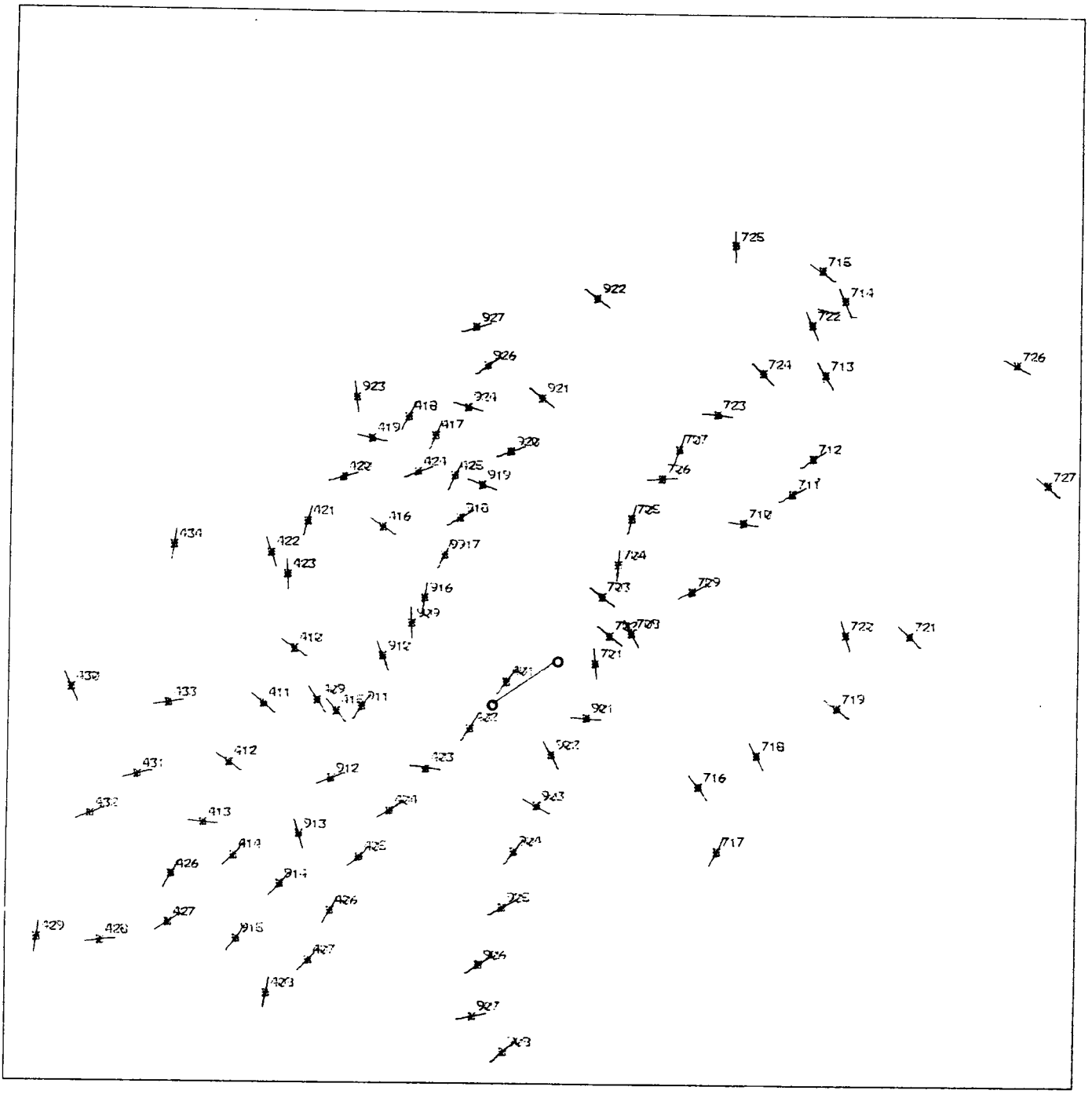

Figure A18. Directions of electric fields measured from source 6.

Appendix B. Listing of resistivity values computed for rotation of source bipoles.

N : Identification number of observation point

R : Distance from the common point of a source bipole pair to an observation point, in kilometers.

BEAR : Bearing of the line from the source common point to an observation point, degrees from north.

RMEAN : The average of maximum and minimum apparent resistivity values found on rotation, in ohm-meters.

CMEAN : The average of maximum and minimum apparent conductance values found on rotation, in mhos.

RMAX : The maximum apparent resistivity computed on rotation, in ohm-meters

RMIN : The minimum apparent resistivity computed on rotation, in ohm-meters.

Appendix B: Sources 1 and 2

N	R	BEAR	RMEAN	CMEAN	RMAX	RMIN
201	v.930	297.	4621.	1.	8971.	271.
2	2.140	209.	*******	0.	*******	1117.
3	3.130	209.	3884.	2.	7502.	266.
4	2.880	88.	1416.	9.	2744.	87.
5	3.000	161.	1420.	10.	2746.	93.
6	1.000	85.	2225.	3.	4323.	127.
7	2.150	80.	1380.	2.	2425.	334.
8	3.900	155.	2725.	7.	5225.	224.
9	4.750	149.	894.	6.	1430.	357.
10	4.180	171.	4462.	4.	8603.	321.
11	5.140	180.	4805.	7.	9431.	178.
12	6.440	188.	8548.	11.	16964.	131.
13	7.430	195.	12695.	9.	25211.	179.
14	7.950	191.	32412.	4.	64317.	506.
15	8.320	184.	25192.	16.	50142.	242.
16	NO SIGNAL					
17	6.550	171.	416.	13.	664.	168.
18	4.750	149	733.	31.	1402.	64.
19	5.420	158.	708.	5.	804.	613.
20	5.960	150.	679.	22.	1274.	83.
21	NO SIGNAL					
22	NO SIGNAL					
23	6.140	85.	1415.	3.	1778.	1052.
24	5.030	95.	1068.	4.	1420.	716.
25	3.200	105.	2270.	2.	3960.	581.

Appendix B: Sources 1 and 2

N	R	BEAR	RMEAN	CMEAN	RMAX	RMIN
226	4.410	110.	241.	13.	281.	201.
27	4.650	134.	286.	13.	412.	159.
28	4.700	141.	1017.	4.	1403.	631.
29	8.100	54.	1082.	6.	1363.	802.
30	8.320	61.	1828.	7.	3013.	643.
31	7.620	69.	746.	20.	1380.	112.
32	7.200	81.	3066.	6.	5636.	496.
33	7.100	91.	533.	21.	880.	186.
34	NO SIGNAL					
35	6.120	123.	702.	8.	1158.	246.
36	6.230	132.	429.	41.	811.	48.
37	7.730	160.	1342.	9.	2414.	270.
38	8.680	166.	152.	47.	239.	64.
39	5.420	158.	902.	9.	1581.	224.
40	6.900	164.	893.	17.	1659.	127.
501	0.750	226.	1247.	14.	2453.	41.
2	1.630	0.	402.	7.	625.	178.
3	2.130	18.	685.	7.	1233.	138.
4	2.850	40.	1817.	5.	3394.	240.
5	3.870	36.	4468.	3.	8355.	581.
6	5.050	34.	13859.	0.	23317.	4401.
7	6.600	38.	2794.	2.	3948.	1640.
8	7.650	46.	2378.	12.	4532.	224.
9	8.530	48.	1591.	9.	2767.	414.
10	8.140	78.	2499.	10.	4717.	282.

Appendix B: Sources 1 and 2

511	8.190	88.	1957.	28.	3786.	128.
12	7.210	75.	2955.	4.	5322.	588.
13	5.480	72.	23906.	1.	45641.	2171.
14	6.000	61.	1720.	13.	3197.	242.
15	4.900	59.	4563.	2.	8206.	920.
16	4.550	51.	4519.	1.	6810.	2227.
17	4.400	19.	4387.	6.	8495.	280.
18	5.800	14.	1182.	13.	2199.	166.
19	7.000	7.	2002.	12.	3826.	178.
20	5.980	357.	382.	15.	541.	223.
21	4.850	350.	396.	25.	694.	98.
22	4.150	328.	370.	12.	564.	176.
23	5.740	317.	2239.	3.	3274.	1203.
24	6.200	302.	42454.	10.	84615.	294.
25	6.510	283.	866.	27.	1627.	104.
26	2.250	277.	1079.	5.	1946.	212.
27	3.600	258.	455.	10.	794.	115.
28	4.750	260.	450.	23.	836.	64.
29	5.780	250.	606.	19.	1127.	86.
30	7.350	246.	2073.	6.	3736.	410.
31	2.050	305.	283.	34.	523.	43.
32	2.480	252.	1996.	2.	3581.	411.
33	3.650	220.	4625.	16.	9205.	45.
34	4.320	209.	3918.	7.	7712.	125.
35	5.730	215.	10370.	1.	19390.	1349.

Appendix B. Sources 3 and 4

N	R	BEAR	RMEAN	CMEAN	RMAX	RMIN
301	3.810	214.	976.	4.	1080.	872.
2	4.560	226.	1414.	20.	2715.	114.
3	5.720	236.	2001.	11.	3812.	190.
4	7.310	233.	666.	127.	1305.	27.
5	6.750	242.	1636.	5.	2710.	563.
6	7.800	242.	4809.	4.	8831.	787.
7	7.660	249.	804.	10.	1305.	303.
8	8.900	242.	1558.	41.	3042.	73.
9	9.950	240.	1581.	13.	2799.	364.
10	11.150	237.	1584.	17.	2942.	225.
11	11.860	232.	1956.	17.	3595.	317.
12	11.640	238.	1567.	9.	2476.	658.
13	12.250	243.	507.	30.	792.	223.
14	9.310	251.	2794.	13.	5354.	233.
15	6.950	256.	1100.	8.	1852.	348.
16	6.760	264.	489.	11.	650.	328.
17	7.600	273.	328.	29.	574.	83.
18	7.370	284.	243.	40.	433.	54.
19	6.900	292.	238.	221.	468.	8.
20	5.550	304.	215.	66.	407.	22.
21	7.900	237.	3253.	38.	6414.	92.
22	9.050	234.	45332.	0.	76552.	14112.
23	10.200	232.	372943.	0.	733962.	11924.
24	11.700	229.	1047.	24.	1852.	243.
25	13.200	226.	3585.	3.	4764.	2405.

Appendix B. Sources 3 and 4

N	R	BEAR	RMEAN	CMEAN	RMAX	RMIN
326	12.920	247.	3412.	12.	6311.	513.
27	NO SIGNAL					
28	NO SIGNAL					
29	5.880	221.	1072.	14.	1910.	234.
30	7.300	220.	634.	317.	1256.	12.
31	8.500	220.	1312.	61.	2553.	71.
32	9.000	258.	369.	56.	691.	46.
33	NO SIGNAL					
601	2.650	52.	14679.	3.	29235.	122.
2	4.460	53.	11972.	1.	23026.	918.
4	6.830	54.	32196.	3.	63902.	489.
5	7.790	57.	4629.	2.	7724.	1533.
6	6.550	66.	10657.	1.	19548.	1765.
7	5.080	70.	6905.	6.	13604.	206.
8	8.710	53.	2537.	13.	4785.	289.
9	10.050	49.	6409.	2.	11588.	1230.
10	11.250	47.	4969.	2.	8078.	1861.
11	13.080	46.	3104.	23.	5927.	280.
12	11.860	51.	2436.	6.	4278.	594.
13	NO SIGNAL					
14	2.950	170.	453.	9.	674.	231.
15	3.640	149.	1224.	4.	1970.	478.
16	4.750	137.	485.	11.	672.	297.
17	5.900	133.	1366.	7.	2120.	411.

Appendix B: Sources 3 and 4.

N	R	BEAR	RMEAN	CMEAN	RMAX	RMIN
618	6.510	117.	1011.	7.	1510.	512.
19	6.520	104.	3370.	8.	6423.	316.
20	7.220	96.	5452.	9.	10679.	226.
21	8.670	89.	2505.	5.	4434.	575.
22	9.050	78.	982.	25.	1763.	201.
23	NO SIGNAL					
24	NO SIGNAL					
25	3.580	194.	846.	11.	1549.	144.
26	5.180	194.	4052.	2.	7321.	782.
27	6.240	188.	1086.	13.	1955.	216.
28	7.250	189.	1868.	20.	3600.	135.
29	8.550	188.	629.	48.	1173.	85.
30	7.220	200.	847.	22.	1574.	120.
31	8.320	204.	1438.	7.	2345.	530.
32	9.830	208.	1623.	9.	2650.	595.
33	4.590	175.	2716.	14.	5327.	105.
34	3.770	168.	4132.	1.	7223.	1041.
35	4.860	151.	1281.	7.	2330.	231.
36	6.340	143.	598.	35.	1102.	95.
37	NO SIGNAL					
801	2.200	220.	1283.	4.	2180.	386.
2	0.750	220.	2928.	1.	5003.	854.
3	0.650	349.	95961.	2.	191778.	145.
4	1.900	3.	1228.	2.	1969.	486.
5	2.580	6.	3762.	2.	6989.	534.

Appendix B. Sources 3 and 4.

806	4.700	8.	431.	24.	813.	50.
7	5.900	19.	839.	8.	1437.	240.
8	7.450	23.	2736.	6.	5072.	400.
9	8.100	7.	662.	17.	1109.	216.
10	7.240	359.	589.	8.	672.	505.
11	6.450	350.	388.	13.	527.	249.
12	6.150	334.	266.	100.	514.	18.
13	5.760	320.	168.	150.	327.	9.
14	2.320	127.	7548.	1.	13489.	1608.

Appendix B: Sources 5 and 6.

N	R	BEAR	RMEAN	CMEAN	RMAX	RMIN
401	1.400	247.	2115.	3.	3886.	344.
2	2.900	231.	943.	6.	1744.	143.
3	4.500	230.	12164.	1.	22958.	1369.
4	5.980	227.	3467.	3.	6260.	674.
5	7.460	224.	7492.	1.	12095.	2889.
6	9.050	221.	4744.	6.	9128.	360.
7	10.450	219.	4567.	2.	7640.	1495.
8	11.860	220.	1363.	10.	2353.	372.
9	6.500	260.	2097.	24.	4132.	62.
10	7.050	272.	4416.	3.	8298.	535.
11	7.950	261.	2115.	17.	4079.	152.
12	9.200	252.	3336.	4.	5940.	732.
13	10.440	245.	6612.	3.	12130.	1095.
14	10.120	238.	4511.	4.	8398.	623.
15	6.050	257.	1377.	8.	2573.	182.
16	5.900	307.	945.	5.	1374.	516.
17	6.900	331.	909.	8.	1285.	534.
18	7.700	328.	2830.	21.	5488.	172.
19	7.800	320.	321.	63.	579.	64.
20	7.590	310.	62.	190.	104.	20.
21	7.690	299.	66.	100.	100.	33.
22	8.220	290.	165.	55.	264.	65.
23	7.600	287.	424.	15.	639.	209.
24	6.300	323.	2952.	8.	5480.	425.
25	5.680	331.	1873.	7.	3330.	416.

Appendix B. Sources 5 and 6

N	R	BEAR	RMEAN	CMEAN	RMAX	RMIN
426	11.850	240.	9149.	1.	15330.	2969.
27	12.600	235.	5275.	3.	8899.	1652.
28	14.400	238.	3027.	11.	5581.	474.
29	15.850	241.	2105.	18.	3983.	227.
30	13.100	266.	2658.	9.	4868.	448.
31	11.680	254.	1076.	23.	2010.	142.
32	13.200	251.	1639.	62.	3221.	57.
33	10.500	263.	425.	158.	831.	19.
34	10.780	286.	793.	10.	1008.	578.
701	1.100	93.	1351.	2.	2445.	257.
2	1.630	65.	3657.	5.	7187.	127.
3	2.150	36.	1085.	8.	2072.	98.
4	3.100	33.	1274.	5.	2306.	242.
5	4.350	28.	2738.	4.	5112.	364.
6	5.700	30.	932.	6.	1391.	472.
7	6.620	30.	2166.	9.	4070.	261.
8	2.200	70.	2639.	14.	5226.	53.
9	4.150	63.	2570.	38.	5094.	45.
10	6.300	54.	4974.	4.	9447.	500.
11	7.840	55.	13766.	1.	19143.	8390.
12	8.850	52.	2395.	3.	2590.	2200.
13	10.600	43.	17234.	7.	34031.	437.
14	12.440	39.	60667.	1.	118160.	3173.
15	12.730	34.	4104.	11.	7806.	402.
16	5.180	131.	3469.	29.	6858.	80.
17	6.800	139.	2806.	31.	5559.	53.

Appendix B. Sources 5 and 6

N	R	BEAR	RMEAN	CMEAN	RMAX	RMIN
718	6.050	115.	7856.	9.	15485.	228.
19	7.750	99.	1897.	9.	3358.	437.
20	7.900	85.	7329.	8.	14358.	300.
21	9.620	86.	4236.	7.	7838.	635.
22	11.400	37.	3382.	8.	6233.	530.
23	7.950	33.	4413.	2.	7310.	1516.
24	9.550	36.	2188.	9.	3891.	486.
25	12.180	23.	5434.	14.	10594.	275.
26	14.800	57.	4004.	18.	7665.	343.
27	14.140	70.	4189.	5.	7424.	954.
901	1.780	150.	15122.	1.	29376.	868.
2	2.540	181.	2522.	30.	5008.	37.
3	3.940	186.	1098.	6.	1962.	234.
4	5.280	191.	2642.	8.	5073.	211.
5	6.820	191.	1984.	35.	3909.	59.
6	8.470	193.	3531.	11.	6843.	219.
7	9.850	192.	4712.	8.	9033.	391.
8	10.650	187.	3282.	10.	6216.	349.
9	4.000	284.	383.	51.	739.	27.
10	4.650	271.	206.	15.	251.	162.
11	5.350	256.	286.	226.	567.	5.
12	6.800	242.	3642.	3.	6547.	736.
13	8.330	235.	4269.	6.	8222.	316.
14	9.550	230.	2884.	5.	5257.	512.
15	11.400	228.	3760.	3.	5854.	1665.
16	3.910	295.	219.	28.	377.	61.
17	4.140	313.	1289.	3.	1957.	620.

Appendix B. Sources 5 and 6.

18	4.640	326.	267.	18.	418.	115.
19	5.150	337.	1070.	13.	1978.	162.
20	5.790	347.	2526.	12.	4854.	197.
21	7.100	356.	2328.	5.	4006.	651.
22	9.850	6.	21959.	2.	40329.	3590.
23	8.930	322.	58.	5077.	115.	1.
24	7.250	340.	2195.	13.	4108.	281.
25	NO SIGNAL					
26	8.180	346.	3143.	7.	5765.	522.
27	9.250	346.	684.	22.	1203.	164.

APPENDIX C. Tabulation of observed data.

N. Station number, keyed to maps and plates. Stations with numbers beginning with the digits 2 or 5 were associated with sources 1 and 2; stations with numbers beginning with the digits 3, 6 or 8 were associated sources 3 and 4; stations with numbers beginning with the digits 4, 7 or 9 were associated with sources 5 and 6.

R. The distance from the common point of a pair of sources to a receiver station, in kilometers.

BEAR. Bearing from the common point of the sources to a receiver station, in degrees clockwise from north.

B1,B2. The bearing of each line of an orthogonal pair used at the receiver station to measure electric field. Measured in degrees from north.

V1,V2. The voltage measured in the directions B1 and B2, respectively. Two sets of voltages are recorded, one for each of the pair of sources. Voltages are recorded in microvolts.

I. Current, amperes peak to peak.

L. Length of a receiver line, in meters.

L1,L2. The length of a source bipole, in kilometers.

B1,B2. The bearing of a source bipole, referred to the common point of a pair.

Project: Virginia Hot Springs

L1 = 1.22 L2 = 1.60
B1 = 110° B2 = 203°

					SOURCE 1				SOURCE 2			
N	R	Bear	Receiver B1	Receiver B2	V1	V2	I	L	V1	V2	I	L
201	.93	296.5	120	28	102 500	-31 500	6.6	30	45 000	102 000	6.8	30
202	2.14	209	329	46	29 000	-105 000	6.6		11 500 000	44 500 000	6.8	
203	3.13	209	230	130	-1400	3200	6.6		-7700	900	6.8	
204	2.88	88	300	208	-725	-2500	6.6		2850	-5500	6.8	
205	3.00	161	243	323	-875	-163	6.6		6100	-3200	6.8	
206	1.00	85	168	269	40000	-98000	6.6		23850	-20750	6.8	
207	2.15	80	192	285	3400	8200	6.6		5000	-200	6.8	
208	3.90	154.5	265	165	2200	-1000	7.1		7200	-4300	7.4	
209	4.75	149.	142	52	-300	0	7.1		210	-1300	7.4	
210	4.18	170.5	251	328	340	1400	7.1		5750	6100	7.4	

X_1 0 X_2 -.66 X_3 0 X_4 1.14

Y_1 0 Y_2 -1.5 Y_3 0 Y_4 .47

Project: Virginia Hot Springs

					SOURCE 1				SOURCE 2			
N	R	Bear	Receiver B1	Receiver B2	V1	V2	I	L	V1	V2	I	L
211	5.14	180	64	160	360	-350	7.1	30	-1500	-3200	7.4	30
212	6.44	188	147	44	-150	75	7.1		-2900	-90	7.4	
213	7.43	194.5	320	68	130	100	7.1		-2700	530	7.4	
214	7.95	191	280	197	130	-480	7.1		2250	-5100	7.4	
215	8.32	184	174	268	115	-140	7.1		80	-130	7.4	
216	7.38	177	114	204	0	0	7.1		-180	-90	7.4	
217	6.55	171	139	226	-35	-80	7.1		-140	0	7.4	
218	4.75 ~~5.42~~	149	52	142	-300	0	7.1		-1250	210	7.4	
219	5.42	158	110	199	-450	-210	7.1		0	-380	7.4	
220	5.96	150	318	44	170	0	7.1		460	-110	7.4	

Project: Virginia Hot Springs

					SOURCE 1				SOURCE 2			
N	R	Bear	Receiver B1	Receiver B2	V1	V2	I	L	V1	V2	I	L
221	6.55	145	123	233	0	0	7.5	30	-110	140	7.8	30
222	6.95	153	310	45	0	0	7.5		14	-64	7.8	
223	6.14	84.5 ~~95~~	293	20	200	240	7.5		-320	-650	7.8	
224	5.03	95	314	53	350	55	7.5		0	-1050	7.8	
225	3.20	105	270	350	570	5100	7.5		2200	-2650	7.8	
226	4.41	110	215	305	0	180	7.5		300	-220	7.8	
227	4.65	134	258	349	240	40	7.5		200	-200	7.8	
228	4.70	141	52	316	-260	550	7.5		-1500	140	7.8	
229	8.10	53.5	250	350	-120	-140	7.2		0	130	7.5	
230	8.32	61.	158	55	-220	-180	7.2		195	250	7.5	

Project: Virginia Hot Springs

L1 = 1.22
B1 = 110°

L2 = 1.60
B2 = 2030

					SOURCE 1				SOURCE 2			
N	R	Bear	Receiver B1	Receiver B2	V1	V2	I	L	V1	V2	I	L
231	7.62	69	305	30	120	0	7.2	30	-85	30	7.5	30
232	7.20	81	63	337	-100	0	7.2		-500	-1000	7.5	
233	7.10	90.5	310	37	60	-7.5	7.2		-240	-90	7.5	
234	6.19	105	106	11	-230	280	7.2		0	0	7.5	
235	6.12	123	36	302	15	280	7.2		-130	0	7.5	
236	6.23	132	303	33	170	20	7.2		230	-45	7.5	
237	7.73	159.5	249	19	67	65	7.2		350	-35	7.5	
238	8.68	165.5	286	18	-5	20	7.2		-10	-15	7.5	
239	5.42	158	118	213	-60	-230	7.2		-680	-400	7.5	
240	6.90	164	27	296	50	-10	7.2		100	-340	7.5	
241	7.38	178	208	113	0	0	7.2		-100	-225	7.5	

Project: Virginia Hot Springs

200s and 500s are from same sources.

					SOURCE 1				SOURCE 2			
N	R	Bear	Receiver B1	Receiver B2	V1	V2	I	L	V1	V2	I	L
501	0.75	226	335	90	35000	-16000	6.6	31.4	35000	-18000	6.8	31.4
502	1.63	0	337	248	4600	-2700	6.6		4600	-2000	6.8	
503	2.13	18	007	270	2100	1700	6.6		2650	3250	6.8	
504	2.85	40	350	216	1300	-5100	6.6		2300	-4850	6.8	
505	3.87	36	181	269	9100	-1300	6.6		850	-550	6.8	
506	5.05	34	291	320	-1650	450	6.6		1000	-2750	6.8	
507	6.60	38	336	230	-450	185	6.6		240	-630	6.8	
508	7.65	46	184	279	55	180	6.6		-230	-450	6.8	
509	8.53	48	317	283	-42.5	180	6.6		22	-240	6.8	
510	8.14	78	253	156	38	32	7.1		22	600	7.4	

x_1 0 x_2 -.3? x_3 0 x_4 1.14

y_1 0 y_2 -1.5 y_4 -.47

Project: Virginia Hot Springs

					SOURCE 1				SOURCE 2			
N	R	Bear	Receiver B1	Receiver B2	V1	V2	I	L	V1	V2	I	L
511	8.19	87.5	344	93	75	-40	7.1	31.4	500	200	7.4	31.4
512	7.21	74.5	002	116	120	90	7.1		65	780	7.4	
513	5.48	72.	115	003	-10300	690	7.1		7900	-1100	7.4	
514	6.00	60.5	27	114	-1030	-340	7.1		800	340	7.4	
515	4.90	58.5	75	161	-4400	1780	7.1		1420	75	7.4	
516	4.55	51	103	338	3400	-4100	7.1		1600	-95	7.4	
517	4.40	19	110	322	1650	-215	7.1		2680	-415	7.4	
518	5.80	14	127	52	-270	85	7.1		-480	45	7.4	
519	7.00	7	240	352	-60	110	7.1		90	340	7.4	
520	5.98	357	38	152	70	-80	7.1		35	-115	7.4	

Project: Virginia Hot Springs

					SOURCE 1				SOURCE 2			
N	R	Bear	Receiver B1	Receiver B2	V1	V2	I	L	V1	V2	I	L
521	4.85	350	55	177	43	-180	7.1	31.4	0	-250	7.4	31.4
522	4.15	328	143	10	-170	180	7.1		-205	85	7.4	
523	5.74	317	240	140	0	-950	7.1		350	-1100	7.4	
524	6.20	302	10	181	20	-30	7.1		0	-40	7.4	
525	6.51	283	21	302	-35	250	7.1		0	250	7.4	
526	2.25	277	007	155	1460	-5650	7.4		550	-4500	7.8	
527	3.60	258	71	215	-900	320	7.4		-540	560	7.8	
528	4.75	260	72	211	-280	55	7.4		-320	185	7.8	
529	5.78	2495	108	219	-260	180	7.4		-165	200	7.8	
630	7.35	2455	77	16	-95	90	7.4		0	-475	7.8	

Project: Virginia Hot Springs

					SOURCE 1				SOURCE 2			
N	R	Bear	Receiver B1	Receiver B2	V1	V2	I	L	V1	V2	I	L
531	2.05	305	230	110	-525	-2150	7.4	31.4	-375	-2280	7.8	31.4
532	2.48	252	154	252	0	4850	7.4		7000	8300	7.8	
533	3.65	220	253	006	-800	500	7.4		-7600	1800	7.8	
534	4.32	209	69	165	630	960	7.4		2850	-2850	78	
535	5.73	215	58	193	1100	-2720	7.2		3550	-3200	7.2	
536	7.25	216	73	202	1220	-1520	7.2		1480	150	7.2	
537	8.40	215	201	294	55	12	72		-550	-390	7.2	
538	9.25	216.5	114	222	-40	40	7.2		8300	180	7.2	
539	10.50	218	42	301	-10	7	7.2		228	-72	7.2	
640	11.34	218	17	267	-7.5	-15	7.2		-175	120	7.2	

Project: Virginia Hot Springs

					SOURCE 1				SOURCE 2			
N	R	Bear	Receiver B1	Receiver B2	V1	V2	I	L	V1	V2	I	L
541	12.28	221	76	182	-10	17	7.2	31.4	-20	138	7.2	31.4
542	8.18	212.5	224	126	-140	530	7.2		-860	-25	7.2	
543	7.56	211	280	002	-620	-40	7.2		-810	700	7.2	
544	7.87	206.5	285	140	-105	55	7.2		-660	-1080	7.2	

Sources 3,4

Project: Virginia Hot Springs

300's
600's
800's

L1 = 1.65
B1 = 28°

L2 = 1.50
B2 = 352.5°

					SOURCE 1				SOURCE 2			
N	R	Bear	Receiver B1	Receiver B2	V1	V2	I	L	V1	V2	I	L
301	3.81	214	2	96	1000 L	380 L	6.1	30	380 L	670 L	5.1	30
302	4.56	226	35	128	800 L	1325 R	6.1		38 L	45 L	5.2	
303	5.72	235	106	15	775 L	90 L	6.1		1025 L	160 L	5.3	
304	7.31	233	345	90	220 R	70 L	6.2		520 R	260 R	5.3	
305	6.75	242	20	110	160 R	400 L	6.1		280 R	260 L	5.3	
306	7.80	242	330	55	950 R	400 L	6.1		575 R	100 L	5.3	
307	7.66	249	319	224	80 R	120 L	6.3		120 R	60 L	5.5	
308	8.90	242	294	23	140 R	160 R	6.3		120 R	140 R	5.5	
309	9.95	240	129	227	160 L	NS	6.1		130 L	30 L	5.1	
310	11.15	237	26	157	10 R	80 L	6.1		23 R	80 L	5.1	

X_1 0 X_2 1.29 X_3 0 X_4 -1.61

Y_1 0 Y_2 1.1 Y_3 0 Y_4 1.48

Project: Virginia Hot Springs

					SOURCE 1				SOURCE 2			
N	R	Bear	Receiver B1	Receiver B2	V1	V2	I	L	V1	V2	I	L
311	11.86	232	17	297	25 L	115 R	6.1	30	30 R	85 R	5.1	30
312	11.64	238	309	35	90 R	42 L	6.1	↓	70 R	NS	5.1	↓
313	12.25	243	358	267	30 L	15 R	6.2		18 R	NS	5.2	
314	9.31	251	139	62	340 L	15 R	6.2	↓	170 L	38 R	5.2	↓
315	6.95	256	193	286	70 L	280 R	6.2		135 L	120 R	5.2	
316	6.76	264	130	216	110 L	75 R	6.2		NS	115 L	5.2	
317	7.60	273	173	91	35 L	NS	6.2		60 L	48 R	5.2	
318	7.37	284	317	41	20 L	35 R	6.1		NS	35 R	5.2	
319	6.90	292	113	36	NS	40 R	6.1		NS	80 R	5.2	
320	5.55	303.5	28	118	45 R	50 L	6.1		75 R	145 R	5.2	

Project: Virginia Hot Springs

					SOURCE 1				SOURCE 2			
N	R	Bear	Receiver B1	Receiver B2	V1	V2	I	L	V1	V2	I	L
321	7.90	237	53	151	150 L	875 R	6.1	30	38 L	290 R	5.2	30
322	9.05	234	41	126	7500 L	2000 R	6.2		440 L	1200 R	5.2	
323	10.20	232	9	111	660 R	720 L	6.2		500 R	450 L	5.2	
324	11.70	228.5	8	269	70 L	NS	6.2		30 R	NS	5.2	
325	13.20 ~~12~~	226	33	298	90 L	NS	6.2		30 L	110 R	5.2	
326	12.92	246.5	198	283	175 R	50 R	6.1		175 L	30 L	5.1	
327	13.95	249	—		—		6.1		—		5.1	
328	10.05	257	—		—		6.1		—		5.1	
329	5.88	221	35	297	565 L	180 R	6.1		380 L	180 R	5.2	
330	7.30	220	33	303	220 L	NS	6.1		120 L	NS	5.2	

Project: Virginia Hot Springs

					SOURCE 1				SOURCE 2			
N	R	Bear	Receiver B1	Receiver B2	V1	V2	I	L	V1	V2	I	L
331	8.50	220	8	98	290 L	55 L	6.2	30	150 L	30 L	5.2	30
332	9.00	258	120	5	NS	20 R	6.2	30	10 R	45 R	5.2	30
333			319	140	32 R	75 L	6.2	30	NS	100 L	5.2	30
334												
335												
336												
337												
338												
339												
340												

Project: Virginia Hot Springs

					SOURCE 1				SOURCE 2			
N	R	Bear	Receiver B1	Receiver B2	V1	V2	I	L	V1	V2	I	L
601	2.65	52	132	48	~~-0-~~ ~~200~~	-3500 ~~200~~	6.1	31.4	-39700 ~~340~~	3600 ~~-4500~~	5.1	31.4
602	4.46	53	224	85	8200	-890	6.1		5600	-1250	5.2	
603	5.52	56	245	343	-800	500	6.1		0	650	5.3	
604	6.83	54	202	71	160	45	6.2		7700	-1870	5.3	
605	7.79	57	260	171	1620	-15	6.1		110	-220	5.3	
606	6.55	66	344	207	-1700	550	6.1		-1700	-25	5.3	
607	5.08	70	20	118	200	200	6.3		-4500	340	5.5	
608	8.71	52.5	200	120	650	-170	6.1		-375	-230	5.2	
609	10.05	48.5	200	270	220	-75	6.1		440	400	5.2	
610	11.25	47	269	15	-200	300	6.1		-220	45	5.2	

x_1 0 x_2 1.5 1 x_3 0 1.1 -1.61

y_1 0 y_2 1.1 y_3 0 3.4 1.18

Project: Virginia Hot Springs

					SOURCE 1				SOURCE 2			
N	R	Bear	Receiver B1	Receiver B2	V1	V2	I	L	V1	V2	I	L
611	13.08	46	265	40	240	-30	6.2	31.4	-85	10	5.2	31.4
612	11.86	51	341	63	-32	45	6.2		-120	-25	5.2	
~~613~~	—		~~294~~	~~55~~	—	—			-	-		
614	2.95	170	320	84	-460	-80	6.2		0	-860	5.2	
615	3.64	149	26	145	700	-100	6.2		360	840	5.2	
616	4.75	137	272	187	-140	-95	6.2		-390	90	5.2	
617	5.90	133	278	41	440	-230	6.2		480	-35	5.2	
618	6.51	117	223	308	-75	-100	6.2		330	-185	5.2	
619	6.52	104	215	299	-20	-95	6.2		1350	-340	5.2	
620	7.22	95.5	194	105	-880	110	6.2		-1100	235	5.2	

Project: Virginia Hot Springs

					SOURCE 1				SOURCE 2			
N	R	Bear	Receiver B1	Receiver B2	V1	V2	I	L	V1	V2	I	L
621	8.67	89	136	38	-380	150	6.2	31.4	70	120	5.1	31.4
622	9.05	78	312	57	820	-110	6.2		-360	90	5.1	
~~623~~												
~~624~~												
625	3.58	193.5	86	180	438	-188	6.1		1000	625	5.1	
626	5.18	194	128	002	219	1016	6.1		-391	-328	5.1	
627	6.24	188	163	57	294	138	6.1		66	-50	5.2	
628	7.25	189	223	98	59	25	6.1		375	25	5.2	
629	8.55	188	310	204	-119	-41	6.1		-44	9	5.2	
630	7.22	200	92	205	28 ~~311~~	26	6.2		160 ~~80~~	54	5.2	

Project: Virginia Hot Springs

					SOURCE 1				SOURCE 2			
N	R	Bear	Receiver B1	Receiver B2	V1	V2	I	L	V1	V2	I	L
631	8.32	204	201	80	131	68.8	6.2	31.4	-25	-43.8	5.1	31.4
632	9.83	207.5	346	90	-162	-83	6.2		-0-	-43.8	5.1	
633	4.59	175	238	133	-562	-0-	6.2		1125	531	5.1	
634	3.77	168	116	340	1312	781	6.2		-719	-781	5.1	
635	4.86	151	192	262	-388	175	6.2		112	0	5.1	
636	6.34	143	282	164	-25	25	6.2		-288	81	5.1	
637	8.03	144	322	42	0	0	6.2		62	-75	5.1	

* Questionable value.
DEFINITELY not Reliable
IF ROTATED.

SOURCE 1 SOURCE 2

	N	R	Bear	Receiver B1	Receiver B2	V1	V2	I	L	V1	V2	I	L	
A1	801	2.20	220	298	28	~~975 L~~ ~~175 R~~	8000 R ~~50 R~~	6.1	30	210 R ~~175 L~~	8000 R ~~30 L~~	5.1	30	*
A2	802	0.75	220	300	30	137500 L	106 000 R	6.1		137500 L	100 000 R	5.1		*
A3	803	0.65	349	346	256	10000 R	2800 L	6.1		2.4×10^6 L	2.45×10^6 L	5.1		
A4	804	1.90	3	51	321	6400 R	2350 L	6.1		2375 L	8200 L	5.1		
A5	805	2.58	6	169	295	310 L	2750 L	6.2		4350 R	3450 R	5.1		
A6	806	4.70	8	281	5	248 L	—	6.2		530 R	110 L	5.1		*
A7	807	5.90	18.5	196	104	80 R	150 R	6.2		440 R	25 L	5.1		
A8	808	7.45	23	321	46	22 L	500 L	6.2		218 L	675 L	5.2		
A9	809	8.10	7	146	46	100 R	80 L	6.2		160 R	50 L	5.2		
A10	810	7.24	358.5	153	51	50 R	120 L	6.2		180 L	50 R	5.2		

x_1 0 x_2 1.81 x_3 0 x_4 -1.61

y_1 0 y_2 1.1 y_3 0 y_4 1.43

Project: Virginia Hot Springs

						SOURCE 1				SOURCE 2			
	N	R	Bear	Receiver B1	Receiver B2	V1	V2	I	L	V1	V2	I	L
A11	811	6.45	350	139	46	70 R	70 R	6.2	30	210 R	40 L	5.2	30
A12	812	6.15	334	334	60	100 R	40 R	6.2		85 L	20 R	5.2	
A13	813	5.76	320	150	237	18 L	65 L	6.2		18 R	40 L	5.2	
AH	814	2.32	127	25	235	1050 L	6750 L	6.2		16250 L	6000 L	5.2	

Project: Virginia Hot Springs

N-S
SMITH CREEK RD SOURCE
SOURCE 1

E-W
SOURCE 2

N	R	Bear	Receiver B1	Receiver B2	V1	V2	I	L	V1	V2	I	L
401	1.40	246.5	303	190	54000R	90600 R	11.3	30	2000R	3200R	8.8	30
402	2.90	231	300	224	9750L	~~1995R~~ 37500 R	11.3	↓	525 R	1975 R	8.8	↓
403	4.50	229.5	112	28	7900L	1650 L	11.3	↓	18[illegible]R	11800 R	8.8	
404	5.98	227	320	43	1700L	6000R	11.4		160R	1240L	8.9	
405	7.46	224	240	133	4250L	675 L	11.4		1180R	260R	8.9	
406	9.05	221	312	190	~~145R~~ 400L	980L	11.4		~~580R~~ 145R	380R	8.9	
407	10.45	218.5	326	56	220R	710R	11.4		90L	295L	8.9	
408	11.86	220	32	128	140R	45L	11.4		63L	~~[illegible]~~ 18 R	8.9	
409	6.50	260.5	265	163	120L	290R	11.3		450 L	410 L	8.8	
410	7.05	272	30	295	280L	1850 L	11.3		20R	950 R	8.9	

x_1 0 x_2 -1.63 x_3 0 x_4 .64

y_1 0 y_2 -1.12 y_3 0 y_4 -.93

Project: Virginia Hot Springs

					SOURCE 1				SOURCE 2			
N	R	Bear	Receiver B1	Receiver B2	V1	V2	I	L	V1	V2	I	L
411	7.95	261	215	307	20R	750L	11.3	30	~~NS~~	450R	8.9	30
412	9.20	252	197	112	175R	680R	11.3		75R	380L	8.9	↓
413	10.44	244.5	36	129	700R	850R	11.3		400L	320L	8.9	
414	10.12	238	346	240	135R	325L	11.3		180L	380R	8.9	
415	6.05	256.5	208	118	280R	400R	11.3	↓	130L	500L	8.9	
416	5.90	307	30	298	60L	720L	11.3		180R	200R	8.9	
417	6.90	331	143	52°	100R	140L	11.3		260L	80R	8.9	
418	7.70 ~~6.30~~	328	197	287	220L	30L	11.3		~~90~~ 740R	220R	8.9	
419	7.80	319.5	326	257	15L	20L	11.4		35L	65R	8.9	
420	7.59	310	75	172	10L	NS	11.4		15L	10R	8.9	

Project: Virginia Hot Springs

					SOURCE 1				SOURCE 2			
N	R	Bear	Receiver B1	Receiver B2	V1	V2	I	L	V1	V2	I	L
421	7.69	298.5	43	151	20L	10R	11,4	30	—	10L	8.8	30
422	8.22	290	78	340	—	20L	11,4	↓	30L	NS	8.8	↓
423	7.60	287	280	197	70L	160 R	11,4		35 R	40R	8.8	
424	6.30	323	211	116	210R	140L ~~1425L~~	11.4		190 L	1425 L	8.8	
425	5.68	330,5	333	53	220L	290 L	11.4		950R	110 L	8.8	
426	11.85	240	42	306	500 R	85 R	11.3		220 L	350 L	8.8	
427	12.60	235	350	223	120L	370 L	11,4		NS	160 R	8.8	
428	14.40	237.5	37	278	120R	250 L	11.4		60L	80R	8.8	
429	15.85	241	223	133	15 L	8 L	11.3		40R	25 R	8.8	
430	13.10	266	222	130	30L	50L	11.3		40R	95 R	8.8	

Project: Virginia Hot Springs

					SOURCE 1				SOURCE 2			
N	R	Bear	Receiver B1	Receiver B2	V1	V2	I	L	V1	V2	I	L
431	11.68	254	245	343	35 L	5 L	11.3	30	60 R	25 L	8.8	30
432	13.20	251	5	267	20 R	40 L	11.2	↓	40 L	60 R	8.7	↓
433	10.50	263	152	60	10 R	20 R	11.2	↓	12 L	35 L	8.7	
434	10.78	286	188	98	100 R	NS	11.2		NS	40 L	8.7	
901 B1	1.78	150	91	0	95000 R	3150 L	11.3		275000 L	150000 R	8.8	
902 B2	2.54	181	323	51	1360 L	135 L ~~9000 L~~	11.3		27500 L	9000 L ~~[illegible]~~	8.8	
903 B3	3.94	186	269	1°	700 L	300 L	11.3		1650 R	2750 R	8.8	
904 B4	5.28	191	92	351	220 L	190 L	11.4		1700 R	2150 R	8.9	
905 B5	6.82	191	126	39	60 L	110 L	11.4		60 L	1000 R	8.9	
906 B6	8.47	193	138	40	50 L	130 L	11.4		93 L	840 R	8.9	
	x_1 0		x_2 -1.63		x_3 0	x_4 .64						
	y_1 0		y_2 -.112		y_3 0	y_4 -.93						

Sources 5,6

Project: Virginia Hot Springs

700's
400's
900's

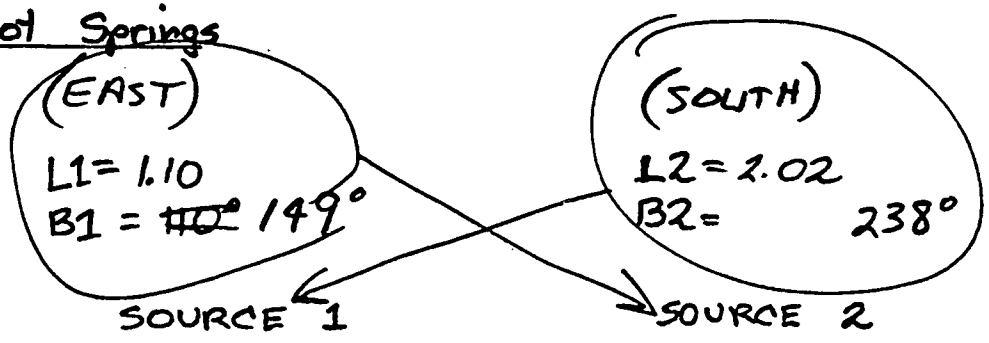

N	R	Bear	Receiver B1	Receiver B2	V1	V2	I	L	V1	V2	I	L
701	1.11	93	67	325	6250	9750	11.2	31.4	-15000	-95000	8.8	31.4
702	1.63	65	188	308	812	24000	11.4		-4188	-37200	8.8	
703	2.15	36	245	135	890	-3750	11.4		-2344 &	3375	8.9	
704	3.10	33	270	006	-87.5	-2343	11.4		781	1312	8.9	
705	4.35	28	253	18	-68.8	-1012	11.4		437	1250	8.9	
706	5.70	30	205	286	-175	-356	11.4		206	-175	8.9	
707	6.62	30	342	63	125	87.5	11.4		21.9	609	8.9	
708	2.20	70	227	322	-780	3940	11.3		-2750	-23440	8.9	
709	4.15	63	317	241	-580	-5500	11.3		-380	2190	8.9	
710	6.30	53.5	207	118	-260	510	11.4		140	1830	8.9	

X_1 0 X_2 -1.63 X_3 0 X_4 .64

Y_1 0 Y_2 -1.1 Y_3 0 Y_4 -.93

Project: Virginia Hot Springs

					SOURCE 1				SOURCE 2			
N	R	Bear	Receiver B1	Receiver B2	V1	V2	I	L	V1	V2	I	L
711	7.84	54.5	146	242	-20	4440	11.3	31.4	-1090	-780	8.9	31.4
712	8.85	51.5	135	237	10	600	11.3		-160	20	8.9	
713	~~10.42~~ 10.60	43	255	150	10	-530	11.4		-190	1250	8.8	
714	~~12.44~~ 12.44	38.5	54	339	-190	2690	11.4		440	-2130	8.8	
715	12.73	34	40	135	30	130	11.4		0	200	8.8	
716	5.18	130.5	51	319	-20	-310	11.4		-450	5380	8.8	
717	6.80	139	295	23	-150	1530	11.4		-40	250	8.8	
718	6.05	114.5	28	142	-297	1125	11.4		572	-4875	8.8	
719	7.75	99	224	128	-22	538	11.4		150	-613	8.8	
720	7.90	84.5	285	337	-269	1625	11.4		-213	650	8.8	
~~721~~			103	320	281	-788			-213	500		

Project: Virginia Hot Springs

					SOURCE 1				SOURCE 2			
N	R	Bear	Receiver B1	Receiver B2	V1	V2	I	L	V1	V2	I	L
721	9.62	85.5	103	320	281	-788	11.4	31.4	-213	500	8.8	31.4
722	11.40	37	55	331	28	234	11.3		75	-203	8.7	
723	7.95	33	16	260	150	+438	11.4		-46.7	-625	8.8	
724	9.55	35.5	235	128	-53	-362	11.4		-87	250	8.8	
725	12.18	23	105	16	-25	62.5	11.3		200	225	8.8	
726	14.80	57	211	296	0	312	11.2		0	-75	8.8	
727	14.14	70	0	240	-38	-25	11.2		50	87.5	8.8	

Project: Virginia Hot Springs

						SOURCE 1				SOURCE 2			
	N	R	Bear	Receiver B1	Receiver B2	V1	V2	I	L	V1	V2	I	L
	907 B7	9.85	192	87	5	125L	15L	11.4	30	480R	560R	8.9	30
	908 B8	10.65	186.5	295	230	NS	60R	11.4		80R	325L	8.9	
C1	909	4.00	284	218	347	50L	140R	11.3		600R	600L	8.8	
C2	910	4.65	271	111	344	80R	420L	11.3		60L	60L	8.9	
C3	911	5.35	256	191	51	190R	220L	11.3		140R	150L	8.9	
C4	912	6.80	241.5	180	73	200L	2050R	11.3		640R	925L	8.9	
C5	913	8.33	235	176	93	850L	160L	11.3		650R	270R	8.9	
C6	914	9.55	230	102	198	250R	400L	11.3		45L	290R	8.9	
C7	915	11.40	228	330	30	50L	310R	11.3		40L	180L	8.9	
C8	916	3.91	295	212	312	850R	320L	11.3		170L	40R	8.9	

Project: Virginia Hot Springs

				SOURCE 1					SOURCE 2			
	N	R	Bear	Receiver B1	Receiver B2	V1	V2	I	L	V1	V2	I	L
C9	917	4.14	313	270	25	50R	1975L	11.3	30	170R	750R	8.9	30
C10	918	4.64	3255	328	240	NS	400R	11.3	↓	70R	90R	8.9	↓
C11	919	5.15	336.5	137	86	320L	310L	11.3	↓	385L	110R	8.9	↓
C12	920	5.79	347	320	226	100R	180R	11.4		1050R	480L	8.9	
C13	921	7.10	356	313	215	270R	25R	11.4		260R	430L	8.8	
D1	922	9.85	6	31	326	1450L	4400R	11.4		600L	2400R	8.8	
D2	923	8.93	322	352	250	15R	NS	11.4		8R	NS	8.8	
D3	924	7.25	340	129	226	200L	75R	11.4		700L	—	8.8	
D4	926	8.18	346	235	308	110R	NS	11.3		140L	500R	8.8	
D5	927	9.25	345.5	157	245	10L	55R	11.3		50L	45L	8.8	

APPENDIX D; Apparent resistivity in a uniform anisotropic medium.

Bath county, where the surveys described in this report were carried out, lies in the Appalachian folded belt. Here, rocks of early Paleozoic age have been severly folded into elongate structures, trending generally from northeast to southwest in Bath county. The individual layers making up the sedimentary section consist of carbonates and clastic rocks, with very strong resistivity contrasts between the two types of rock. A laminated sequence of materials with differing resistivities will exhibit of the property of electrical anisotropy, with conduction taking place more readily along the planes of separation than normal to these planes. This anisotropy exists, even though the layering is macroscopic. Keller (1968) has compiled values for the anisotropy due to layering in a number of sedimentary sections by making use of electric logs which record the actual resistivities in the individual layers. For a limestone-shale sequence, it was found that the anisotropy may be very great, with the coefficient of anisotropy being as large as 10 in Paleozoic limestone-shale sections. The coefficient of anisotropy is defined as the square root of the ratio of resistivity measured across the bedding to that measured along the bedding, so a coefficient of 10 corresponds to a resistivity change of 100;1.

Normally, sedimentary sections are primarily flat-lying, so that the vertical resistivity is much larger than the horizontal resistivity, and the horizontal resistivity will not depend on

direction. In an area like the Appalachians where the section is severely folded, there is a strong likelihood that anisotropy will exist also between the direction along the strike of the structure and the direction across the strike. So long as the section is flat-lying, the effect of anisotropy is undetectable on resistivity measurements made along the surface of the earth. On the other hand, if anisotropy causes a dependence of resistivity on direction in the horizontal plane, one might expect the patterns of resistivity measured with a surface-based survey to be affected. For this reason, some calculations were done to predict the effect of anisotropy on the patterns of resistivity measured in dipole mapping.

The theory for current flow in an anisotropic uniform medium is straingtforward, and has been described by Keller and Frischknecht (1966, pp100-104). In effect, the mathematical problem of determining the potential caused by current flow in an anisotropic medium is solved by transforming the coordinate system to stretch the dimension in the direction of high resistivity; thus converting the problem to one of determining potential in a uniform isotropic medium. The potential, U, observed at a point on the surface of an anisotropic uniform earth, caused by a current I flowing from a single electrode is:

$$U = \frac{IN\rho_1}{2\pi(x^2 + N^2y^2)^{1/2}}$$

where x and y are the coordinates of the observation point on the

surface, referred to an origin at the single current electrode, and N is the coefficient of anisotropy, as defined previously. In dipole mapping, the electric field is measured, rather than the potential. The electric field is determined by taking the negative gradient of the potential:

$$\vec{E}_1 = \frac{INx\rho_1\vec{i}}{2\pi(x^2+N^2Y^2)^{3/2}} + \frac{IN^3y\rho_1\vec{j}}{2\pi(x^2+N^2y^2)^{3/2}}$$

where ρ_1 is the longitudinal resistivity, or that measured in the direction of lowest resistivity.

In dipole mapping, the contribution to the electric field from a second source electrode at the return end of the source cable must be added to this quantity. A computer program was written to carry out the calculations of electric field components described in the equation above for one quadrant of the area around a bipole source, with the anisotropy coefficient a variable parameter. Calculations were restricted to one quadrant by making calculations only for a source bipole oriented along one of the principal directions of anisotropy. That is, only the cases in which the bipole source was oriented in the direction of maximum resistivity or minimum resistivity were treated, and in these cases, the symmetry of the potential field makes the resistivity patterns in each of the four quadrants the same. This did not comprise a serious restriction on the applicability of the results, because in the field surveys, the sources were oriented in these prime directions.

Computations were carried out for values of the coefficient of anisotropy (AN) ranging from 1.00 to 10. A coefficient of 1.00 corresponds to an isotropic earth; these calculations were done to check the validity of the program, and to provide a reference for comparison for the results obtained with anisotropy coefficients other than unity. The results are presented in a set of 32 maps accompanying this Appendix. The maps are organized as follows:

Figures D1-D8. Contour maps of apparent resistivity for the source bipole oriented along the direction of minimum resistivity. The coefficient of anisotropy increases through the sequence of maps, both in this and in the subsequent sets of maps.

Figures D9-D16. Maps with lines plotted indicating the direction of the electric field vector at each point on a grid where calculations were made. The source bipole is oriented along the direction of low resistivity for this set of maps. (It should be mentioned that the direction of current flow does not necessarily coincide with the direction of the electric field vector in an anisotropic medium, and so, this map does not exactly reflect the current flow paths.)

Figures D17-D24. Contour maps of apparent resistivity for the case in which the source bipole is oriented in the direction of highest resistivity.

Figures D25-D32. Maps showing the electric field directions when the source bipole is oriented along the direction of highest resistivity.

Some generalizations about the effect of anisotropy in the horizontal plane may be drawn from an examination of these maps.

Generalization 1: The effect of moderate anisotropy is moderate, while the effect of strong anisotropy is profound. For anisotropy ratios up to 2.0, the effect of anisotropy is not so marked that it would mask structural changes in resistivity. Beyond a coefficient of 2, the effect of anisotropy becomes so strong that it might be difficult to recognize any resistivity effects caused by structures other than the anisotropy.

Generalization 2: The largest apparent resistivities are observed at stations offset in the direction of lowest resistivity, no matter whether the source is oriented along the direction of maximum resistivity or the direction of minimum resistivity. At first thought, this result may seem inappropriate, but it is an example of the "paradox of anisotropy" which has long been recognized for the more conventional electrode arrays used in resistivity surveys. According to the paradox of anisotropy, if an electrode array is rotated on the surface of an anisotropic medium such as has been defined here, the maximum apparent resistivity will be recorded when the array is oriented along the direction of least resistivity, and the minimum apparent resistivity will be observed when the array is oriented in the direction of maximum resistivity.

Generalization 3; For the case in which the source bipole is oriented along the direction of highest resistivity, for large anisotropy coefficients, over most of the area around the bipole,

the electric field will also be directed along the axis of maximum resistivity. This may seem inconsistent, because most of the current will be flowing in the direction of lowest resistivity. However, in an anisotropic medium, electric field directions and current flow directions are not coincident. A small component of current flow in the direction of high resistivity will cause a high electric field component, and so, the electric field directions will be rotated toward the high resistivity axis with reference to the surrent flow direction.

References

Keller, G. V., and Frischknecht, F. C., 1966, Electrical methods in geophysical prospecting: Pergamon Press, Oxford.

Keller, G. V., 1968, Electrical Prospecting for Oil: Colo. School of Mines Quarterly.

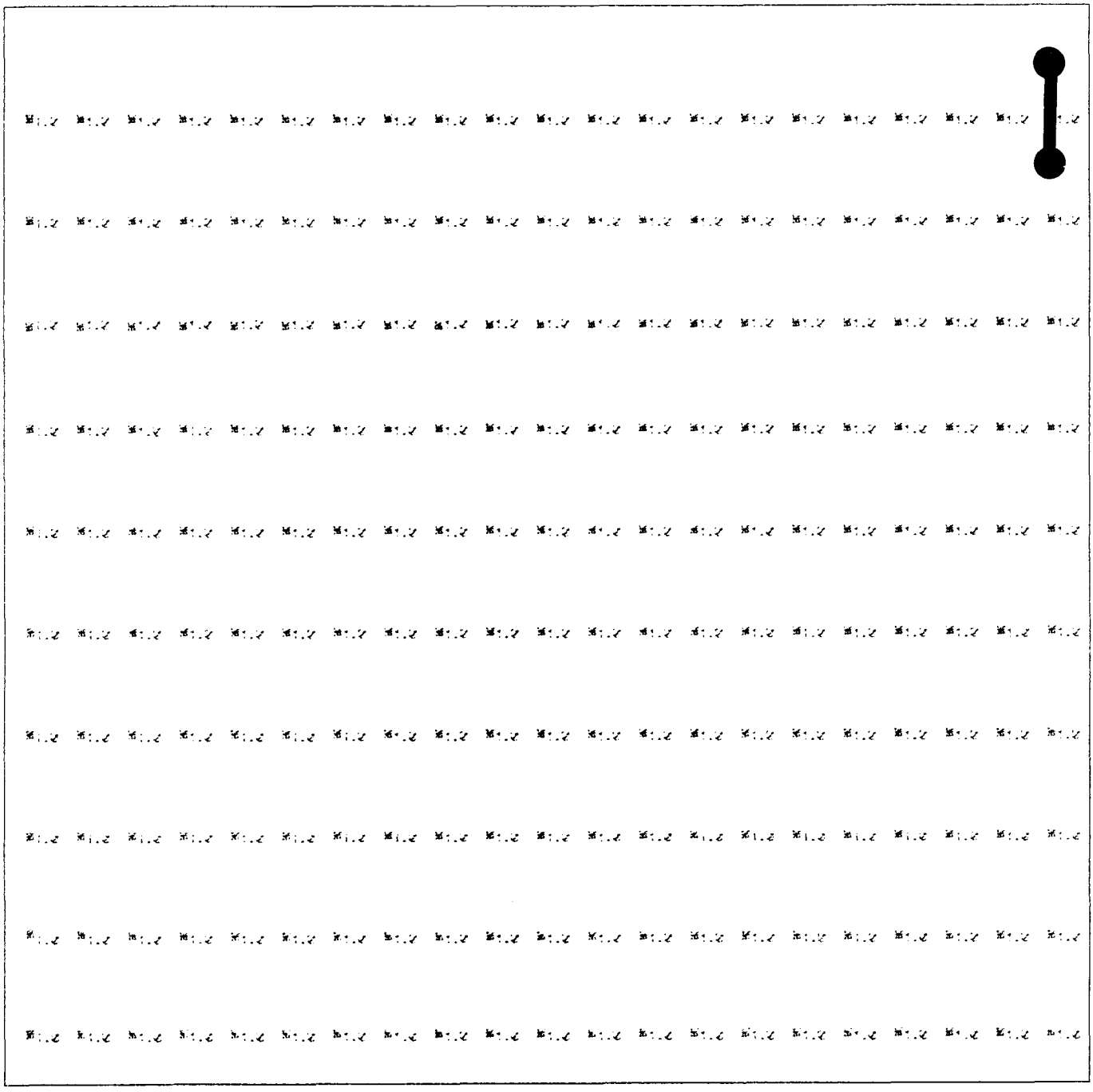

UNIFORM ANISOTROPIC EARTH WITH AN = 1.00

Figure D1.

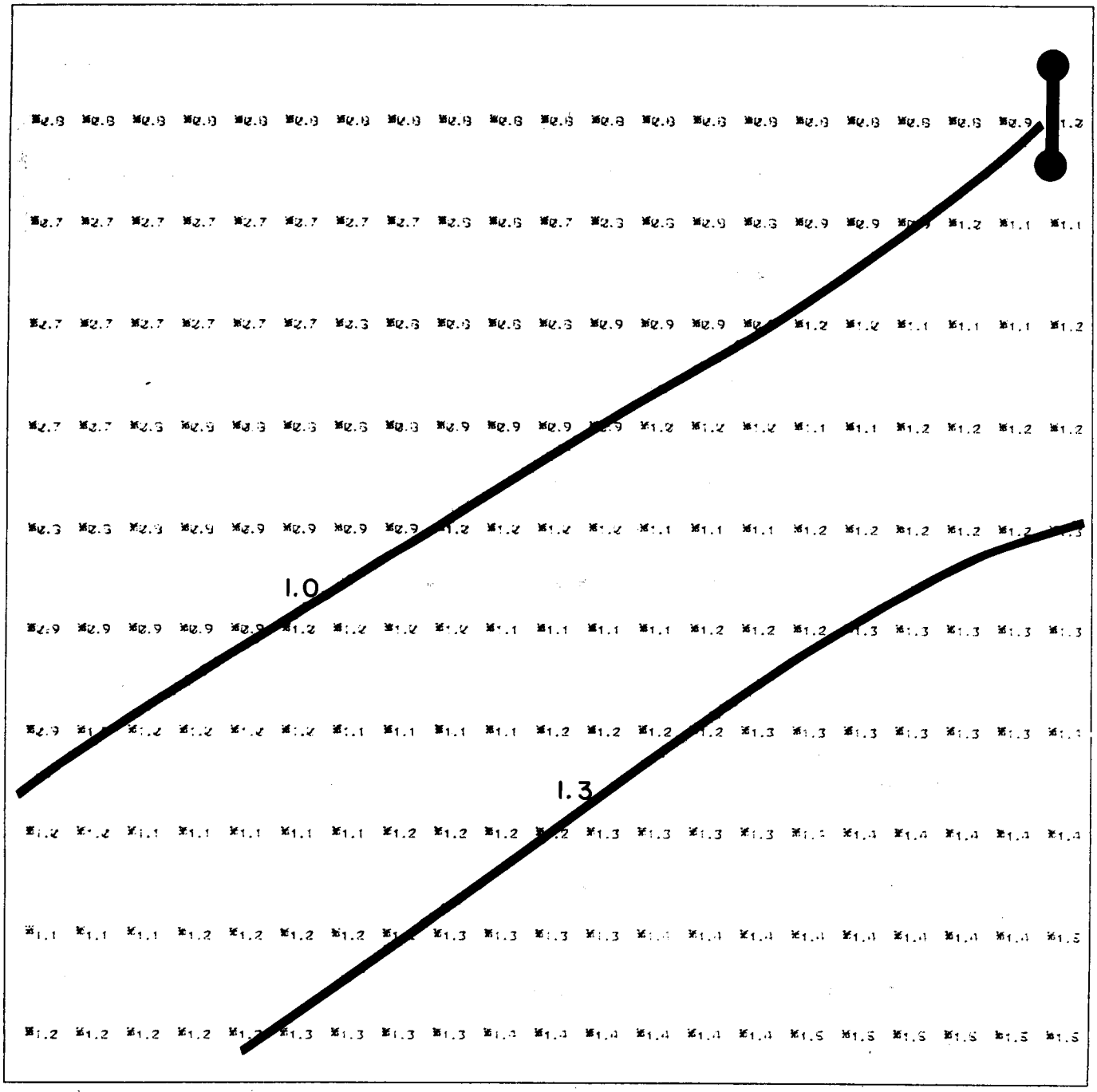

UNIFORM ANISOTROPIC EARTH WITH AN=1.100

Figure D2

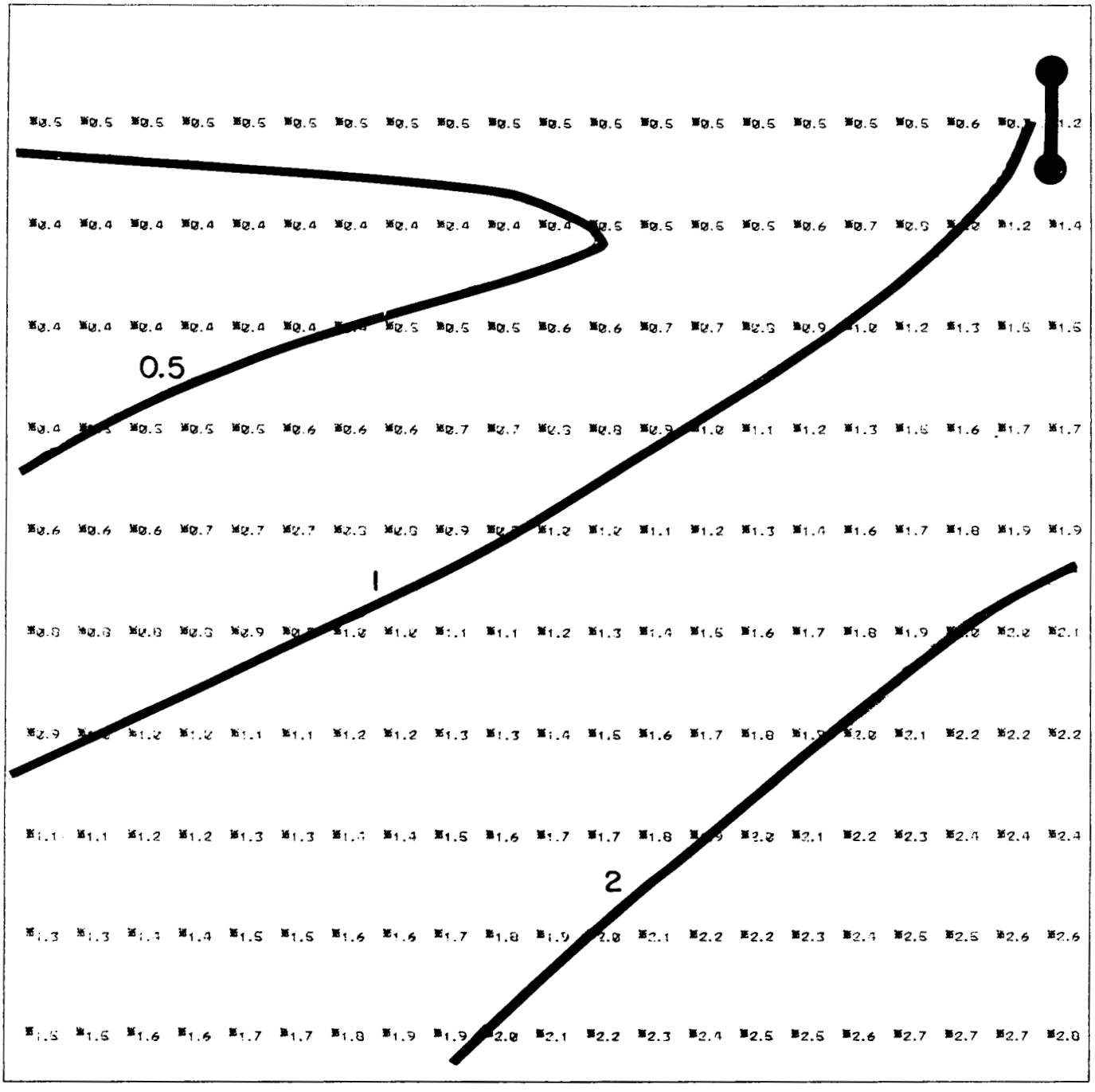

UNIFORM ANISOTROPIC EARTH WITH AN = 1.35

Figure D3.

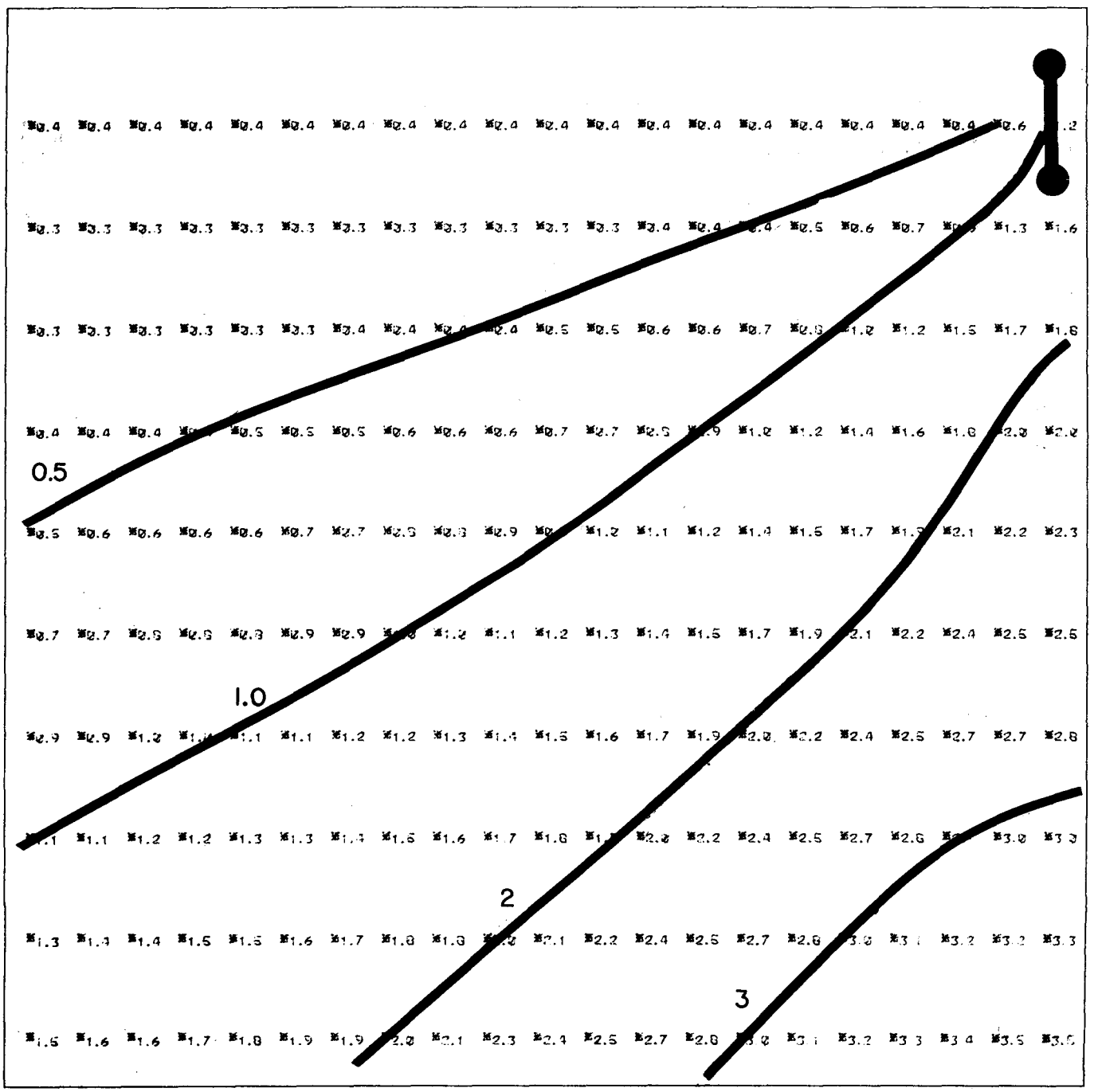

UNIFORM ANISOTROPIC EARTH WITH AN =1.500

Figure D4.

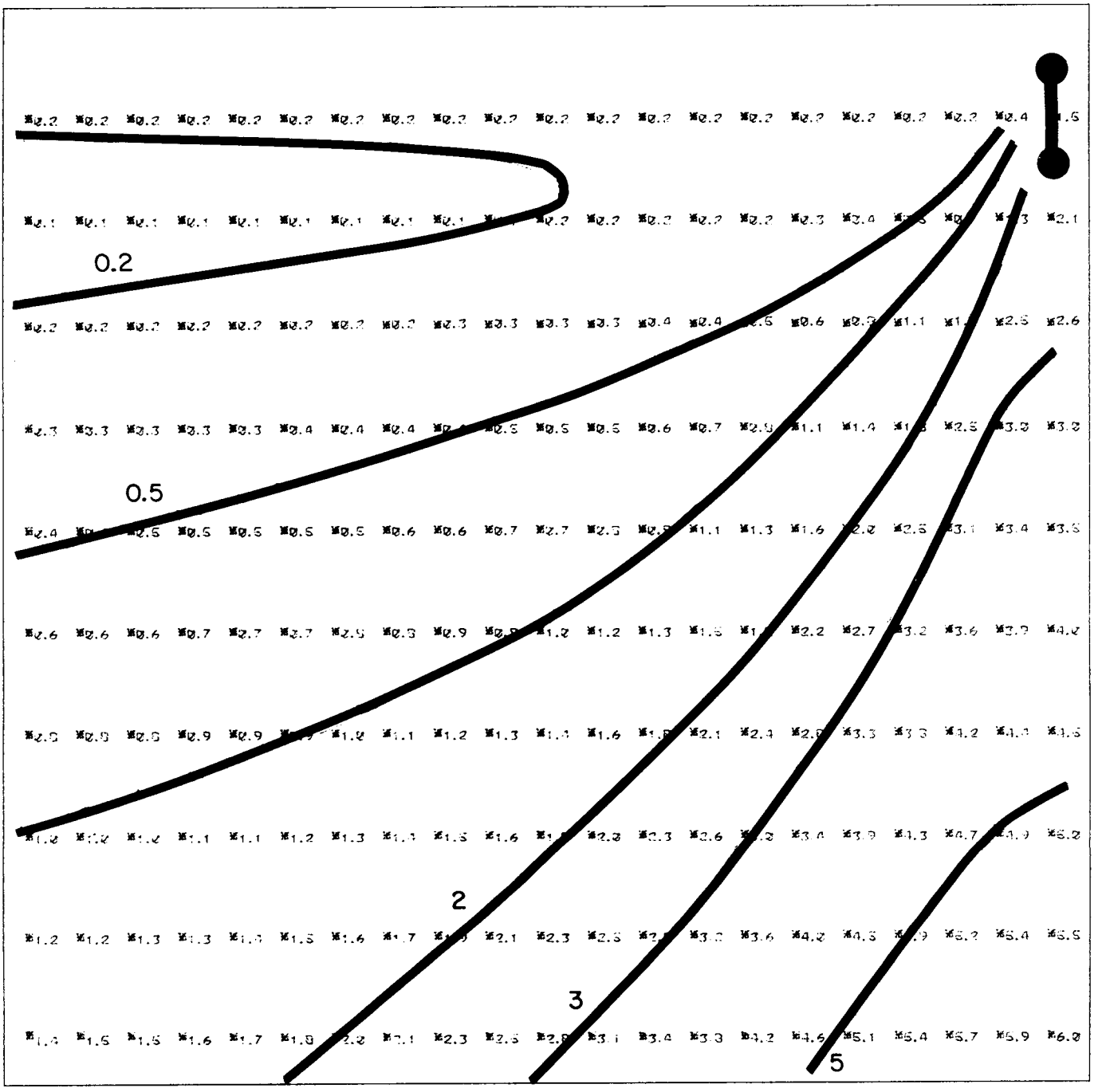

UNIFORM ANISOTROPIC EARTH WITHJ AN=2.000

Figure D5.

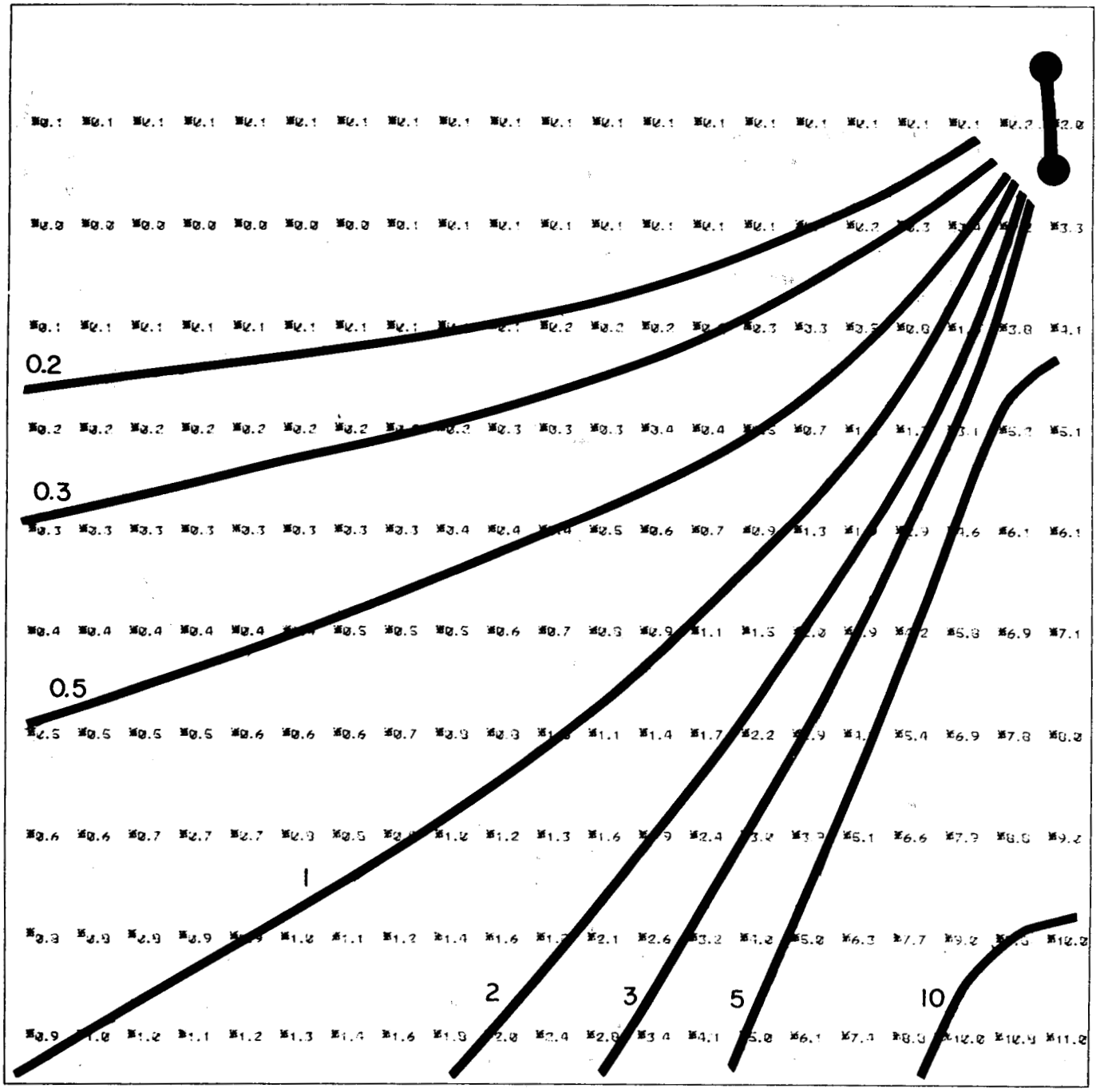

UNIFORM ANISOTROPIC EARTH WITH AN =3.000

Figure D6.

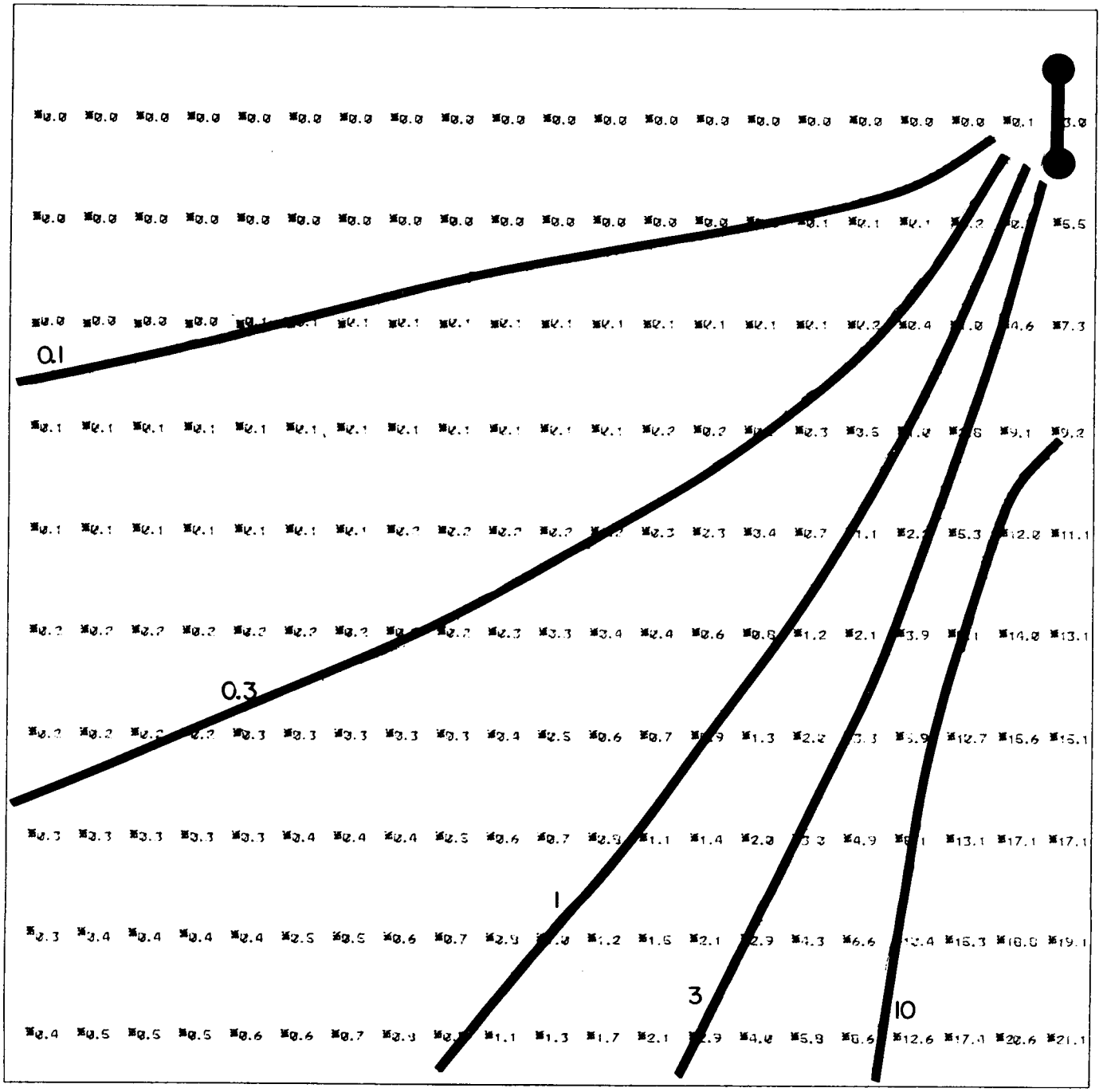

UNIFORM ANISOTROPIC EARTH WITH AN = 5.00

Figure D7.

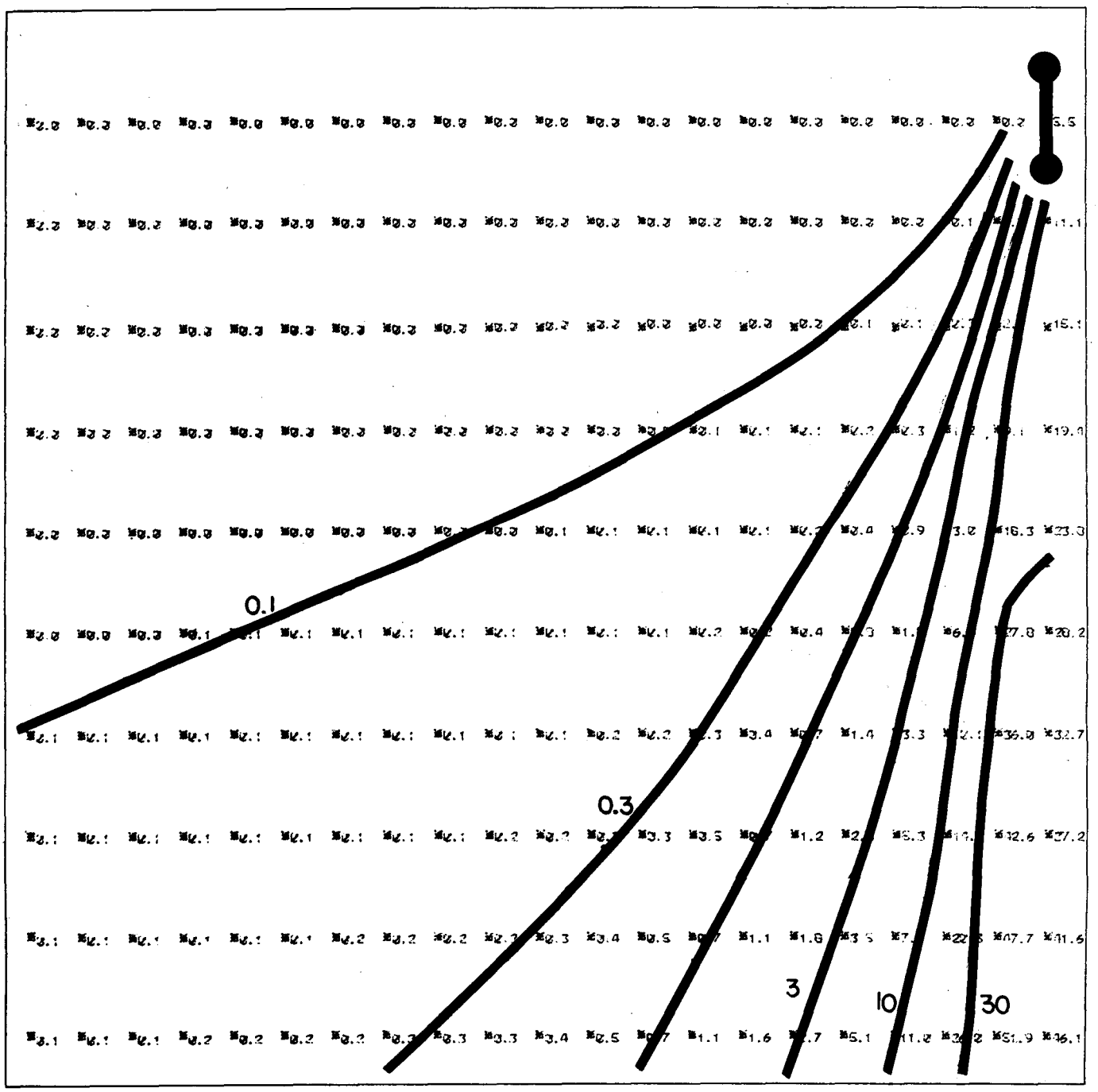

UNIFORM ANISOTROPIC EARTH WITH AN = 10.0

Figure D8.

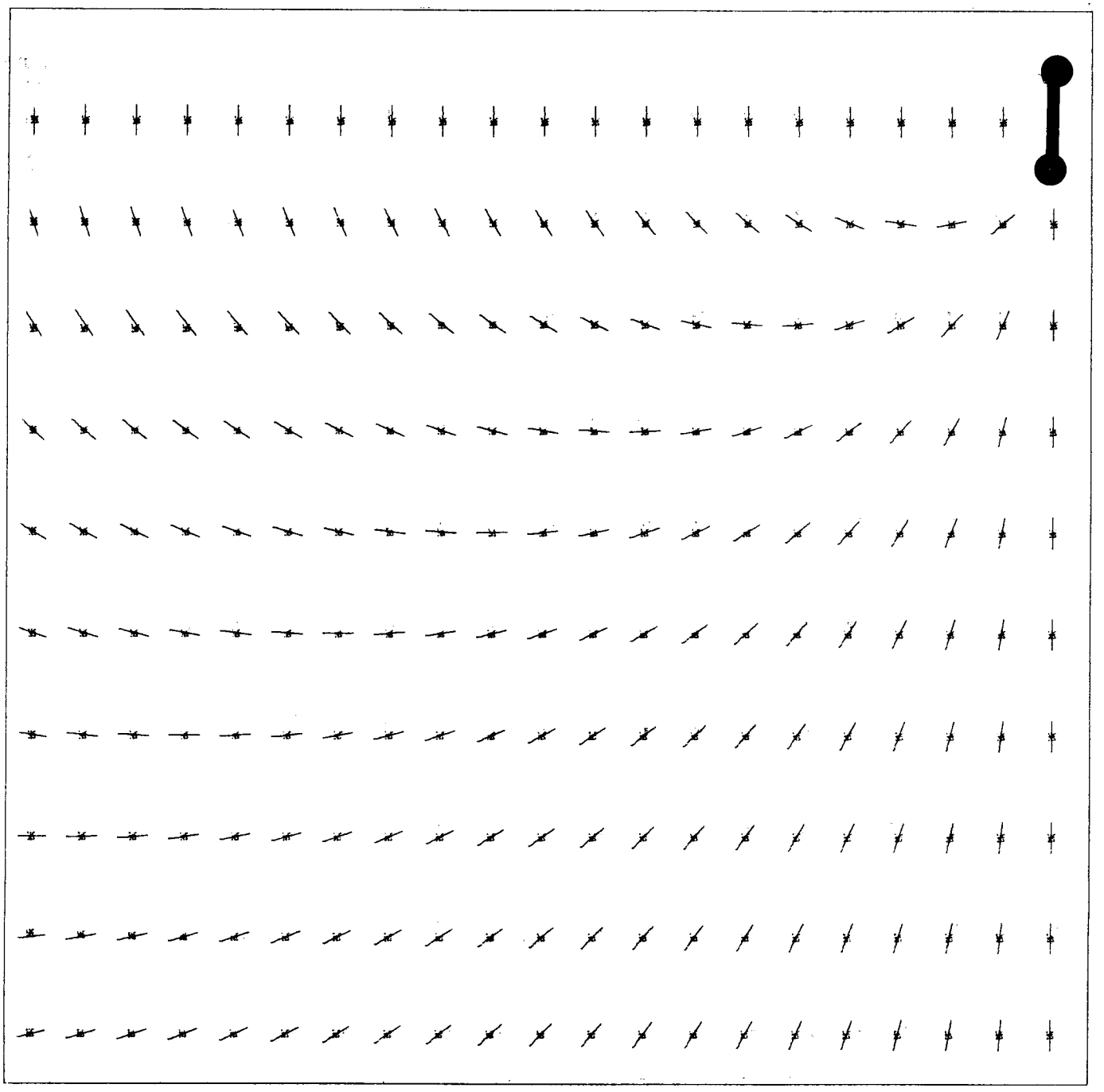

Figure D9.

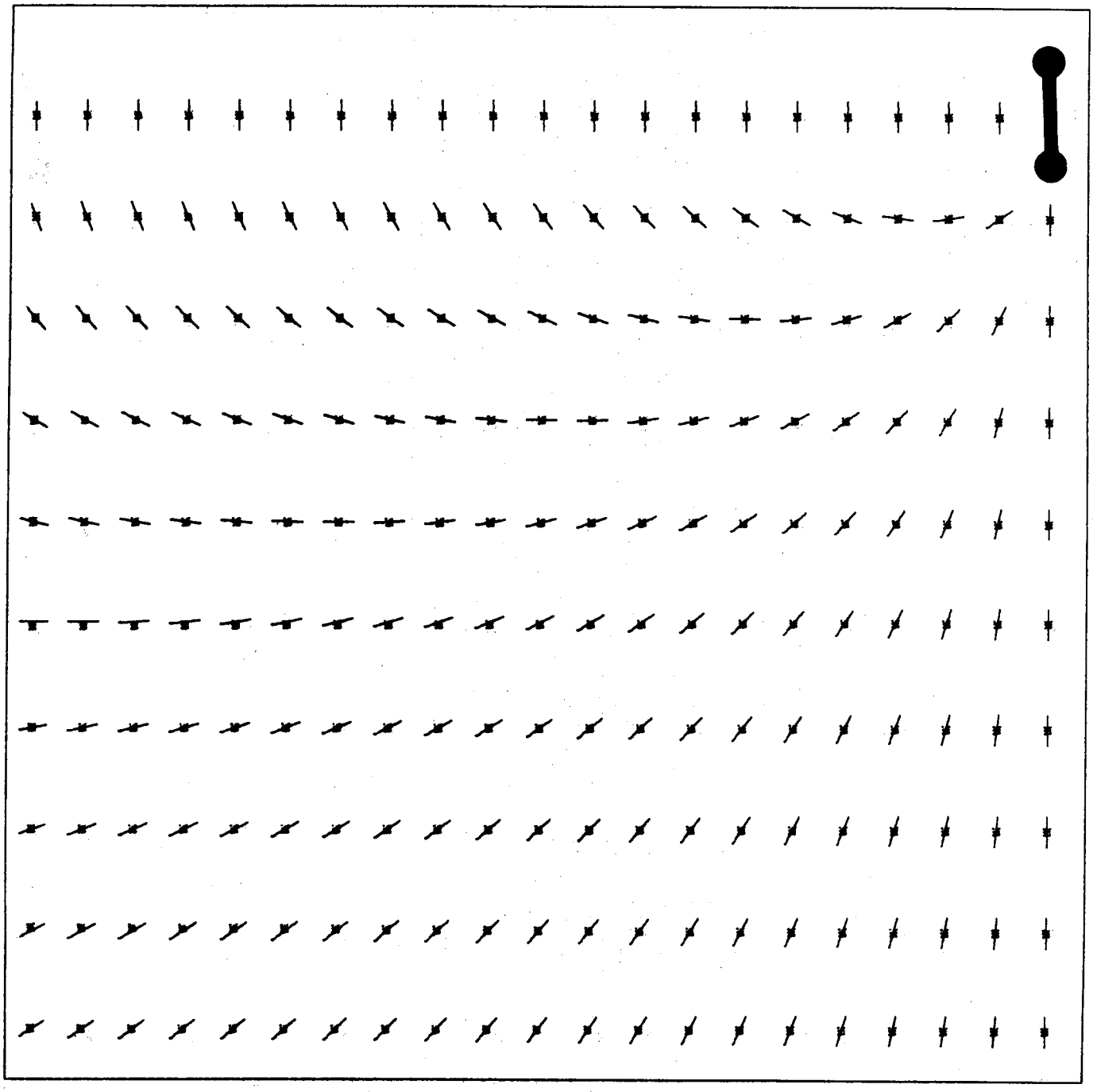

UNIFORM ANISOTROPIC EARTH WITH AN=1.100

Figure D10.

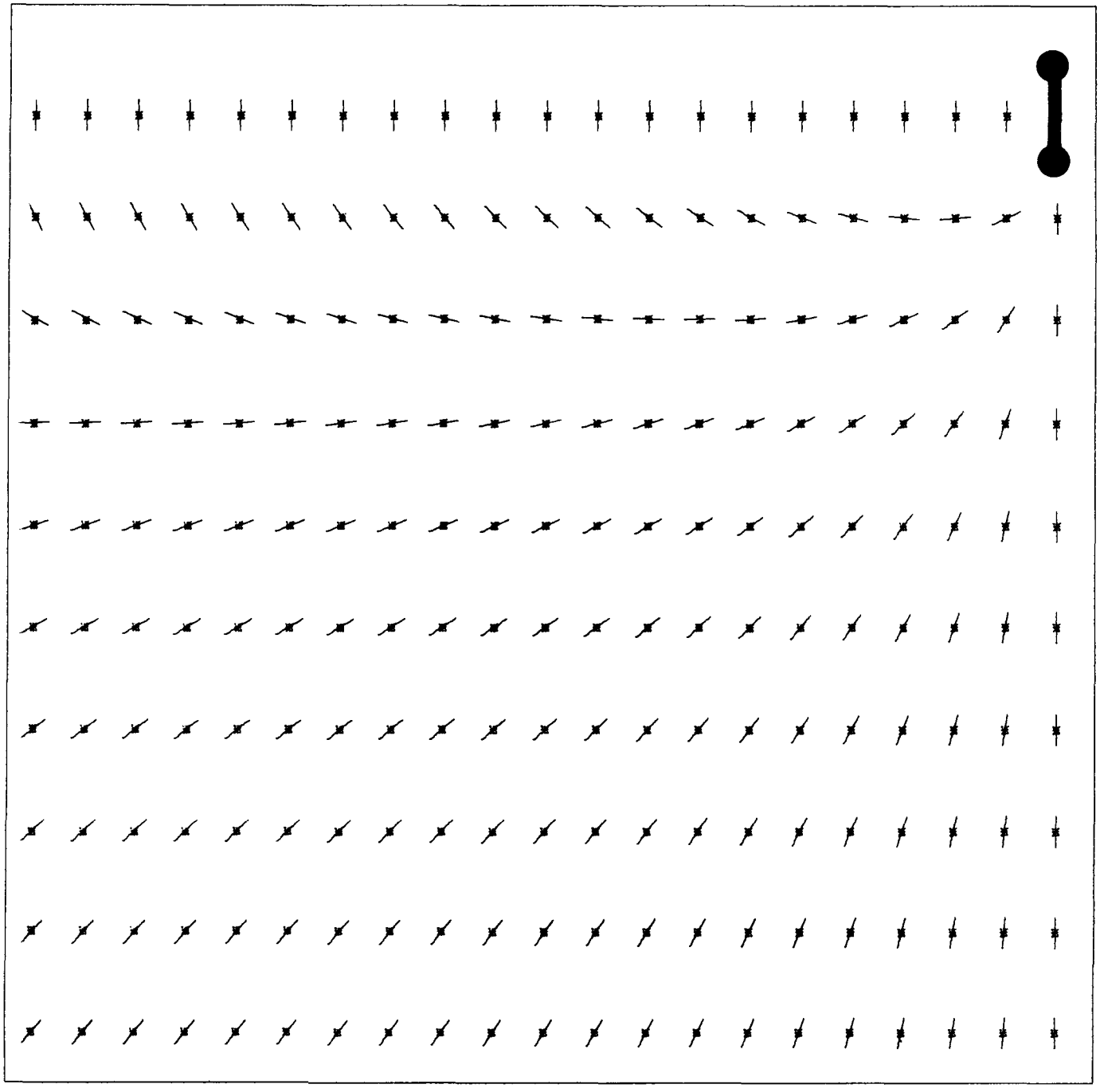

Figure D11.

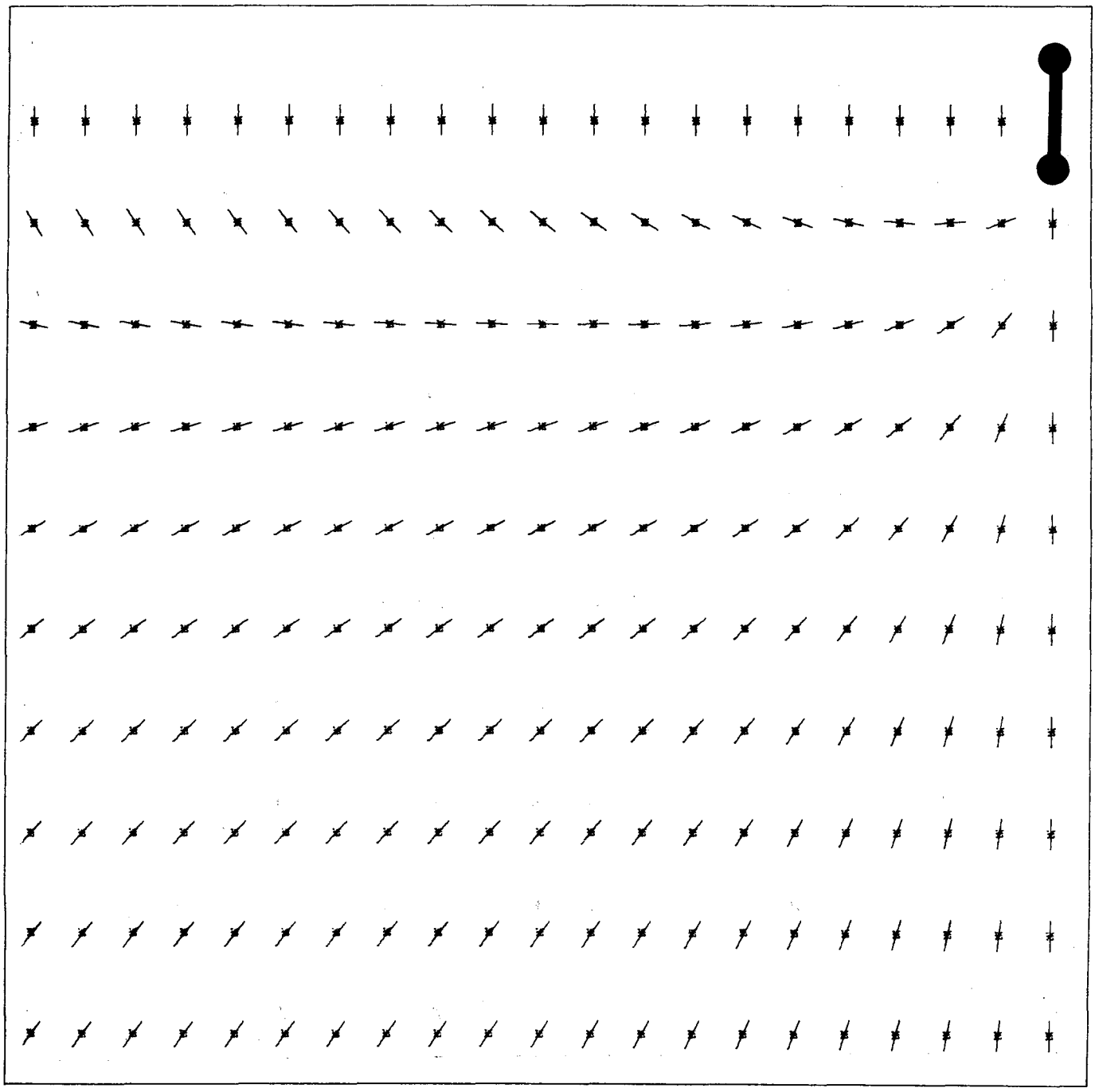

UNIFORM ANISOTROPIC EARTH WITH AN =1.500

Figure D12.

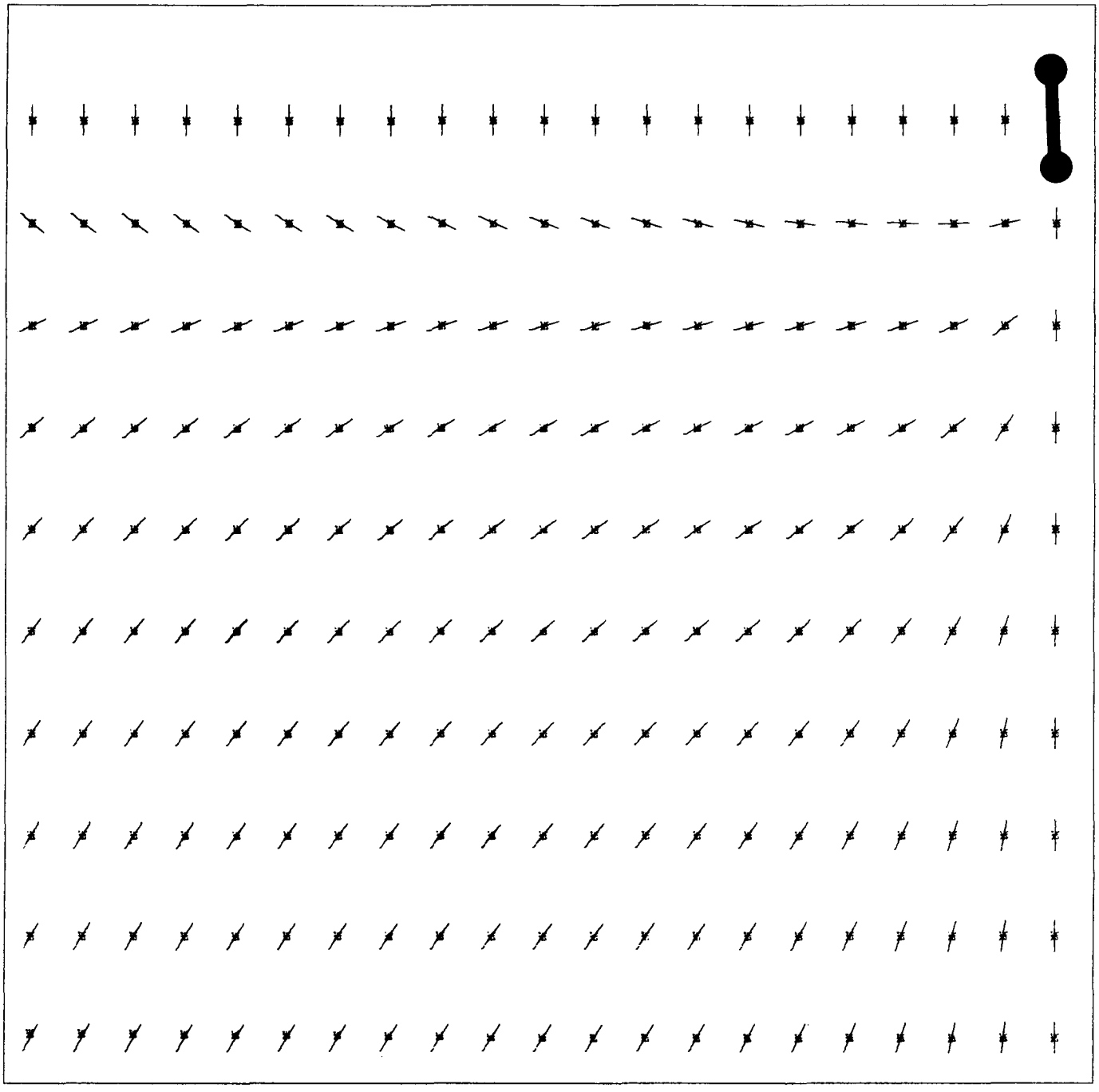

Figure D13.

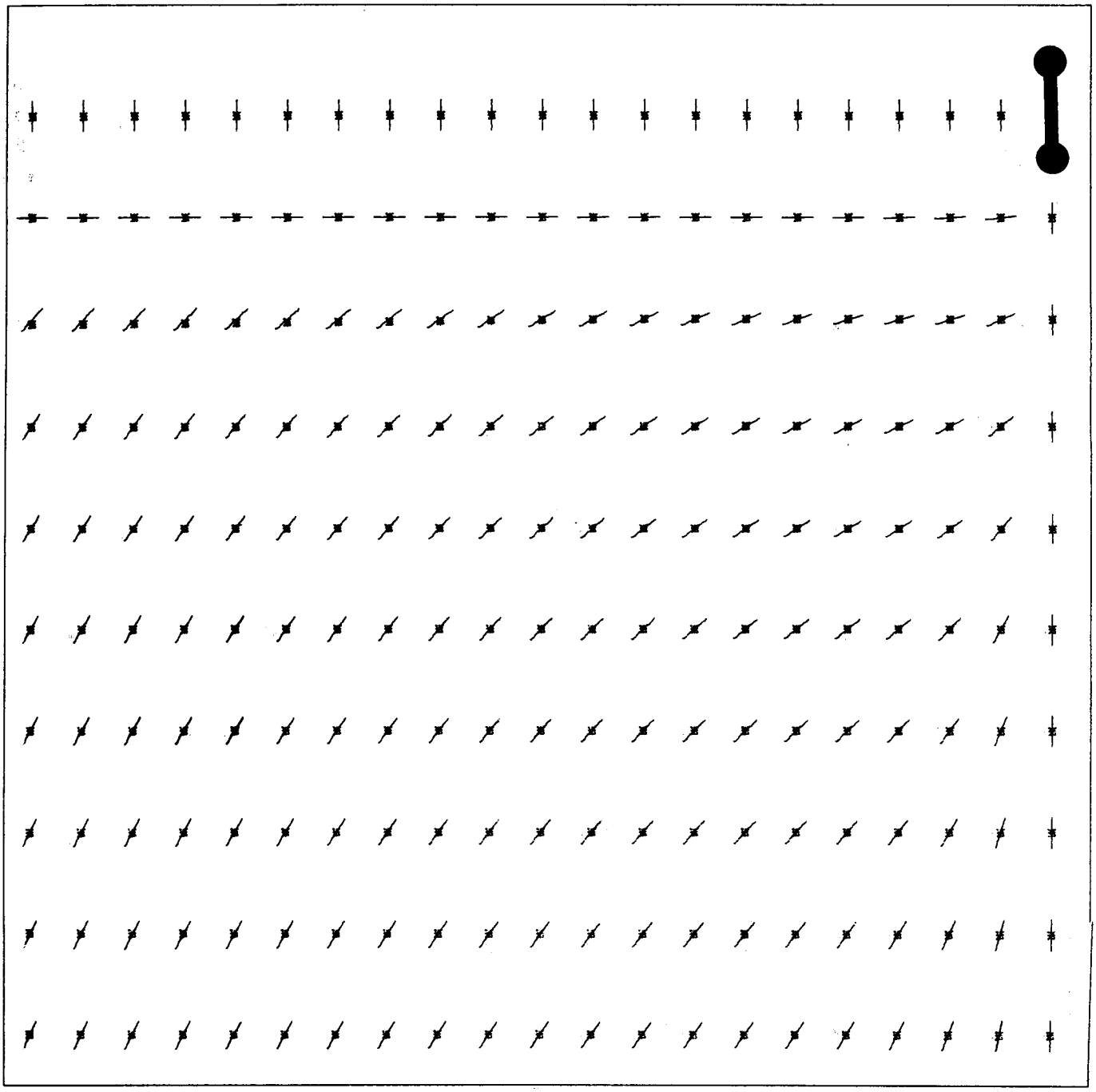

Figure D14.

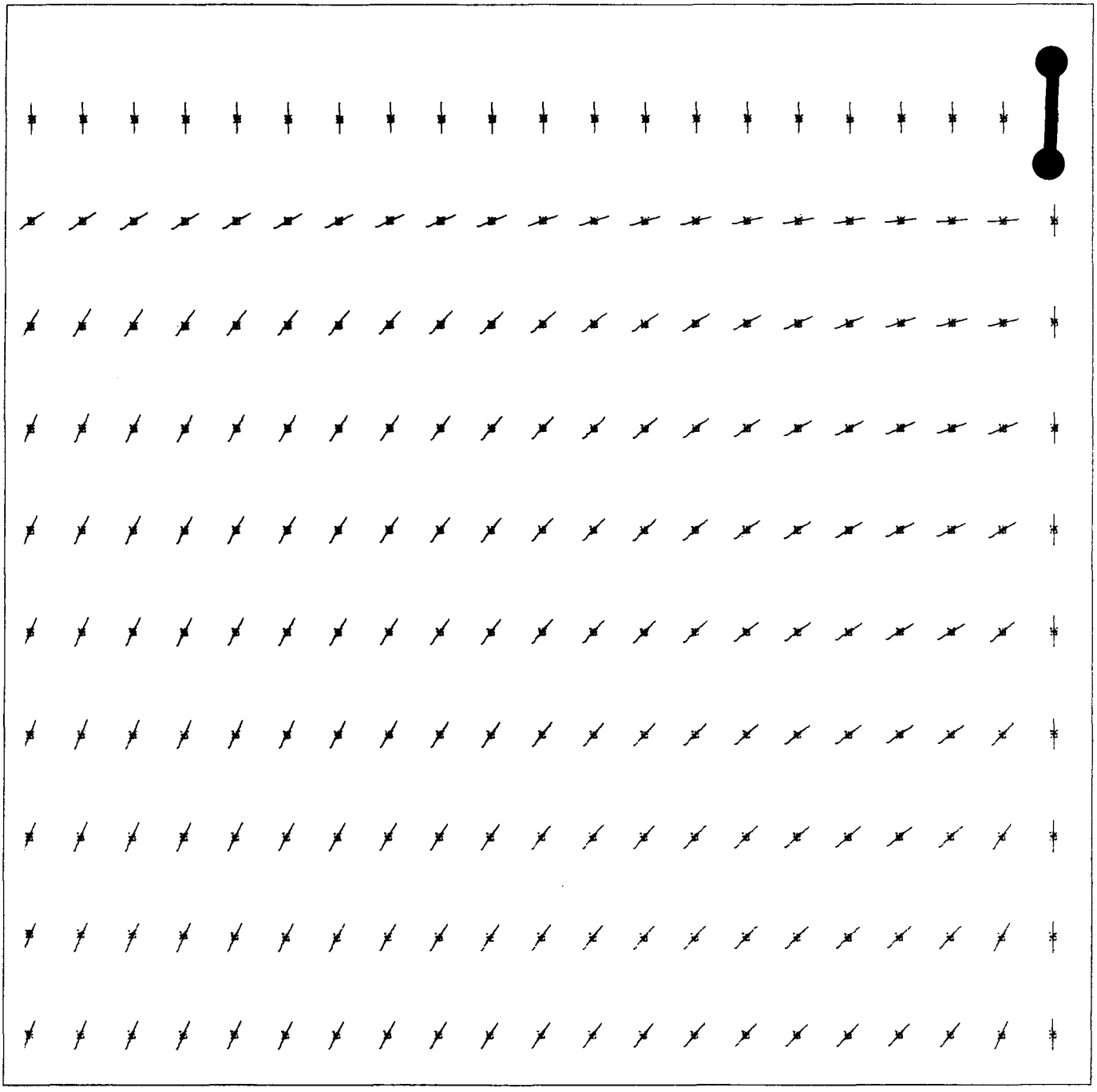

Figure D15.

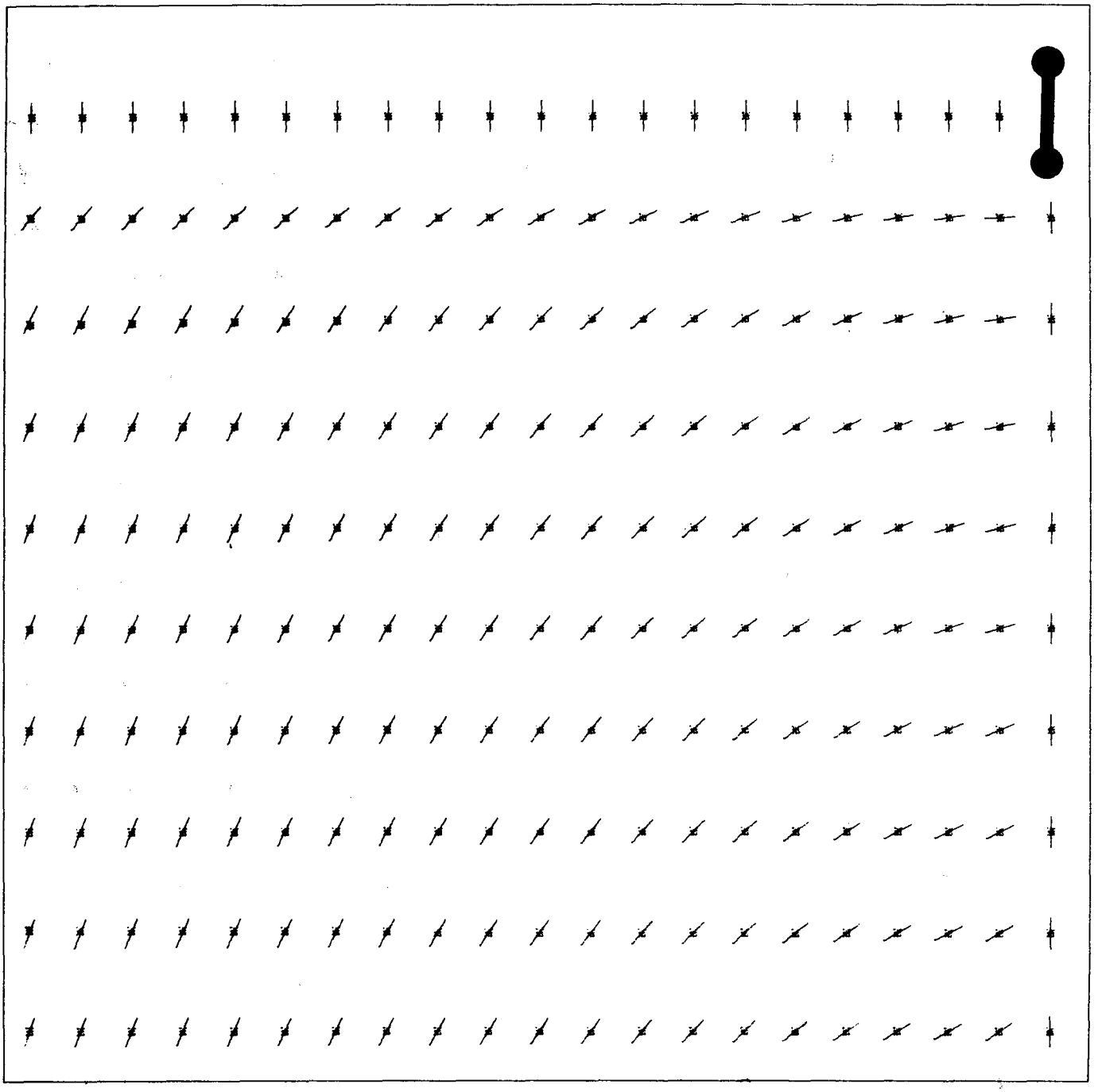

UNIFORM ANISOTROPIC EARTH WITH AN = 10.0

Figure D16.

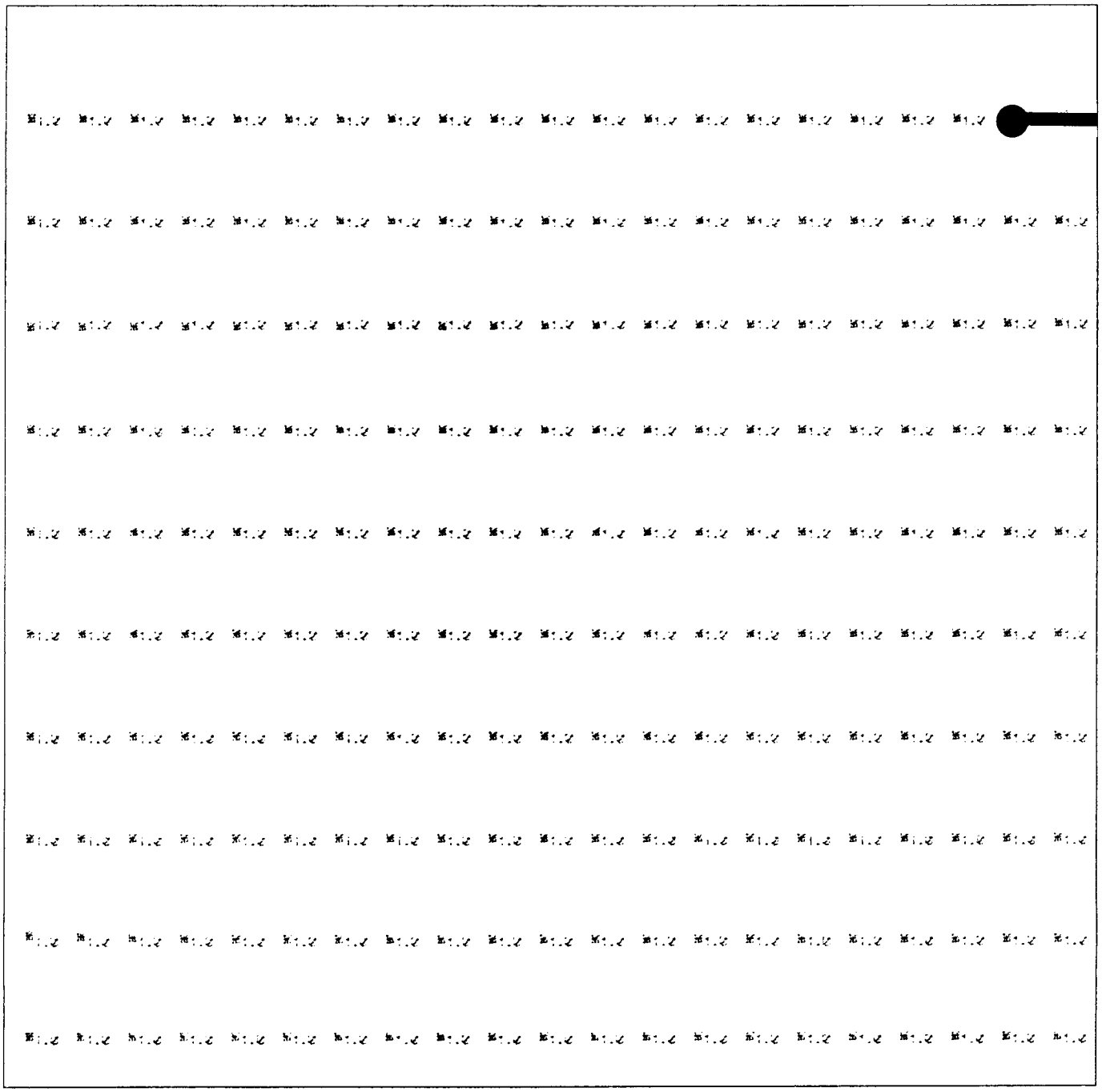

UNIFORM ANISOTROPIC EARTH WITH AN = 1.00

Figure D17.

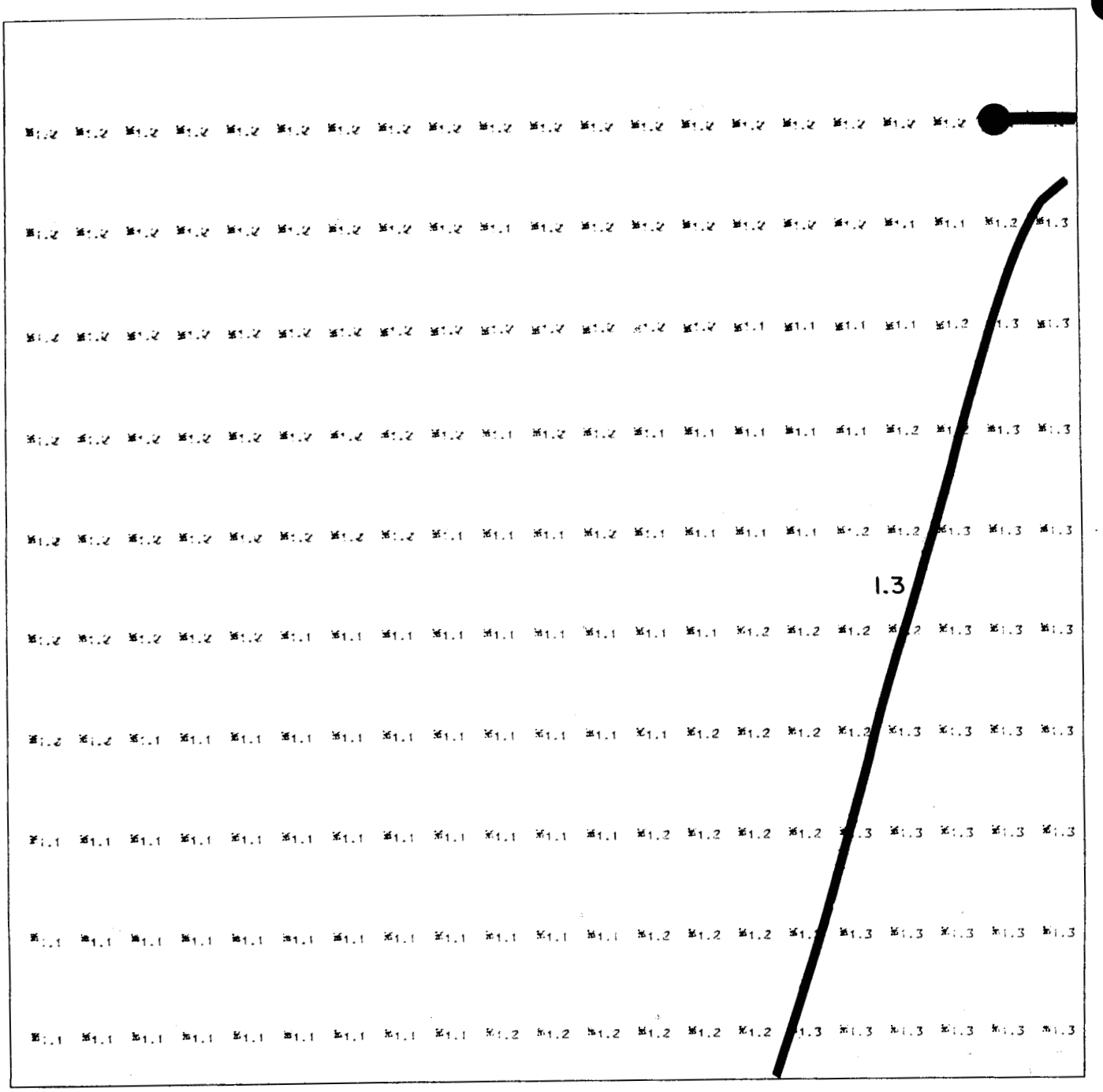

UNIFORM ANISOTROPIC EARTH WITH AN=1.100

Figure D18.

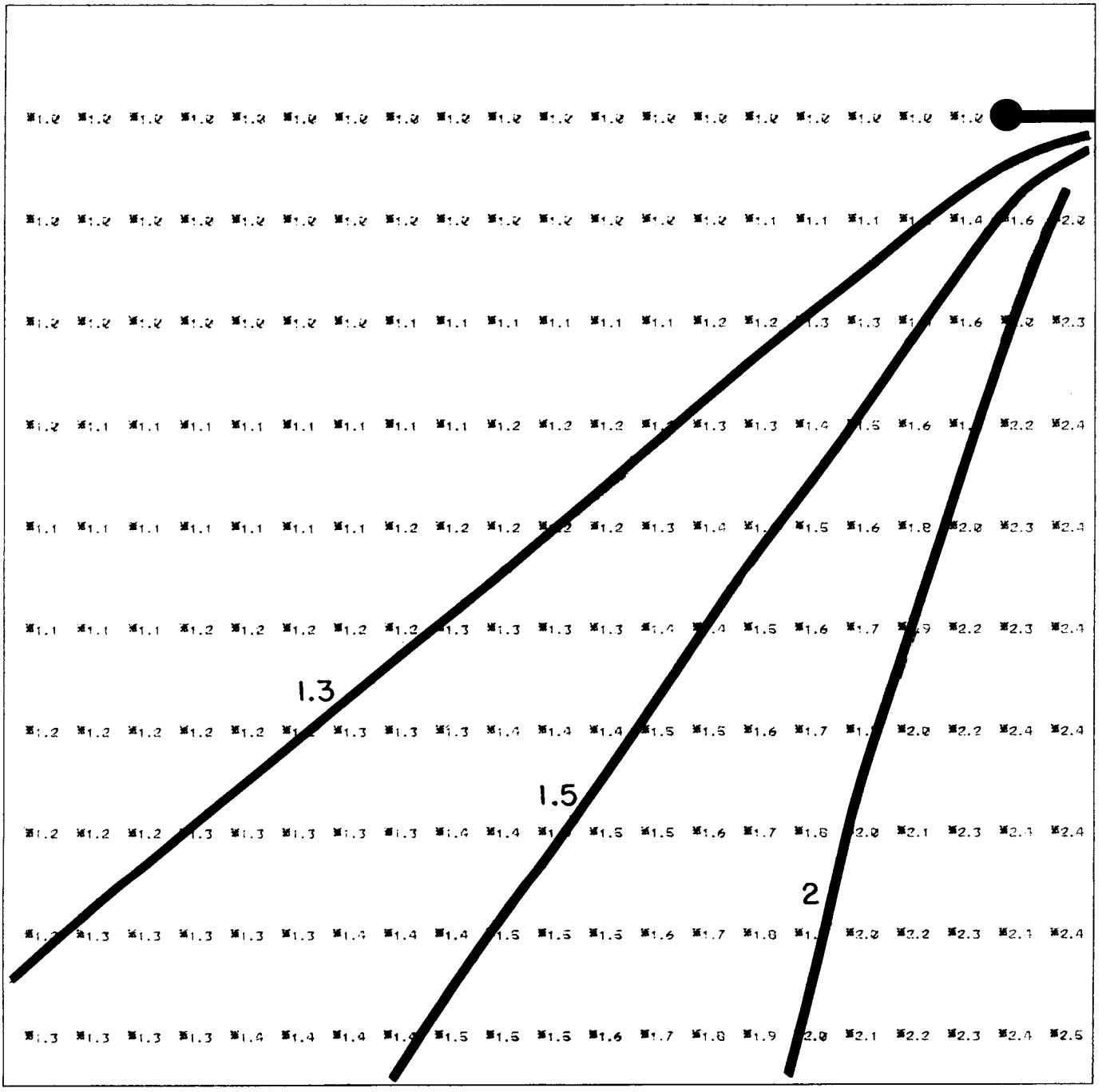

UNIFORM ANISOTROPIC EARTH WITH AN = 1.35

Figure D19.

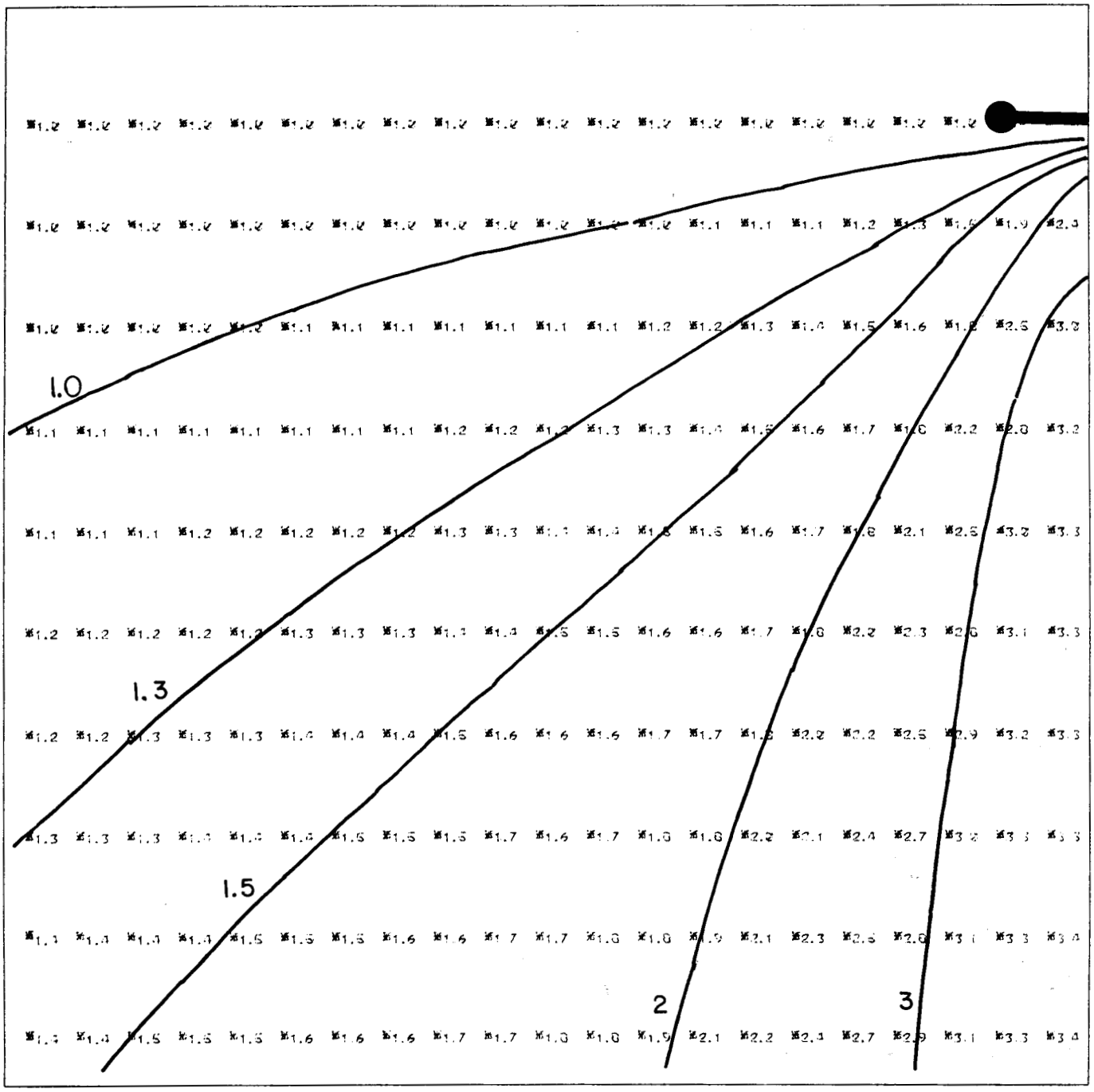

UNIFORM ANISOTROPIC EARTH WITH AN =1.500

Figure D20.

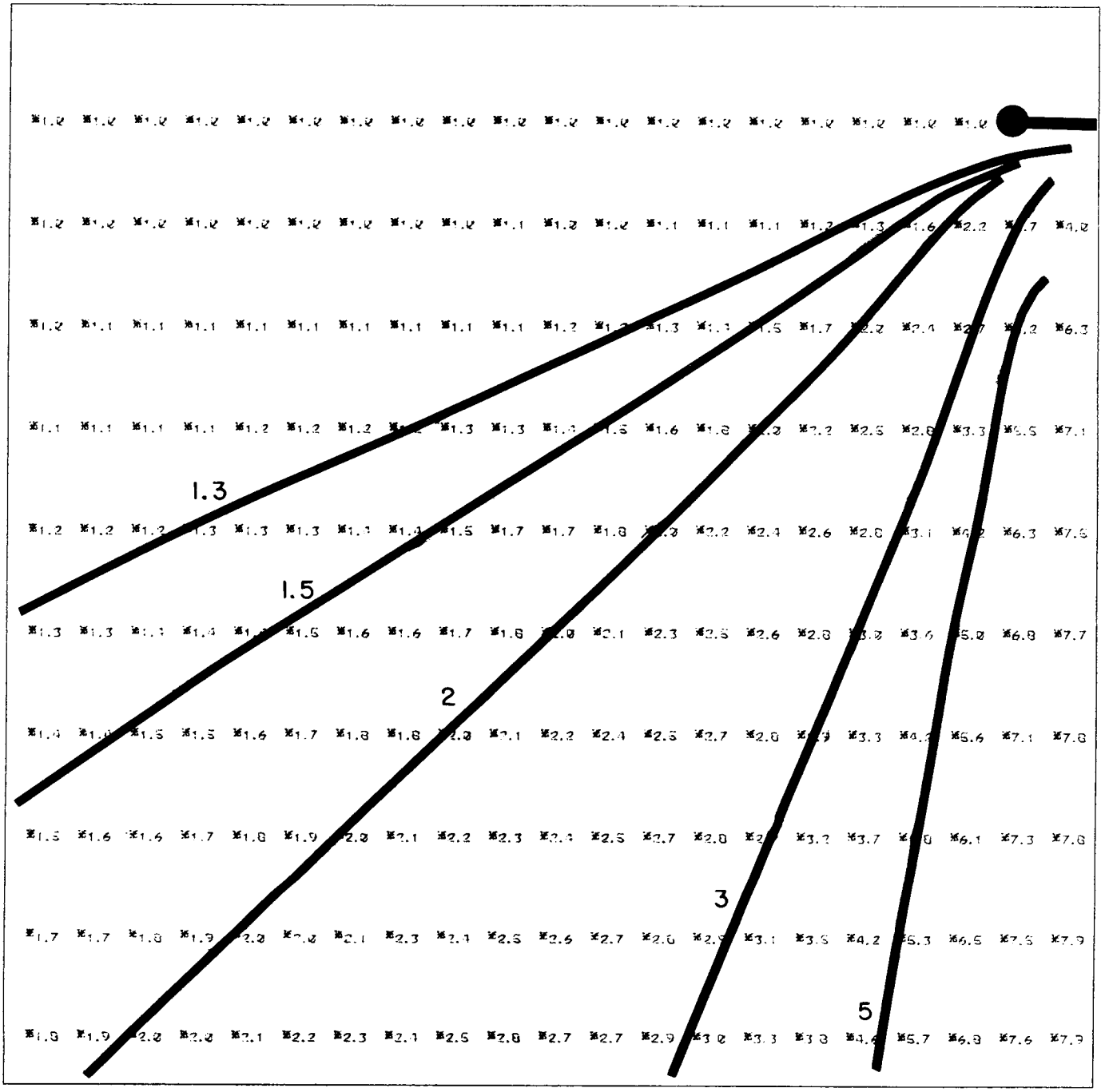

UNIFORM ANISOTROPIC EARTH WITHJ AN=2.000

Figure D21.

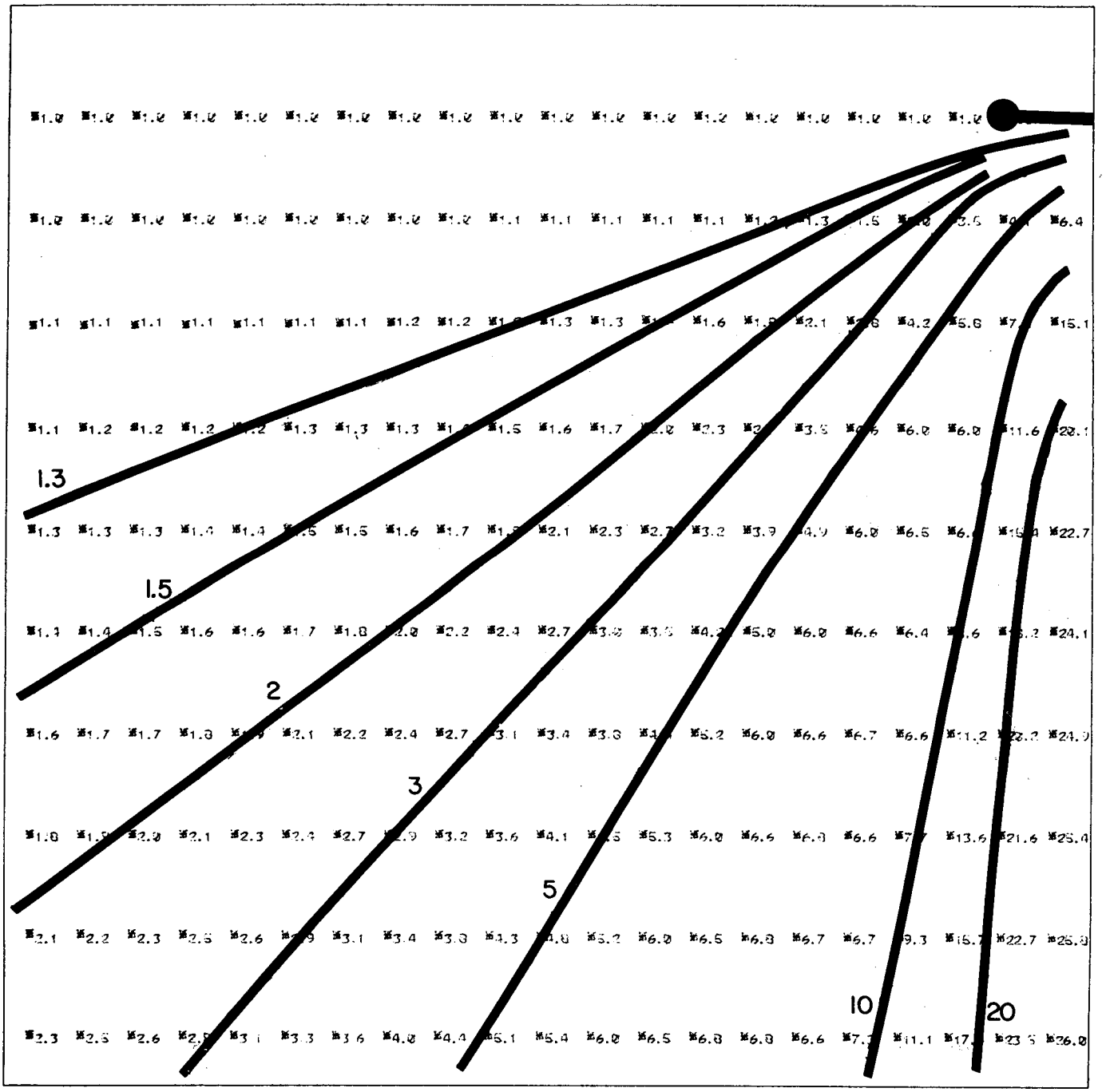

UNIFORM ANISOTROPIC EARTH WITH AN =3.000

Figure D22.

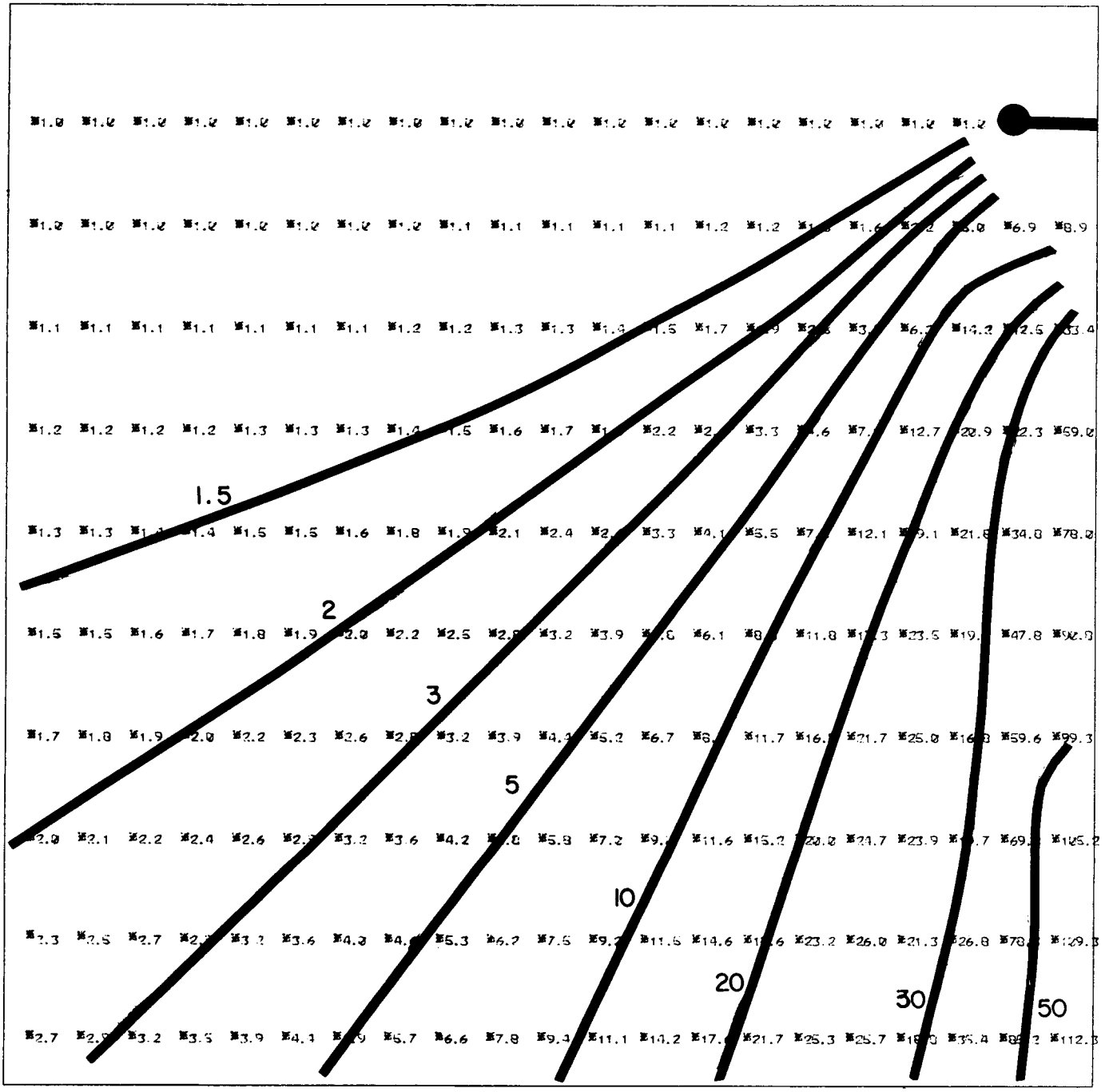

UNIFORM ANISOTROPIC EARTH WITH AN = 5.00

Figure D23.

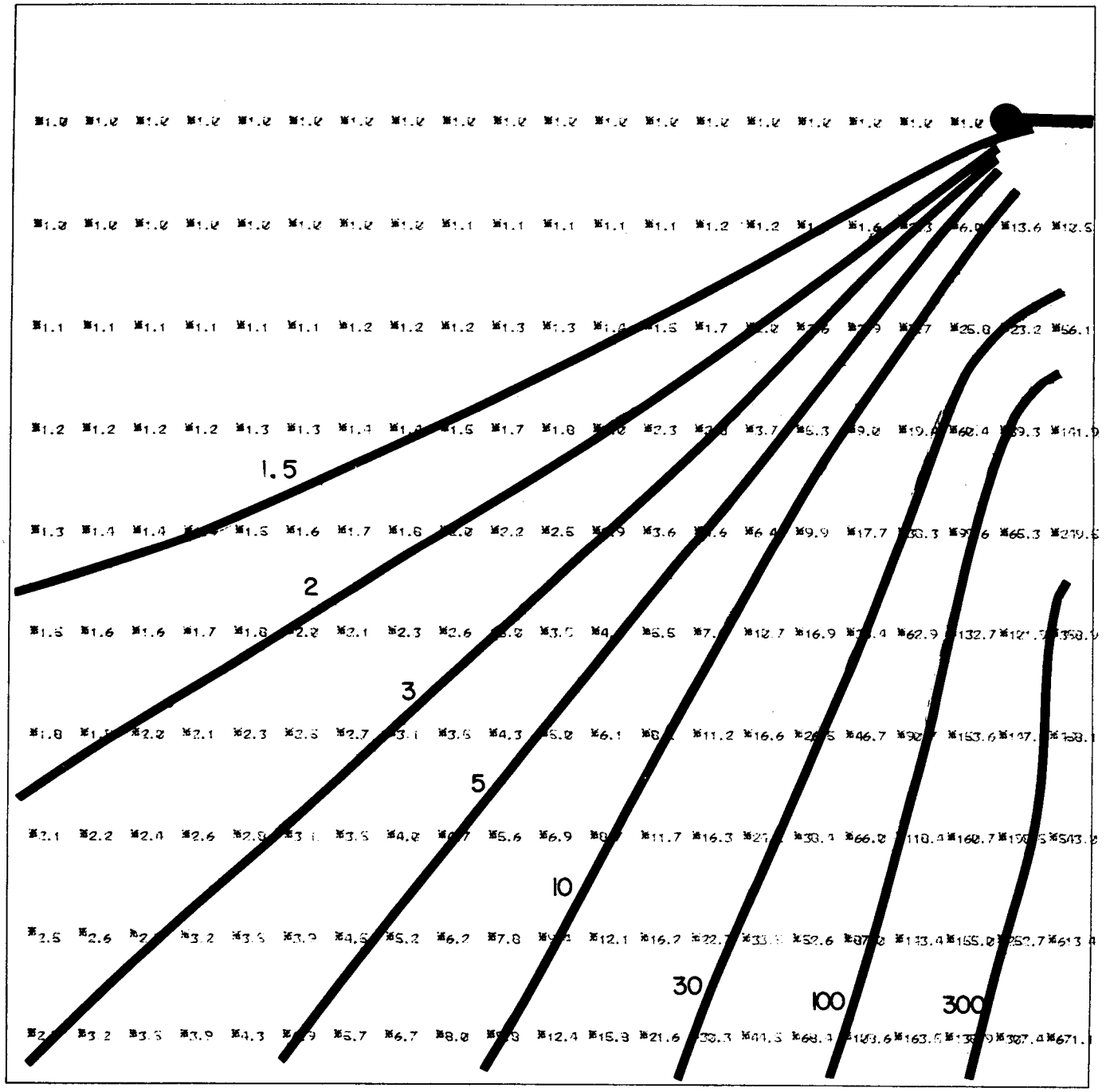

UNIFORM ANISOTROPIC EARTH WITH AN = 10.0

Figure D24.

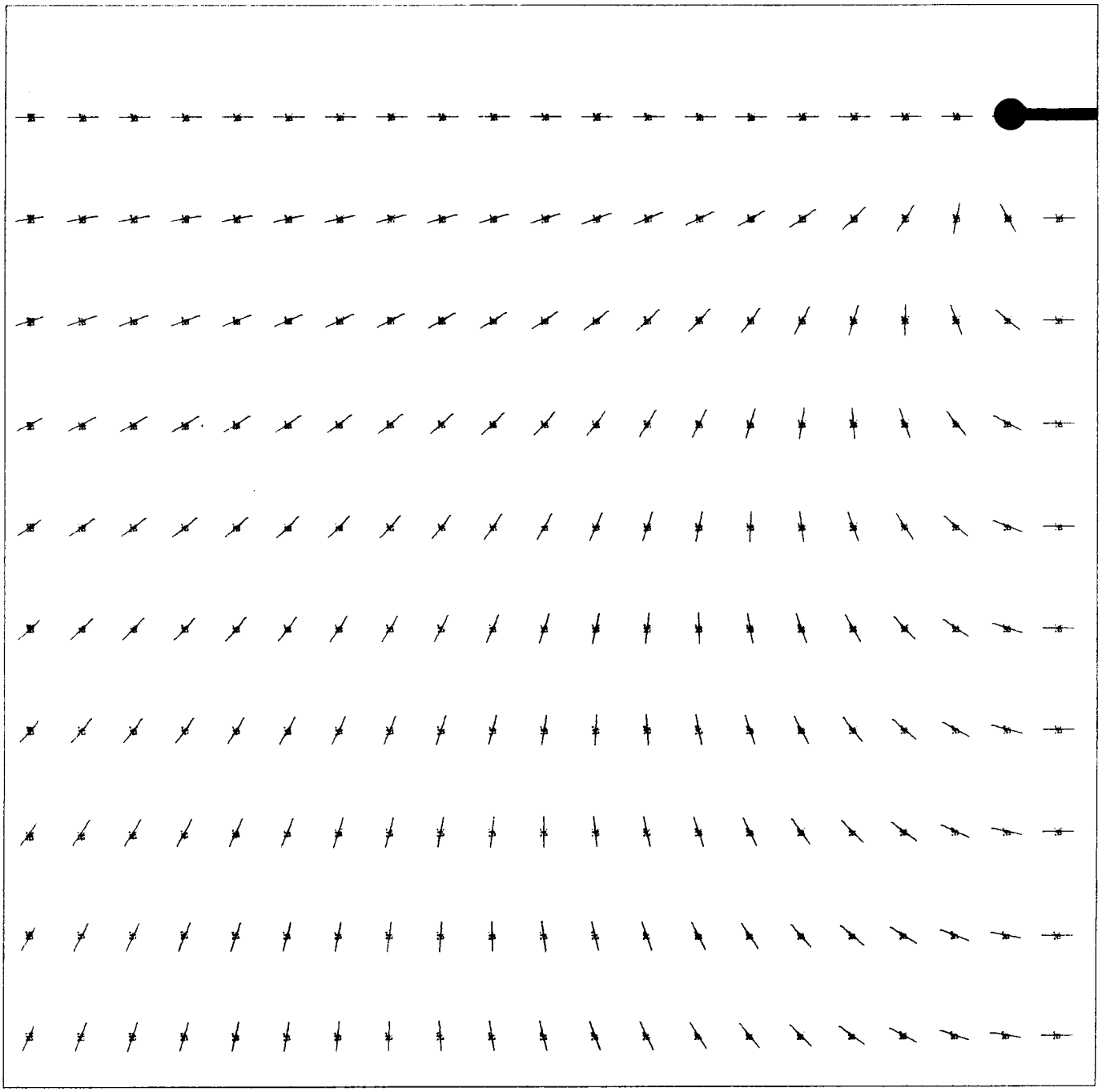

Figure D25.

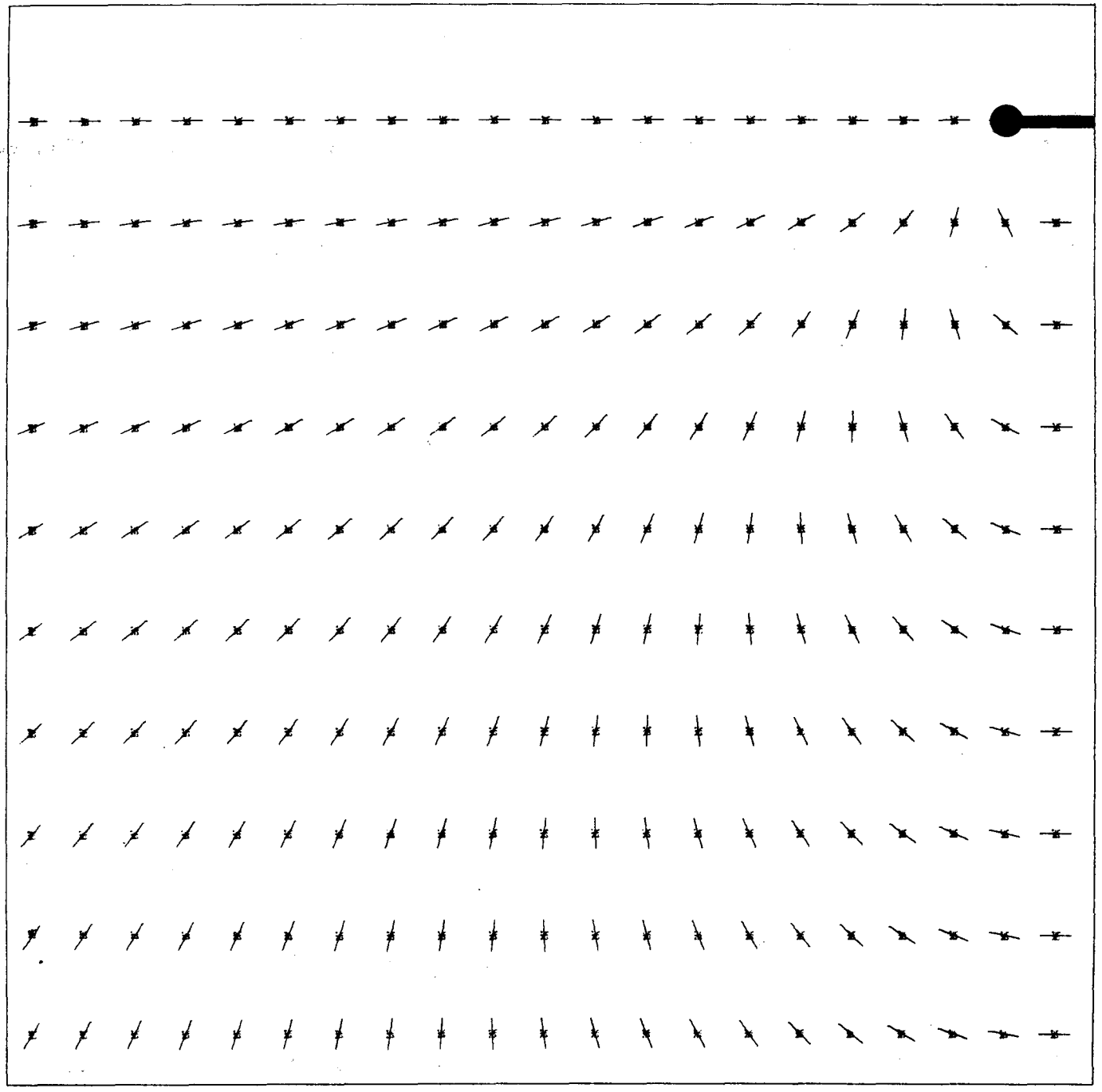

Figure D26.

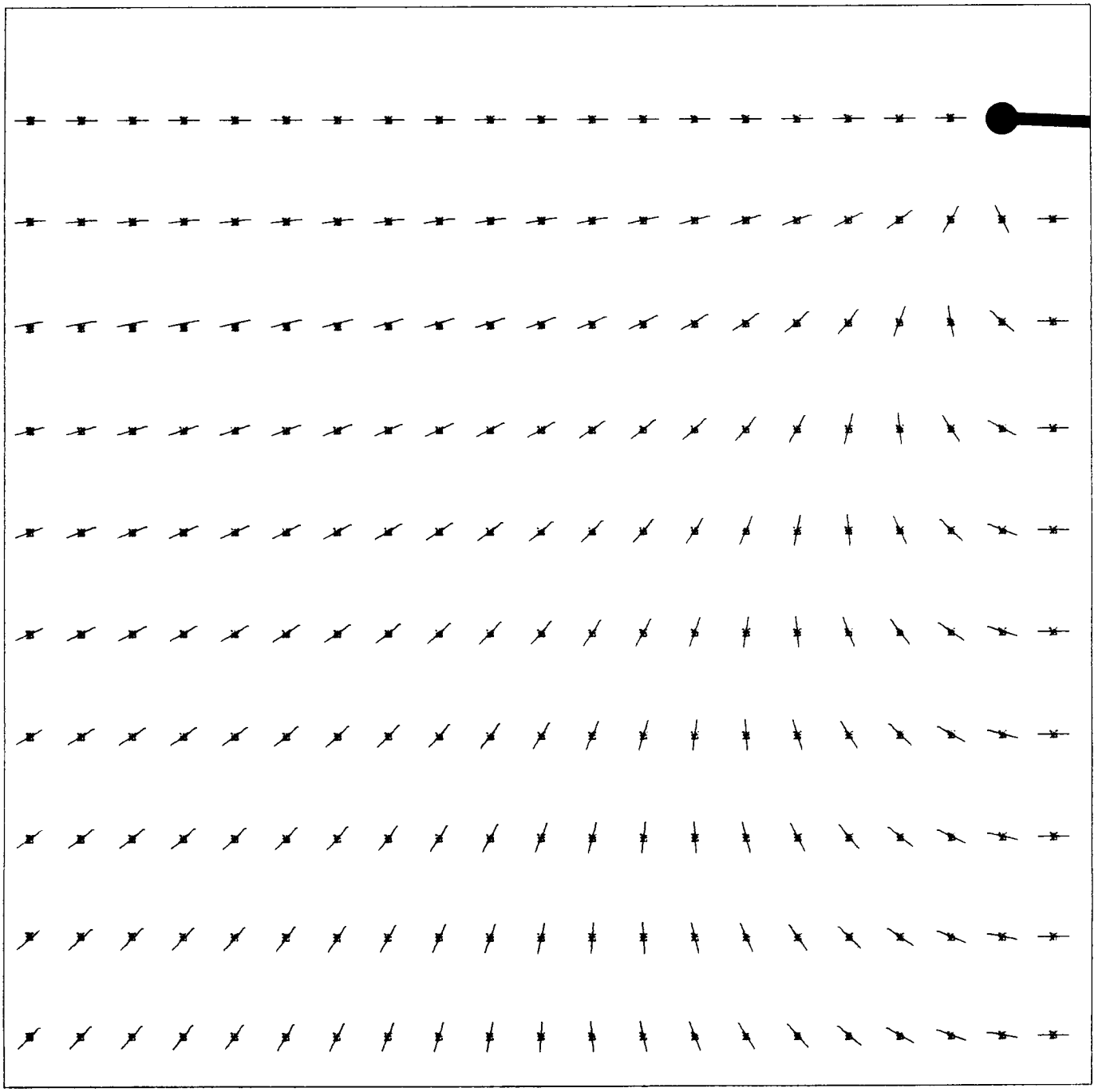

Figure D27.

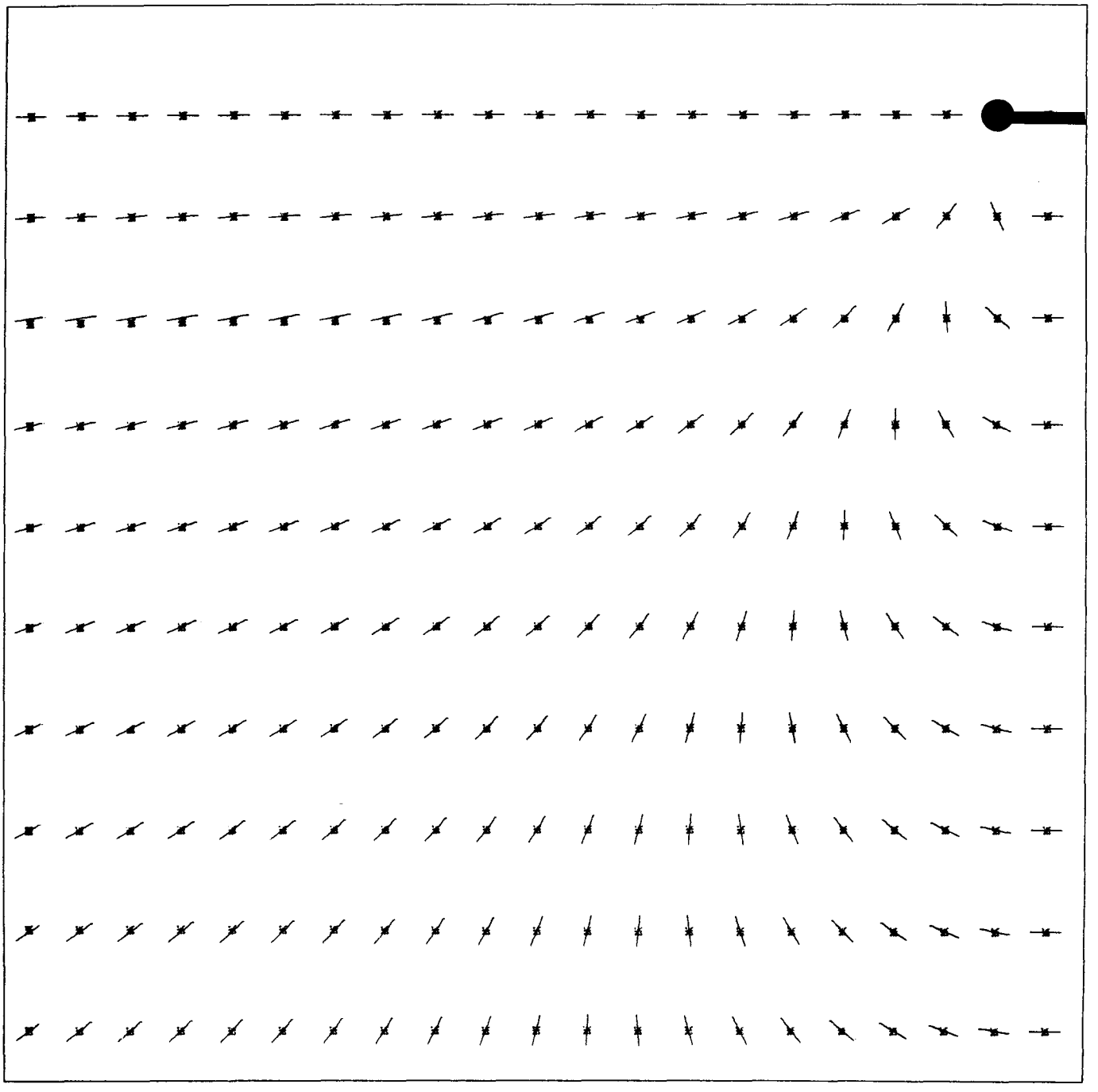

Figure D28.

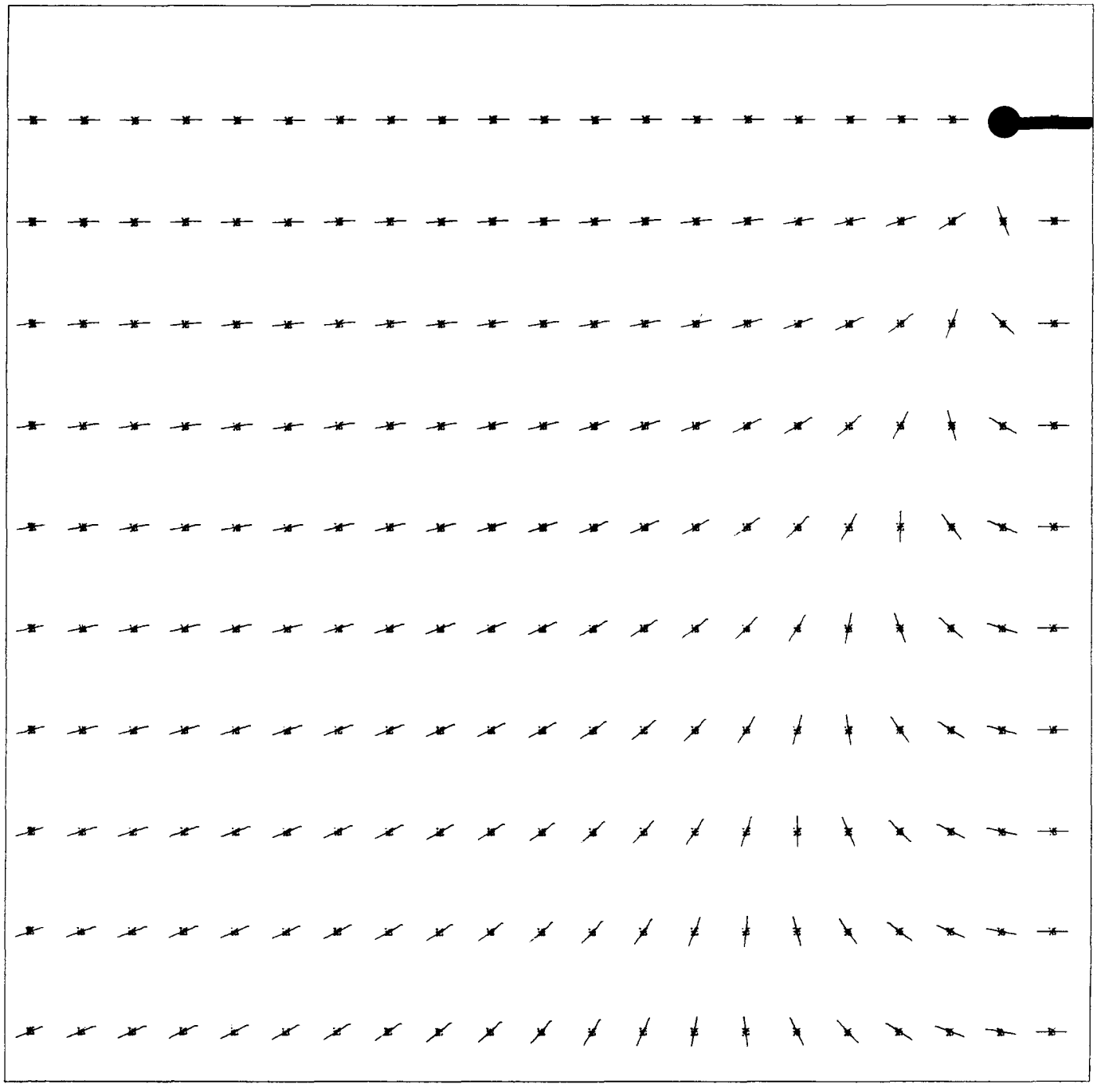

Figure D29.

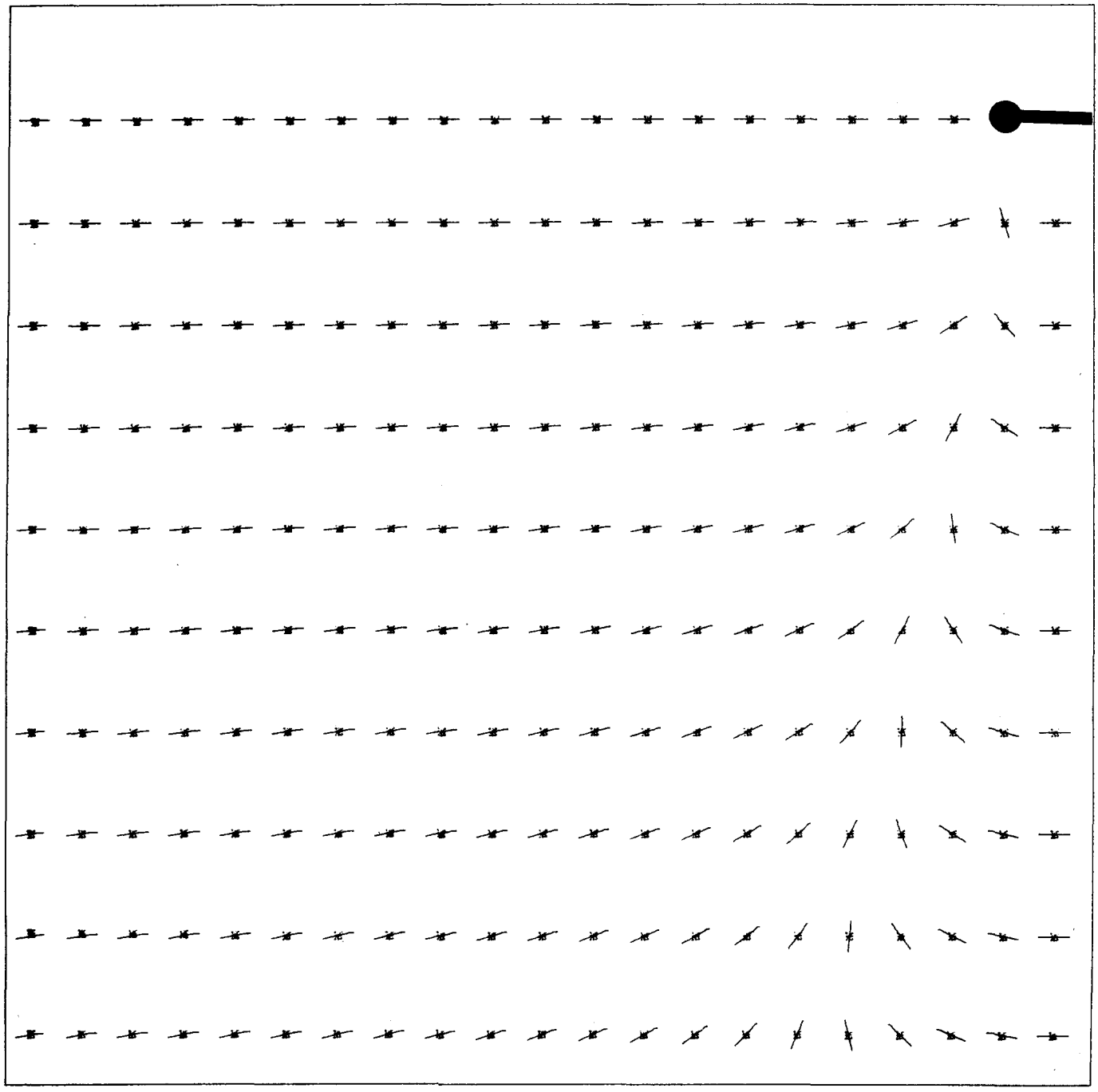

Figure D30.

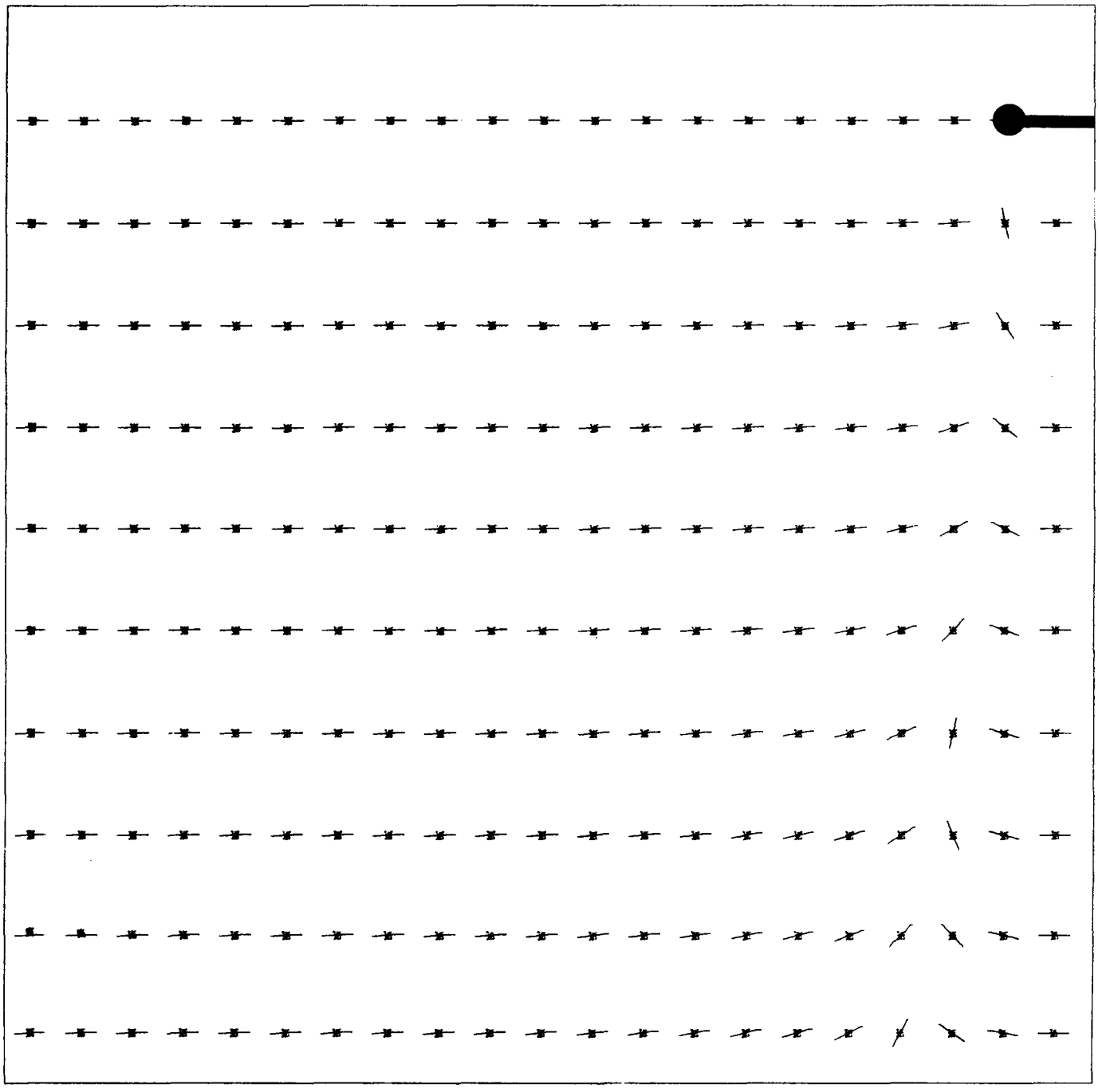

Figure D31.

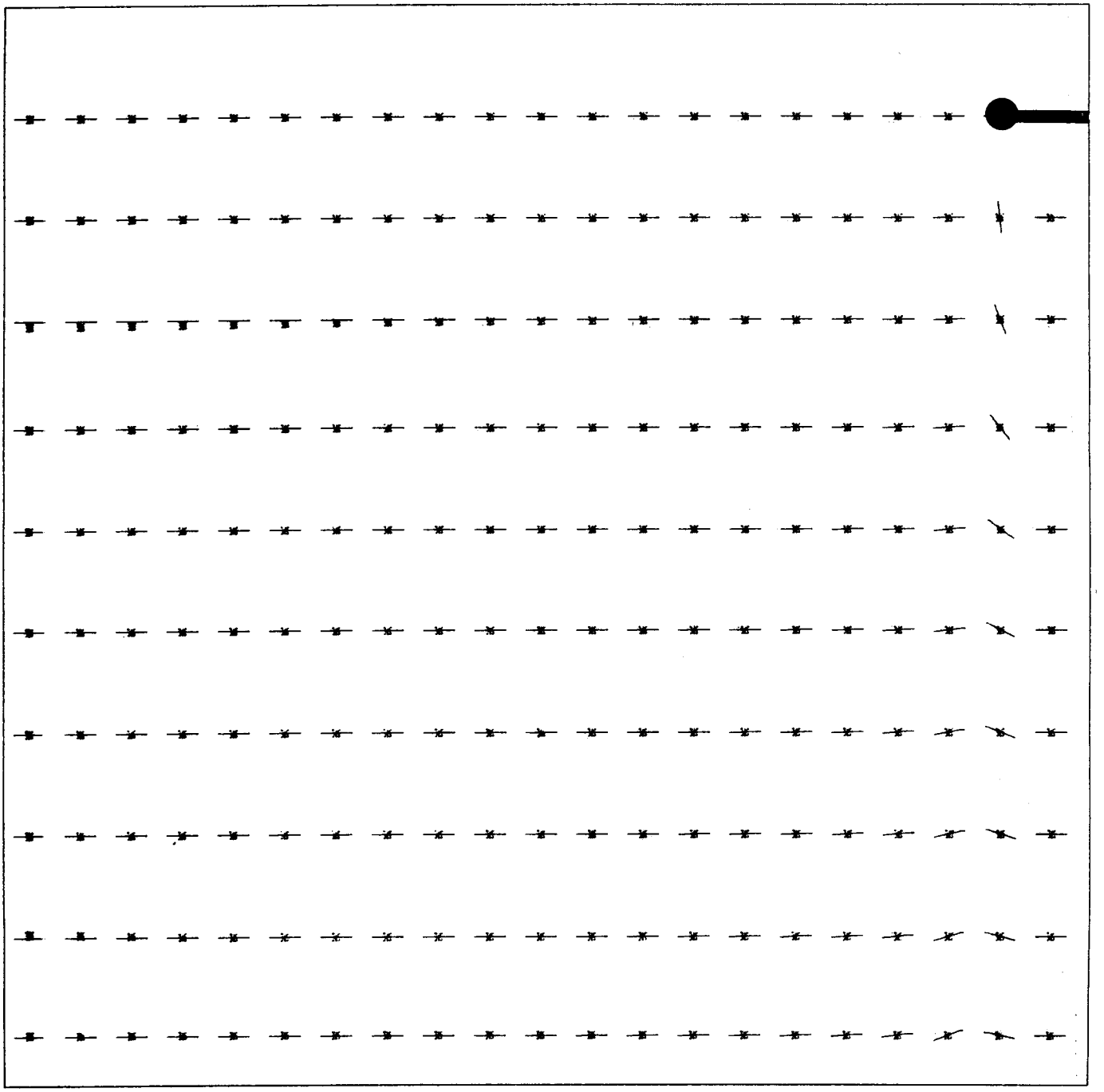

UNIFORM ANISOTROPIC EARTH WITH AN = 10.0

Figure D32.

☆U.S. GOVERNMENT PRINTING OFFICE: 1978-740-092/337